UNIVERSITY OF CALIFORNIA
RIVERSIDE

# Long-Term Plasticity of Astrocytic Metabotropic Neurotransmitter Receptors Driven by Changes in Neuronal Activity in Hippocampal Slices

A Dissertation submitted in partial satisfaction
of the requirements for the degree of

Doctor in Philosophy

in

Neuroscience

by

Xiaoqiao Xie

August 2011

Dissertation Committee:

Dr. Todd A. Fiacco, Chairperson
Dr. Iryna M. Ethell
Dr. Peter W. Hickmott

The Dissertation of Xiaoqiao Xie is approved:

_____

_____

_____

Committee Chairperson

University of California, Riverside

ABSTRACT OF THE DISSERTATION

Long-Term Plasticity of
Astrocytic Metabotropic Neurotransmitter Receptors
Driven by Changes in Neuronal Activity
in Hippocampal Slices

by

Xiaoqiao Xie

Doctor of Philosophy, Graduate Program in Neuroscience
University of California, Riverside, August 2011
Dr. Todd A. Fiacco, Chairperson

In addition to synaptic communication between neurons, there is now strong evidence for neuron-to-astrocyte receptor signaling in the brain. During trains of action potentials or repetitive stimulation, neurotransmitter spills out of the synapse to activate astrocytic Gq protein-coupled receptors (Gq GPCRs). To date, very little is known about the ability of astrocytic receptors to exhibit plasticity as a result of long-term changes in neuronal firing rates. Here we describe for the first time bidirectional scaling of astrocytic group 1 metabotropic glutamate receptor (mGluR) signaling in acute mouse hippocampal slices on a rapid timescale following either long-term blockade or increase in neuronal synaptic transmission. Plasticity of astrocytic mGluRs was measured by recording changes in spontaneous and evoked astrocyte $Ca^{2+}$ elevations in both astrocytic soma as well as fine processes. In response to 4 to 6 hour blockade of CA3-CA1 neurotransmission, the following changes in astrocyte $Ca^{2+}$ signaling were observed: 1) a significant increase in the percentage of astrocytes in the slice population exhibiting

spontaneous $Ca^{2+}$ elevations; 2) significantly faster rise times of the spontaneous $Ca^{2+}$ transients; 3) a significant increase in response probability to the group I mGluR agonist; 4) significantly faster rise times of evoked $Ca^{2+}$ responses; 5) significantly shorter response latencies of evoked $Ca^{2+}$ responses in astrocyte microdomains; and 6) a dose-dependent shift in astrocytic responses to DHPG in TTX vs. control incubated slices. In response to 4 to 6 hour elevation of CA3-CA1 neurotransmission, the opposite effects on the previous parameters were observed. Further study using transgenic mice expressing a novel Gq GPCR suggested that the changes observed in astrocytic group I mGluR $Ca^{2+}$ signaling were due to changes in expression of the group I mGluRs in astrocytes, while the intracellular signaling pathway activated by the Gq GPCRs remained unchanged. This study introduces a sensitive assay for recording changes in astrocytic Gq GPCR expression levels, and the results demonstrate active astrocytic detection of basal and elevated frequencies of neuronal action potentials that lie within a physiological range.

## TABLE OF CONTENTS

LIST OF FIGURES

# LIST OF ABBREVIATIONS

| | |
|---|---|
| 20-HETE | 20-Hydroxyeicosatetraenoic Acid |
| 4C3HPG | (S)-4-Carboxy-3-hydroxy-phenylglycine |
| 4CPG | 4-carboxy-phenylglycine |
| AA | arachidonic acid |
| AC | adenylate cyclase |
| ACSF | artificial cerebrospinal fluid |
| ALS | amyotrophic lateral sclerosis |
| AMPA | 2-amino-3-(5-methyl-3-oxo-1,2-oxazol-4-yl)propanoic acid |
| AP | action potential |
| ATP | Adenosine-5'-triphosphate |
| BSA | bovine serum albumin |
| C1q | subunit of first component of the classical complement pathway |
| CaMKIV | calcium/calmodulin-dependent protein kinase type IV |
| CNPase | 2', 3'-cyclic nucleotide 3'-phosphodiesterase |
| CNS | central nervous system |
| COX-1 | cyclooxygenase |
| CREB | cAMP response element-binding |
| DHPG | (R,S)-3,5-dihydroxyphenylglycine |
| DIC | differential interference contrast |
| DMSO | dimethyl sulfoxide |
| dox | doxyxyxline |
| EDTA | ethylenediaminetetraacetic acid |
| ER | endoplasmic reticulum |
| FACS | fluorescence-activated cell sorter |

| | |
|---|---|
| FLRFa | FLRFamide (Phe-Leu-Arg-Phe-$NH_2$) |
| FMRFa | FMRFamide (Phe-Met-Arg-Phe-$NH_2$) |
| GFAP | glial fibrillary acidic protein |
| GDP | guanosine diphosphate |
| GFP | green fluorescent protein |
| GTP | guanosine triphosphate |
| GLAST | glutamate/aspartate transporter |
| GLT-1 | glutamate transporter 1 |
| GPCR | G protein coupled receptor |
| GRK | G protein coupled kinase |
| GS | glutamine synthetase |
| H1R | histamine H1 receptor |
| iGluR | ionotropic glutamate receptors |
| IP3 | inositol trisphosphate |
| LTP | long-term potentiation |
| LY367385 | (+)-2-methyl-4-carboxyphenylglycine |
| mAchR | muscarinic acetylcholine receptor |
| MAPK | mitogen-activated protein kinase |
| MCPG | α-methyl-4-carboxyphenylglycine |
| mEPSC | miniature excitatory postsynaptic currents |
| mGluR | metabotropic glutamate receptor |
| mIPSC | miniature inhibitory postsynaptic current |
| MPEP | 2-methyl-6-(phenylethynyl)pyridine |
| MS | multiple sclerosis |
| MrgA1 | Mas-related geneA1 |
| NBQX | 2,3-dihydroxy-6-nitro-7-sulfamoyl-benzo[f]quinoxaline-2,3-dione |

| | |
|---|---|
| NMDA | N-methyl-D-aspartate |
| NO | nitric oxide |
| NOS | nitric oxide synthase |
| OGB-1 | Oregon Green BAPTA-1 |
| P2YR | purinergic receptor |
| PBS | phosphate buffered saline |
| PIP2 | phosphatidylinositol (4,5) bisphosphate |
| PLA2 | phospholipases A2 |
| PLC | phospholipase C |
| ROIs | regions of interest |
| SIC | slow inward current |
| s. r. | stratum radiatum |
| SR101 | sulforhodamine |
| tACPD | trans-ACPD (1-amino-1,3-dicarboxycyclopentane) |
| tetO | tetracycline operator |
| TMN | tuberomammillary nucleus |
| TNFα | Tumor necrosis factor-alpha |
| tTA | tetracycline transactivator |
| TTX | tetrodotoxin |

# Chapter 1: Introduction

## 1.1 Astrocytes are the most predominant glial cell type in the central nervous system (CNS)

Astrocytes are the predominant glial cell type in central nervous system (CNS), constituting approximately one-third of mouse brain cells and nearly half of human brain cells (Cahoy et al., 2008). Astrocytes could be as heterogeneous as neurons. They fall into at least two main categories which can be distinguished by morphology, antigenic phenotype, location and function (Barres, 2008). Protoplasmic astrocytes are mainly located in gray matter. Their processes intensively ensheath synapses as well as contacting blood vessels. In white matter, the majority of astrocytes are called fibrillary astrocytes. Fibrillary astrocytes (or fibrous astrocytes) contact blood vessels and nodes of Ranvier on neuronal axons.

There are also astrocytes that are specialized in certain brain structures. For example, Müller cells in vertebrate retina ensheath many synapses, similar to protoplasmic astrocytes in gray matter. However, as a specialized type of astrocyte in retina, Müller cells also have distinguished neurogenic capacity (Pinto and Götz, 2007). In intact zebrafish retina, Müller cells express low levels of the multipotent progenitor marker paired box gene 6 (Pax6), and proliferate at a low frequency. In response to injury to retina and neuronal loss, Müller cells have the ability to undergo de-differentiation and become multipotent progenitor cells, which give rise to several retinal cell types, including photoreceptor cells (Bernardos et al., 2007).

Another well-known type of specialized astrocyte is the Bergmann glia of the cerebellum. The cell bodies of Bergmann glia reside in the Purkinje cell layer while their processes extend into the molecular layer of the cerebellum, forming distinct morphological structures to interact with cerebellar neurons (Grosche et al., 1999; Grosche et al., 2002). Unlike most cortical areas of the brain where only 40% to 60% of synapses are associated with astrocytic processes, 100% of synapses in the cerebellum are wrapped by processes from Bergmann glia. In addition, all the synapses are covered by at least two inter-digitating glial microdomains, and synaptic clefts are entirely surrounded by glial protrusions. Interestingly, many small neuronal terminals without vesicles are also completely ensheathed by glial caps, representing novel glial-neuronal structures with unknown function (Grosche et al., 2002).

### 1.2 Astrocytes play important roles in CNS

What do astrocytes do in the CNS? Similar morphologies of astrocytes in Drosophila and in mammalian CNS suggest that the functions of astrocytes are likely to be highly conserved (Doherty et al., 2009). Given the complexity of interactions between individual astrocyte processes and synapses or fine blood vessels (Ventura and Harris, 1999; Bushong et al., 2002), one can imagine the possibility of communication between neuronal synapses, the cerebrovasculature, and astrocyte processes. Within the CA1 stratum radiatum (s.r.) of the hippocampus, an individual astrocyte has a soma diameter of 7 to 9 millimeter (mm) and, with its fine processes,

occupies a non-overlapping domain of about 66,000 $mm^3$ (Bushong et al., 2002; Agulhon et al., 2008).

In gray matter, protoplasmic astrocytes help to control extracellular concentration of some ions such as potassium ($K^+$) ions and neurotransmitters in the extracellular space. The fine processes of an individual astrocyte are connected to one another and to processes of other astrocytes through gap junctions (Konietzko and Muller, 1994), which enables astrocytes to take up extracellular $K^+$ ($[K^+]_o$) and quickly redistribute $K^+$ further away from active synapses through the astrocyte syncytium. A recent transcriptome study has shown that astrocytes express a full cassette of ion transporters, pumps, and channels (Cahoy et al., 2008).

Astrocytes can also sense nearby neuronal activity and regulate blood flow either through vasoconstriction (Mulligan and MacVicar, 2004; Metea and Newman, 2006) or vasodilation (Zonta et al., 2003; Metea and Newman, 2006; Takano et al., 2006). In fact, 99% of the cerebrovascular surface in the CNS is ensheathed by astrocyte processes (Simard et al., 2003; Haydon and Carmignoto, 2006; Takano et al., 2006). Neuronal activity activates astrocytic surface receptors which lead to calcium ($Ca^{2+}$) elevations in astrocytes. $Ca^{2+}$ responses then propagate to astrocytic endfeet, which are directly in contact with arterioles. Astrocytes mediate vasodilation through calcium-mediated synthesis of phospholipases A2 (PLA2), which is converted into prostaglandins by cyclooxygenase (COX-1) and leads to arachidonic acid (AA) production (Zonta et al., 2003; Takano et al., 2006). In contrast, vasoconstriction

following $Ca^{2+}$ transients in astrocytic endfeet *in situ* was shown to involve a different signaling cascade, resulting in the release of AA by astrocyte processes which then diffuses to vascular smooth muscle cells, leading to the production of the major vasoconstrictive metabolite 20-Hydroxyeicosatetraenoic Acid (20-HETE) (Mulligan and MacVicar, 2004). It is not clear why some groups observe vasodilation while other groups observe vasoconstriction after astrocyte stimulation. The different outcomes of blood flow both involve activation of astrocytic receptors by neurotransmitter and $Ca^{2+}$ transients. Vasoconstriction has been suggested to be an artifact of the slice preparation due to the lack of vascular tone and blood flow cessation (Takano et al., 2006). Another explanation of the different type of vasomotor response is the effect of nitric oxide (NO). Inhibitors of nitric oxide synthase (NOS) enzymes completely eliminate vasoconstrictions, whereas NO donors block vasodilations or even transform vasodilations into vasoconstrictions (Metea and Newman, 2006).

Astrocytes are known to release many trophic factors, which promote synaptogenesis and enhance synaptic function (Barres, 2008). Astrocyte-derived cholesterol also powerfully enhances presynaptic function (Mauch et al., 2001). Thrombospondin, a large matrix-associated protein secreted by cultured astrocytes, can increase the number of synapses formed between retinal ganglion cells in culture (Ullian et al., 2001; Christopherson et al., 2005). Thrombospondins 1 and 2 are shown to be sufficient to induce synapses that have normal presynaptic and postsynaptic ultrastructure as well as normal clustering of presynaptic and postsynaptic proteins,

while other proteins are needed to induce the response of postsynaptic glutamate receptors such as α-amino-3-hydroxy-5-methyl-4-isoxazolepropionic acid (AMPA) receptors (Christopherson et al., 2005). During development, the secretion of thrombospondins by immature astrocytes is controlled by neuronal release of ATP and other neurotransmitters, which suggested a novel pathway of synaptogenesis required by local neuronal activity (Tran and Neary, 2006). In 2009, Gabapentin receptor α2β-1 was identified as the neuronal thrombospondin receptor that is involved in CNS synapse formation (Eroglu et al., 2009). Surprisingly, transplantation of immature astrocytes into adult primary visual cortex can robustly restore ocular dominance plasticity (Muller and Best, 1989). Interestingly, thrombospondin is confirmed as one of the few genes that is highly upregulated in human brain compared to the brains of other primates, which might underlie the greatly enhanced brain plasticity of humans.

It has also been shown that astrocytes also help to control synapse elimination in the developing CNS by inducing neurons to express and secrete C1q (subunit of first component of the classical complement pathway), which becomes synaptically localized and leads to activation of the classical complement cascade (Stevens et al., 2007). In adult CNS, neuronal C1q is normally downregulated. Upon injury or disease, reactive astrocytes induce C1q expression in neurons and relocalize it to synapses (Stevens et al., 2007). This study suggests a model in which unwanted synapses are tagged by complement for elimination and that complement-mediated synapse elimination may become aberrantly reactivated in neurodegenerative disease.

Astrocytes are also the one type of glial cell known to release tumor necrosis factor-alpha (TNFα). Glial TNFα has been shown to play diverse roles in brain function including synaptogenesis (Ullian et al., 2004), enhancing release of gliotransmitters (Bezzi et al., 1998) as well as contributing to the process of homeostatic plasticity in neurons (Beattie et al., 2002).

### 1.3 Reciprocal astrocyte-to-neuron communication

It has been a long-term debate whether astrocytic G protein coupled (metabotropic) receptor (Gq GPCR) activation can induce release of glutamate, Adenosine-5'-triphosphate (ATP) and other neuroactive substances such as D-serine from astrocytes back to synapses, known as gliotransmission. There have been many reports on cultured astrocytes releasing glutamate and ATP through different mechanisms, including swelling-induced activation of volume-regulated anion channels (Kimelberg et al., 2006), connexin hemichannels (Stout et al., 2002; Ye et al., 2003; Kang et al., 2008), pore-forming P2X7 purinergic receptors (Duan et al., 2003; Fellin et al., 2006), and reversal of glutamate transporters (Anderson and Swanson, 2000). Astrocytic Gq GPCR signaling cascades have been proposed to trigger $Ca^{2+}$-dependent release of gliotransmitters for reciprocal astrocyte-to-neuron communication to regulate fast synaptic transmission as well as long-term potentiation (LTP) (Henneberger et al.; Yang et al., 2003; Fiacco and McCarthy, 2006) but some labs have been unable to find evidence for calcium-induced release of

glutamate onto postsynaptic neurons (Fiacco et al., 2007; Agulhon et al., 2008; Fiacco et al., 2009).

However, whether astrocytes *in vivo* release glutamate in quanta has never been directly demonstrated. Given the difference between astrocytes in intact CNS, and cultured astrocytes which often exhibit a phenotype of reactive astrocytosis only seen in pathological conditions *in vivo*, there is very little evidence that astrocytes *in vivo* secrete and release glutamate back to neurons via a $Ca^{2+}$-dependent vesicular pathway. Furthermore, glutamine synthetase (GS), the enzyme responsible for degrading glutamate to glutamine, is highly enriched in astrocytes (Norenberg and Martinez-Hernandez, 1979). It has been shown that there is a very low level of cytoplasmic glutamate in astrocytes (Innocenti et al., 2000; Fiacco et al., 2008). In addition, it is still controversial whether astrocytes *in vivo* express the right components for vesicular release of glutamate as in neurons (Cahoy et al., 2008; Fiacco et al., 2008).

Recent studies reveal that astrocytes are nevertheless highly secretory cells (Cahoy et al., 2008). The mechanisms by which astrocytes secrete neuroactive substances remains to be clarified. It was reported that astrocytes *in vivo* can induce regulated secretion from secretory lysosomes upon $Ca^{2+}$ elevations (Jaiswal et al., 2007; Zhang et al., 2007; Li et al., 2008). It has also been reported *in vivo* that astrocytes release ATP and in turn regulate CNS synaptic transmission, potentially from secretory lysosomes (Pascual et al., 2005). Further investigation is required to

determine if this is a universal mechanism of gliotransmission from astrocytes throughout the CNS.

### 1.4 Neuron-astrocyte communication through astrocytic Gq GPCRs

#### 1.4.1 Expression profile of Gq GPCRs on astrocytes

Unlike neurons, astrocytes generally do not express ionotropic neurotransmitter receptors as neurotransmitter binding to astrocytic receptors does not lead to changes in membrane properties. Astrocytes - including fibrous and protoplasmic astrocytes as well as Bergmann and Müller glia - express an incredible array of G-protein-coupled metabotropic receptor types including glutamatergic, GABAergic, adrenergic, purinergic, serotonergic, muscarinic, and peptidergic receptors (Porter and McCarthy, 1997). Expression of these receptors can be detected both *in situ* and *in vivo*, and they can be activated by neurotransmitters released from synaptic terminals. Upon activation, metabotropic receptors on astrocytes signal through activation of phospholipase C (PLC) or adenylate cyclase (AC), following the typical Gq GPCR signaling pathways.

#### 1.4.2 Intracellular $Ca^{2+}$ release mediated by Gq GPCR signaling in astrocytes

The excitability of astrocytes has been defined predominantly by activation of Gq GPCRs which are linked to activation of PLC, conversion of phosphatidylinositol bisphosphate ($PIP_2$) to inositol triphosphate ($IP_3$), and .release of calcium from the endoplasmic reticulum (ER). There is much evidence showing that Gq GPCRs can be

activated by presynaptic neurotransmitter release *in situ* and *in vivo* (Porter and McCarthy, 1995, 1996; Pasti et al., 1997; Kang et al., 1998; Araque et al., 2002; Perea and Araque, 2005a; Wang et al., 2006; Navarrete and Araque, 2008), suggesting that astrocytes are actively sensing neuronal activity *in vivo*. More specifically, astrocytic group I metabotropic glutamate receptors (mGluRs), has been demonstrated to mediate astrocytic $Ca^{2+}$ elevations when stimulation involves glutamatergic afferents in hippocampus (Porter and McCarthy, 1996; Perea and Araque, 2005b). Recently a number of studies performed in awake, mobile mice show that intracellular calcium transients in astrocytes are closely correlated with neuronal activity (Wang et al., 2006; Dombeck et al., 2007; Schummers et al., 2008). The current hypothesis is that astrocytes can respond to sensory stimulation with distinct temporal and spatial patterns. Unlike earlier observations in cultured astroglia, calcium waves generally do not propagate to other astrocytes *in vivo* (Schummers et al., 2008).

### 1.4.3 G-protein-independent signaling by GPCRs

GPCRs can also interact with other cellular proteins, leading to G-protein-independent signaling (Heuss and Gerber, 2000). In CA3 hippocampal pyramidal neurons, mGluR1 can change membrane ion conductance through possible G-protein-independent modulation that involves Src-family non-receptor tyrosine kinase (Heuss et al., 1999). Another example is β3-adrenoceptor, which can bind c-Src directly and activate ERK (Cao et al., 2000). The binding between β3-adrenoceptor and c-Src

family protein are via proline-rich regions (PXXP motifs) in the C-terminal domains of the receptor, which are also present in multiple Gq GPCRs including mGlu1a, $mGlu_{5a}$ and $mGlu_{5b}$ receptors (Cao et al., 2000). In neurons, this type of G-protein-independent signaling by GPCRs often initiates activation of mitogen-activated protein kinase (MAPK) and is involved in internalization and desensitization of Gq GPCRs (Lefkowitz, 1998).

### 1.4.4 Constitutive activity of Gq GPCRs

Astrocytes also exhibit spontaneous calcium oscillations that occur independent of neuronal input (Ango et al., 2001; Hermans and Challiss, 2001; Milligan, 2003; Bond and Ijzerman, 2006; Sweger et al., 2007) or application of agonist (Parri et al., 2001; Nett et al., 2002; Zur Nieden and Deitmer, 2006). It was shown that spontaneous astrocytic $Ca^{2+}$ oscillations still require $IP_3R$ mediated $Ca^{2+}$ release from internal stores, indicating the involvement of Gq GPCR signaling (Nett et al., 2002; Petravicz et al., 2008). This led to the hypothesis that the spontaneous astrocyte $Ca^{2+}$ transients may be driven by constitutive activity of astrocytic Gq GPCRs, which promotes guanosine triphosphate (GTP)/guanosine diphosphate (GDP) exchange and activation of G-proteins in the absence of agonist (de Ligt et al., 2000; Hermans and Challiss, 2001). Consistent with this theory, previous work has shown that the amount of constitutive activity is proportional to the expression levels of the GPCRs (Prezeau et al., 1996; Ango et al., 2001; Milligan, 2003).

### 1.5 Metabotropic glutamate receptors (mGluRs) signaling on astrocytes

#### 1.5.1 Expression profile of group I mGluRs on astrocytes

The expression of neurotransmitter receptors by astrocytes *in situ* exhibits regional and intraregional heterogeneity, and changes during development (Porter and McCarthy, 1997). In hippocampal astrocytes, mGluR3 and mGluR5 are the predominant metabotropic glutamate receptor mRNAs expressed. Eighty-two percent of glial fibrillary acidic protein (GFAP)-positive hippocampal astrocytes acutely isolated from P1 to P10 rats responded to glutamate application with transient intracellular calcium increases via activation of the group 1 metabotropic glutamate receptor. Metabotropic GluR5 mRNA was detected in 100% of the GFAP positive cells acutely isolated from postnatal day 1 (P1) to P10 rats, with “a” type splice variant being dominant (Schools and Kimelberg, 1999). In hippocampal astrocytes acutely isolated from P11 to P20 rats, a smaller percentage (77%) of GFAP positive cells showed detectable mGluR5 mRNA expression and responded to glutamate application (Cai et al., 2000). Only 36% of GFAP positive cells from P25 to P35 rats expressed mGluR5 mRNA and 33% responded to glutamate application (Cai et al., 2000). Both mGluR5a and mGluR5b were expressed with equal frequency in cells from P11 to P20 rats, and the “b” form predominated in cells from P25 to P35 rats. These studies show that the percentage of hippocampal astrocytes that express mGluR5 decreases with age, with the "a" splice variant declining to a greater extent than the "b" splice variant. This data correspond to the developmental changes shown

in total tissue for mGluR5. There was no detectable mGluR1 mRNA expressed in acutely isolated hippocampal astrocytes.

There is also little evidence of astrocytic mGluR1 expression *in situ* in other brain regions including hippocampus (Shigemoto et al., 1992; Baude et al., 1993; Van den Pol, 1994; Mudo et al., 2007). However, it was reported that some astrocytic processes associated with glutamatergic synapses exhibit intense mGluR5 immunoreactivity (van den Pol et al., 1995). This suggests that glutamatergic increases in $[Ca^{2+}]_i$ in astrocytes may be mediated only by mGluR5 (van den Pol et al., 1995). The proximity of astrocytic mGluR5 expression to glutamatergic synapses suggests that these receptors might be the prime targets for glutamate released from those synapses.

In contrast, another group reported at least two subpopulations of group I mGluRs expressed in cultured hippocampal astrocytes. The mGluR agonists (1*S*,3*R*)-1-aminocyclopentane-1,3-dicarboxylic acid (ACPD) and (*R*,*S*)-3,5-dihydroxyphenylglycine (DHPG) induced $Ca^{2+}$ responses in 76% and 93% of hippocampal astrocytes in culture, respectively. The broad-spectrum mGluR antagonist (+)-$\alpha$-methyl-4-carboxyphenylglycine (MCPG) and the mGluR1 antagonists (*S*)-4-carboxy-3-hydroxyphenylglycine (4C3HPG) and (*S*)-4-carboxyphenylglycine(4CPG) suppressed the agonist-evoked $Ca^{2+}$ responses in about 25% of the cells completely and in about 60% partially, depending on the agonist concentration employed. Truncated splice variants of mGluR1 (mGluR1b, mGluR1c,

mGluR1d) were found by immunohistochemical studies (Lembo et al., 2002). In brain slice preparations, application of the mGluR agonist DHPG or tACPD evokes robust $Ca^{2+}$ transients in cortical astrocytes, while co-application of the mGluR1 antagonist (+)-2-methyl-4-carboxyphenylglycine (LY367385) and the mGluR5 antagonist 2-methyl-6-(phenylethynyl) pyridine (MPEP) *in vivo* reduces the whisker-evoked $Ca^{2+}$ response in astrocytes by more than 70% (Wang et al. 2006). MPEP and LY367385 alone are equally effective in inhibiting the whisker-evoked response (40–50% inhibition), suggesting that both mGluR1 and mGluR5 contribute to astrocyte activation *in vivo* (Wang et al. 2006).

### 1.5.2 Plasticity of astrocytic mGluRs

Plasticity of astrocytic mGluRs has been previously demonstrated in several neuronal disorders, including epileptic seizures (Tang et al., 2002; Mudo et al., 2007), multiple sclerosis (MS) (Geurts et al., 2003), amyotrophic lateral sclerosis (ALS) (Aronica et al., 2001) and Taylor-type focal cortical dysplasia (Aronica et al., 2003). The upregulation of astrocytic mGluR expression level has also been found in several animal models of these neuronal disorders (Aronica et al., 2000; Ulas et al., 2000; Ferraguti et al., 2001; Tseng et al., 2009; Drouin-Ouellet et al., 2011). In these studies looking at the role of reactive astrocytes upon neuroinflammatory insult, expression levels of mGluRs have been shown to increase as astrocytes become reactive, characterized by hypertrophy, proliferation and increased expression of GFAP. However, it is unknown whether astrocytic Gq GPCRs exhibit plasticity as a

physiological response to changes in levels of neuronal synaptic transmission. The focus of my thesis dissertation work is to test the hypothesis that astrocytic Gq GPCRs exhibit long-term plasticity in response to changes in basal levels of neuronal synaptic transmission.

### 1.5.3 Plasticity of astrocytic mGluRs in epilepsy brain

In models of kainate-induced epileptic seizures, mGluR5 immunoreactivity is severely reduced 3 days after kainic acid injection, followed by a progressive reappearance and lasting presence of the receptor protein (Ulas et al., 2000). Receptor mRNA disappeared from the pyramidal cell layer of the lesion in CA3 region. On the other hand, the message level was found to increase persistently in the CA3 stratum lucidum and stratum radiatum, the site of massive astrogliosis. In these sites, mGluR5 mRNA became detectable in double labeling studies in GFAP-positive astrocytes (Ulas et al., 2000). This result was further explored by another group in 2001. Immuno-histochemical analysis showed strong mGluR5 and mGluR2/3 immuno-reactivity in glial cells possessing the morphological features of activated astrocytes within the area of neuronal loss. The mechanical injury produced by the needle insertion in the cerebral cortex also produced enhanced expression of mGluR5 and mGluR2/3 in activated astrocytes proximal to the area of neuronal injury (Ferraguti et al., 2001).

In 2000, it was reported a seizure-induced upregulation of mGluR2/3 and mGluR5 in reactive astrocytes (Aronica et al., 2000). Metabotropic GluR2/3 and

mGluR5 protein expression increased markedly in reactive astrocytes of CA3 and hilus one week after status epilepticus occurred. Twenty-four hours after onset of seizure activity, there was a seizure intensity-dependent increase in vimentin immunoreactivity in astrocytes in CA3 and hilar regions where prominent neuronal loss took place. Such increased vimentin labeling persisted up to 3 months. Associated with a reactive phenotype, astrocytic mGluR2/3 and mGluR5 protein expression increased markedly in CA3 and hilus one week after status epilepticus, and persisted up to 3 months after seizure onset. This study indicated that mGluR2/3 and mGluR5 expression in astrocytes is tightly related to CA3 neuronal loss, suggesting that the plasticity of mGluR expression plays an important role in modulation of glial function and for changes in glial-neuronal communication in the course of epileptogenesis (Aronica et al., 2000).

Challenging these findings is a recent study that found no mGluR5 expression in the area of kainate or ibotenic acid induced hippocampal lesions. Ibotenic acid is an N-Methyl-D-aspartate (NMDA) receptor agonist and injection of ibotenic acid into ventral hippocampus at a critical period of development can cause a significant and persistent astrogliosis and microglial activation, associated with the production of inflammatory mediators (Tseng et al., 2009). Although, an increased expression of mGluR3 in the area of lesion was observed one week after the injury and was localized to GFAP- and 2', 3'-cyclic nucleotide 3'-phosphodiesterase (CNPase)-positive cells. There were no data on the protein expression of mGluR5 in reactive astrocytes in this report (Mudo et al., 2007).

In brain tissue taken from patients with mesial temporal lobe epilepsy, expression of the group I metabotropic glutamate receptors was also detected in the hippocampus, where degenerating neuronal elements were found (Tang et al., 2002). Immuno-cytochemical studies using both light and electron in hippocampus of patients with mesial temporal lobe epilepsy showed mGluR1 and mGluR5 immuno-reactivity in the molecular layer of the dentate gyrus and CA1 area, especially at the border between stratum oriens/alveus. Metabotropic $GluR_5$ immuno-reactivity was demonstrated in both post- and pre-synaptic elements in the molecular layer of the dentate gyrus and CA1 area, and was also found in astrocytes and in the periphery of fibrillary tangles (Tang et al., 2002).

### 1.5.4 Plasticity of astrocytic mGluRs in other neurological disorders

Injection of ibotenic acid into ventral hippocampus at a critical period of development can also cause several neuropsychiatric-related symptoms, including psychostimulant-induced hypersensitivity, impaired working memory and social deficits (Tseng et al., 2009). Neonatal lesion of the ventral hippocampus using ibotenic acid has been considered as a neurodevelopmental model of schizophrenia. Recently, Drouin-Ouellet et al. (2011) reported significantly increased mGluR5 mRNA expression in both reactive astrocytes and activated microglia in the context of neuroexcitotoxicity following neonatal ventral hippocampal lesions in rats with ibotenic acid (Drouin-Ouellet et al., 2011).

It was reported that mGluR2/3 and mGluR5 expression were upregulated in reactive glial cells in both gray and white matter of the spinal cord in patients with amyotrophic lateral sclerosis (Aronica et al., 2001) and Taylor-type focal cortical dysplasia (Aronica et al., 2003). In the patients of the CNS inflammatory demyelinating disease multiple sclerosis, upregulation of mGluR2/3 and mGluR5 was observed in astrocytes present in both acute and chronicactive multiple sclerosis lesions (Geurts et al., 2003). Detectable expression level of mGluR1a was only observed in a subpopulation of reactive astrocytes present in demyelinated area (Geurts et al., 2003). Increased expression glutamate transporter 1 (GLT-1) and unexpected expression of glutamate/aspartate transporter (GLAST) were also detected in reactive astrocytes in MS white matter lesions (Newcombe et al., 2008). A subpopulation of reactive astrocytes also had immunoreactivity for glutamate antibodies and expressed glutamate metabolizing enzymes. Thus, reactive astrocytes in MS white matter lesion are equipped for a protective role in sequestering and metabolizing extracellular glutamate (Newcombe et al., 2008).

At sites of CNS trauma or injury thrombin is one of the first regulatory molecules that appear. Thrombin treatment of differentiated astrocyte cultures led to reduction in the level of mGluR5 mRNA and also reduced levels of mGluR5 receptor protein. This suppressive effect was resistant to pretreatment with various protein kinase and protein phosphatase inhibitors (Miller et al., 1996). In addition, thrombin treatment promotes retraction of astrocytic processes and induction of beta-actin mRNA levels, potentially though a signaling pathway distinct from the one that mediates the

suppressive effects of thrombin on mGluR5 (Miller et al., 1996). These findings suggest that changes in neuronal activity under pathological conditions can influence neurotransmitter receptor expression levels and signaling on astrocytes through modulators such as thrombin.

## 1.6 Do astrocytes exhibit long-term plasticity in response to changes in basal levels of synaptic transmission?

### 1.6.1 A form of long-term receptor plasticity in neurons: homeostatic plasticity

Neuronal synaptic plasticity, defined as long-term changes in synaptic receptor expression levels in response to changes in the frequency of synaptic transmission, has been studied for many years. In addition to plasticity occurring at individual synapses, plasticity has also been found to change the intrinsic properties of neurons or neuronal networks. This homeostatic plasticity or long-term scaling of synaptic receptors occurs throughout the entire neuron without changing the relative ratios between AMPA and NMDA receptors within a cell, suggesting that this type of plasticity does not interfere with synapse-specific mechanisms of information storage (Myme et al., 2003).

It has been a long time since the first study on whether neurons exhibit homeostatic regulation in order to maintain stable firing properties of a single neuron or within a neuronal network. Turrigiano et al. (1994) reported that isolated lobster stomatogastric ganglion neurons lost their normal rhythmic bursting activity in culture. However, after 3 days of isolation in culture, these stomatogastric ganglion

neurons changed their intrinsic activity from tonic firing to burst firing. This change could be reversed by applying rhythmic stimulation, suggesting that neurons can regulate their conductance to maintain stable activity patterns based on their recent history of synaptic input (Turrigiano et al., 1994).

Since 1998, Turrigiano et al. have conducted a series of elegant studies to demonstrate that following long-term changes in synaptic activity, neurons scale their postsynaptic receptors accordingly in an attempt to recover their own firing rates (Turrigiano et al., 1998; Watt et al., 2000; Leslie et al., 2001; Pratt et al., 2003; Wierenga et al., 2005; Ibata et al., 2008a). When neuronal action potential (AP)-mediated glutamate release is blocked by incubation of tissue in the $Na^+$ channel blocker tetrodotoxin (TTX) in primary neuronal culture from visual cortex, the postsynaptic expression of AMPA and NMDA receptors scales up in a compensatory manner to recover glutamate receptor activation in postsynaptic cells (Leslie et al., 2001). As a consequence, miniature excitatory postsynaptic current (mEPSC) amplitudes from postsynaptic neurons are significantly increased, while the frequency of mEPSCs remains unchanged. It was reported that such synaptic scaling induced by blockade of postsynaptic firing is mediated through a drop in somatic calcium influx, reduced activation of calcium/calmodulin-dependent protein kinase type IV (CaMKIV), and an increase in gene transcription for a panel of proteins including AMPA receptor subunits (Ibata et al., 2008b). When NMDA receptor mediated miniature synaptic events (‘‘minis’’) were blocked, synaptic scaling occurred more rapidly, suggesting that NMDAR signaling during miniature synaptic transmission

serves to stabilize synaptic function through active suppression of dendritic protein synthesis (Sutton et al., 2004; Sutton et al., 2006).

Homeostatic scaling of neuronal networks has also been shown in hippocampal slices after chronic activity-blockade *in vivo* (Echegoyen et al., 2007). Following sustained release of TTX from the plastic polymer Elvax 40W implantation for 48 hours *in vivo*, Schaffer collateral stimulation-evoked field responses were enhanced in acute hippocampal slices obtained from these animals ex vivo. In addition, mEPSC amplitudes and intrinsic neuronal excitability both increased. However, the increase in mEPSC amplitudes occurred in juveniles (P15), but not in adults (P30). In contrast to previous reports of homeostatic responses *in vitro*, miniature inhibitory postsynaptic current (mIPSC) amplitudes were enhanced, and the frequencies of mEPSCs in both adult and juvenile mice also increased, indicating presynaptic alterations (Echegoyen et al., 2007). Taken together, these studies provide strong evidence that neurons can sense long-term changes in their own firing rate and scale the surface expression of ionotropic glutamate receptors (iGluRs) accordingly, in the direction of maintaining homeostasis on the firing rate of the postsynaptic neurons.

### 1.6.2 My hypothesis: Astrocytes are able to sense long term changes in basal levels of neuronal activity and to exhibit long-term plasticity of their Gq GPCRs in the direction of maintaining homeostasis of neuron-to-astrocyte Gq GPCR communication.

In addition to neuron-to-neuron communication in the brain, there is now very strong evidence for neuron-to-astrocyte signaling (Porter and McCarthy, 1996; Araque et al., 2002; Wang et al., 2006; Dombeck et al., 2007; Schummers et al., 2008). While the importance of this form of signaling in the brain is under active investigation, its existence suggests that astrocytes may be able to detect long-term changes in levels of neuronal synaptic transmission and initiate long-term plasticity of their Gq GPCR expression levels accordingly. Based on the differences between synaptic vs. neuron-to-astrocyte receptor signaling, it is likely that plasticity of astrocytic mGluRs will be even more robust compared to neuronal receptor scaling when action potentials are blocked. Unlike synaptic communication in which released neurotransmitter diffuses across the narrow synaptic cleft to bind postsynaptic receptors, neuron-to-astrocyte receptor communication is by definition extrasynaptic. Neurotransmitter must spill out of the synapse in sufficient concentration to activate astrocytic receptors which may be located some distance away from the active zone. This is especially the case if the synapse in question does not have an associated astrocyte process, or is only partially ensheathed by an astrocyte process as is the case in the hippocampus and many cortical areas (Witcher et al., 2009). During blockade of neuronal synaptic transmission by TTX, the prolonged timecourse of homeostatic plasticity in neurons is thought to be due to persistence of miniature synaptic events (Sutton et al., 2004; Sutton et al., 2006). Miniature vesicular release of neurotransmitter is much less likely to stimulate astrocytic receptors. To date, stimulation of astrocytic Gq GPCRs requires trains of neuronal action potentials

(Porter and McCarthy, 1996). Astrocytes may therefore be more sensitive detectors of long-term changes in neuronal firing rates and scale their receptor expression levels more rapidly. The goal of my thesis dissertation work is to test the hypothesis that astrocytes will exhibit long-term plasticity of their mGluR signaling, in the direction of maintaining normal or expected levels of stimulation by neuronally released transmitter.

In the present study, we have used acute hippocampal slices from P12-P18 mice. CA3-CA1 action potential mediated synaptic transmission was either blocked by 1 μM TTX, or elevated by incubating brain slices in artificial cerebrospinal fluid (ACSF) containing 5.0 mM $[K^+]$. Previous work suggests that visible spontaneous and evoked $Ca^{2+}$ signals in passive hippocampal astrocytes are driven almost exclusively by Gq GPCR mediated release from internal stores (Carmignoto et al., 1998; Nett et al., 2002; Petravicz et al., 2008). Therefore, changes in expression levels of astrocytic Gq GPCRs were assayed by recording spontaneous and evoked astrocyte $Ca^{2+}$ transients.

## 1.7 References

Agulhon C, Petravicz J, McMullen AB, Sweger EJ, Minton SK, Taves SR, Casper KB, Fiacco TA, McCarthy KD (2008) What is the role of astrocyte calcium in neurophysiology? Neuron 59:932-946.

Anderson CM, Swanson RA (2000) Astrocyte glutamate transport: review of properties, regulation, and physiological functions. Glia 32:1-14.

Ango F, Prezeau L, Muller T, Tu JC, Xiao B, Worley PF, Pin JP, Bockaert J, Fagni L (2001) Agonist-independent activation of metabotropic glutamate receptors by the intracellular protein Homer. Nature 411:962-965.

Araque A, Martin ED, Perea G, Arellano JI, Buno W (2002) Synaptically released acetylcholine evokes Ca2+ elevations in astrocytes in hippocampal slices. J Neurosci 22:2443-2450.

Aronica E, Catania MV, Geurts J, Yankaya B, Troost D (2001) Immunohistochemical localization of group I and II metabotropic glutamate receptors in control and amyotrophic lateral sclerosis human spinal cord: upregulation in reactive astrocytes. Neuroscience 105:509-520.

Aronica E, van Vliet EA, Mayboroda OA, Troost D, da Silva FH, Gorter JA (2000) Upregulation of metabotropic glutamate receptor subtype mGluR3 and mGluR5 in reactive astrocytes in a rat model of mesial temporal lobe epilepsy. Eur J Neurosci 12:2333-2344.

Aronica E, Gorter JA, Jansen GH, van Veelen CW, van Rijen PC, Ramkema M, Troost D (2003) Expression and cell distribution of group I and group II metabotropic glutamate receptor subtypes in taylor-type focal cortical dysplasia. Epilepsia 44:785-795.

Barres BA (2008) The mystery and magic of glia: a perspective on their roles in health and disease. Neuron 60:430-440.

Baude A, Nusser Z, Roberts JD, Mulvihill E, McIlhinney RA, Somogyi P (1993) The metabotropic glutamate receptor (mGluR1 alpha) is concentrated at perisynaptic membrane of neuronal subpopulations as detected by immunogold reaction. Neuron 11:771-787.

Beattie EC, Stellwagen D, Morishita W, Bresnahan JC, Ha BK, Von Zastrow M, Beattie MS, Malenka RC (2002) Control of synaptic strength by glial TNFalpha. Science 295:2282-2285.

Bernardos RL, Barthel LK, Meyers JR, Raymond PA (2007) Late-Stage Neuronal Progenitors in the Retina Are Radial Müller Glia That Function as Retinal Stem Cells. The Journal of Neuroscience 27:7028-7040.

Bezzi P, Carmignoto G, Pasti L, Vesce S, Rossi D, Rizzini BL, Pozzan T, Volterra A (1998) Prostaglandins stimulate calcium-dependent glutamate release in astrocytes. Nature 391:281-285.

Bond RA, Ijzerman AP (2006) Recent developments in constitutive receptor activity and inverse agonism, and their potential for GPCR drug discovery. Trends Pharmacol Sci 27:92-96.

Bushong EA, Martone ME, Jones YZ, Ellisman MH (2002) Protoplasmic astrocytes in CA1 stratum radiatum occupy separate anatomical domains. J Neurosci 22:183-192.

Cahoy JD, Emery B, Kaushal A, Foo LC, Zamanian JL, Christopherson KS, Xing Y, Lubischer JL, Krieg PA, Krupenko SA, Thompson WJ, Barres BA (2008) A transcriptome database for astrocytes, neurons, and oligodendrocytes: a new resource for understanding brain development and function. J Neurosci 28:264-278.

Cai Z, Schools GP, Kimelberg HK (2000) Metabotropic glutamate receptors in acutely isolated hippocampal astrocytes: developmental changes of mGluR5 mRNA and functional expression. Glia 29:70-80.

Cao W, Luttrell LM, Medvedev AV, Pierce KL, Daniel KW, Dixon TM, Lefkowitz RJ, Collins S (2000) Direct binding of activated c-Src to the beta 3-adrenergic receptor is required for MAP kinase activation. J Biol Chem 275:38131-38134.

Carmignoto G, Pasti L, Pozzan T (1998) On the role of voltage-dependent calcium channels in calcium signaling of astrocytes in situ. J Neurosci 18:4637-4645.

Christopherson KS, Ullian EM, Stokes CC, Mullowney CE, Hell JW, Agah A, Lawler J, Mosher DF, Bornstein P, Barres BA (2005) Thrombospondins are astrocyte-secreted proteins that promote CNS synaptogenesis. Cell 120:421-433.

de Ligt RA, Kourounakis AP, AP IJ (2000) Inverse agonism at G protein-coupled receptors: (patho)physiological relevance and implications for drug discovery. British journal of pharmacology 130:1-12.

Doherty J, Logan MA, Taşdemir ÖE, Freeman MR (2009) Ensheathing Glia Function as Phagocytes in the Adult Drosophila Brain. The Journal of Neuroscience 29:4768-4781.

Dombeck DA, Khabbaz AN, Collman F, Adelman TL, Tank DW (2007) Imaging large-scale neural activity with cellular resolution in awake, mobile mice. Neuron 56:43-57.

Drouin-Ouellet J, Brownell AL, Saint-Pierre M, Fasano C, Emond V, Trudeau LE, Levesque D, Cicchetti F (2011) Neuroinflammation is associated with changes in glial mGluR5 expression and the development of neonatal excitotoxic lesions. Glia 59:188-199.

Duan S, Anderson CM, Keung EC, Chen Y, Chen Y, Swanson RA (2003) P2X7 receptor-mediated release of excitatory amino acids from astrocytes. J Neurosci 23:1320-1328.

Echegoyen J, Neu A, Graber KD, Soltesz I (2007) Homeostatic plasticity studied using in vivo hippocampal activity-blockade: synaptic scaling, intrinsic plasticity and age-dependence. PLoS One 2:e700.

Eroglu C, Allen NJ, Susman MW, O'Rourke NA, Park CY, Ozkan E, Chakraborty C, Mulinyawe SB, Annis DS, Huberman AD, Green EM, Lawler J, Dolmetsch R, Garcia KC, Smith SJ, Luo ZD, Rosenthal A, Mosher DF, Barres BA (2009) Gabapentin receptor alpha2delta-1 is a neuronal thrombospondin receptor responsible for excitatory CNS synaptogenesis. Cell 139:380-392.

Fellin T, Sul JY, D'Ascenzo M, Takano H, Pascual O, Haydon PG (2006) Bidirectional astrocyte-neuron communication: the many roles of glutamate and ATP. Novartis Found Symp 276:208-217; discussion 217-221, 233-207, 275-281.

Ferraguti F, Corti C, Valerio E, Mion S, Xuereb J (2001) Activated astrocytes in areas of kainate-induced neuronal injury upregulate the expression of the metabotropic glutamate receptors 2/3 and 5. Exp Brain Res 137:1-11.

Fiacco TA, McCarthy KD (2006) Astrocyte calcium elevations: properties, propagation, and effects on brain signaling. Glia 54:676-690.

Fiacco TA, Agulhon C, McCarthy KD (2008) Sorting out Astrocyte Physiology from Pharmacology. Annu Rev Pharmacol Toxicol.

Fiacco TA, Agulhon C, McCarthy KD (2009) Sorting out astrocyte physiology from pharmacology. Annu Rev Pharmacol Toxicol 49:151-174.

Fiacco TA, Agulhon C, Taves SR, Petravicz J, Casper KB, Dong X, Chen J, McCarthy KD (2007) Selective stimulation of astrocyte calcium in situ does not affect neuronal excitatory synaptic activity. Neuron 54:611-626.

Geurts JJ, Wolswijk G, Bo L, van der Valk P, Polman CH, Troost D, Aronica E (2003) Altered expression patterns of group I and II metabotropic glutamate receptors in multiple sclerosis. Brain 126:1755-1766.

Grosche J, Kettenmann H, Reichenbach A (2002) Bergmann glial cells form distinct morphological structures to interact with cerebellar neurons. J Neurosci Res 68:138-149.

Grosche J, Matyash V, Moller T, Verkhratsky A, Reichenbach A, Kettenmann H (1999) Microdomains for neuron-glia interaction: parallel fiber signaling to Bergmann glial cells. Nat Neurosci 2:139-143.

Haydon PG, Carmignoto G (2006) Astrocyte Control of Synaptic Transmission and Neurovascular Coupling. Physiological Reviews 86:1009-1031.

Henneberger C, Papouin T, Oliet SH, Rusakov DA Long-term potentiation depends on release of D-serine from astrocytes. Nature 463:232-236.

Hermans E, Challiss RA (2001) Structural, signalling and regulatory properties of the group I metabotropic glutamate receptors: prototypic family C G-protein-coupled receptors. Biochem J 359:465-484.

Heuss C, Gerber U (2000) G-protein-independent signaling by G-protein-coupled receptors. Trends Neurosci 23:469-475.

Heuss C, Scanziani M, Gahwiler BH, Gerber U (1999) G-protein-independent signaling mediated by metabotropic glutamate receptors. Nat Neurosci 2:1070-1077.

Ibata K, Sun Q, Turrigiano GG (2008a) Rapid synaptic scaling induced by changes in postsynaptic firing. Neuron 57:819-826.

Ibata K, Sun Q, Turrigiano GG (2008b) Rapid Synaptic Scaling Induced by Changes in Postsynaptic Firing. Neuron 57:819-826.

Innocenti B, Parpura V, Haydon PG (2000) Imaging extracellular waves of glutamate during calcium signaling in cultured astrocytes. J Neurosci 20:1800-1808.

Jaiswal JK, Fix M, Takano T, Nedergaard M, Simon SM (2007) Resolving vesicle fusion from lysis to monitor calcium-triggered lysosomal exocytosis in astrocytes. Proc Natl Acad Sci U S A 104:14151-14156.

Kang J, Jiang L, Goldman SA, Nedergaard M (1998) Astrocyte-mediated potentiation of inhibitory synaptic transmission. Nat Neurosci 1:683-692.

Kang J, Kang N, Lovatt D, Torres A, Zhao Z, Lin J, Nedergaard M (2008) Connexin 43 hemichannels are permeable to ATP. J Neurosci 28:4702-4711.

Kimelberg HK, Macvicar BA, Sontheimer H (2006) Anion channels in astrocytes: biophysics, pharmacology, and function. Glia 54:747-757.

Konietzko U, Muller CM (1994) Astrocytic dye coupling in rat hippocampus: topography, developmental onset, and modulation by protein kinase C. Hippocampus 4:297-306.

Lefkowitz RJ (1998) G protein-coupled receptors. III. New roles for receptor kinases and beta-arrestins in receptor signaling and desensitization. J Biol Chem 273:18677-18680.

Lembo PM, Grazzini E, Groblewski T, O'Donnell D, Roy MO, Zhang J, Hoffert C, Cao J, Schmidt R, Pelletier M, Labarre M, Gosselin M, Fortin Y, Banville D, Shen SH, Strom P, Payza K, Dray A, Walker P, Ahmad S (2002) Proenkephalin A gene products activate a new family of sensory neuron--specific GPCRs. Nat Neurosci 5:201-209.

Leslie KR, Nelson SB, Turrigiano GG (2001) Postsynaptic depolarization scales quantal amplitude in cortical pyramidal neurons. J Neurosci 21:RC170.

Li D, Ropert N, Koulakoff A, Giaume C, Oheim M (2008) Lysosomes are the major vesicular compartment undergoing Ca2+-regulated exocytosis from cortical astrocytes. J Neurosci 28:7648-7658.

Mauch DH, Nagler K, Schumacher S, Goritz C, Muller EC, Otto A, Pfrieger FW (2001) CNS synaptogenesis promoted by glia-derived cholesterol. Science 294:1354-1357.

Metea MR, Newman EA (2006) Glial cells dilate and constrict blood vessels: a mechanism of neurovascular coupling. J Neurosci 26:2862-2870.

Miller S, Sehati N, Romano C, Cotman CW (1996) Exposure of astrocytes to thrombin reduces levels of the metabotropic glutamate receptor mGluR5. Journal of neurochemistry 67:1435-1447.

Milligan G (2003) Constitutive activity and inverse agonists of G protein-coupled receptors: a current perspective. Mol Pharmacol 64:1271-1276.

Mudo G, Trovato-Salinaro A, Caniglia G, Cheng Q, Condorelli DF (2007) Cellular localization of mGluR3 and mGluR5 mRNAs in normal and injured rat brain. Brain Research 1149:1-13.

Muller CM, Best J (1989) Ocular dominance plasticity in adult cat visual cortex after transplantation of cultured astrocytes. Nature 342:427-430.

Mulligan SJ, MacVicar BA (2004) Calcium transients in astrocyte endfeet cause cerebrovascular constrictions. Nature 431:195-199.

Myme CI, Sugino K, Turrigiano GG, Nelson SB (2003) The NMDA-to-AMPA ratio at synapses onto layer 2/3 pyramidal neurons is conserved across prefrontal and visual cortices. J Neurophysiol 90:771-779.

Navarrete M, Araque A (2008) Endocannabinoids mediate neuron-astrocyte communication. Neuron 57:883-893.

Nett WJ, Oloff SH, McCarthy KD (2002) Hippocampal astrocytes in situ exhibit calcium oscillations that occur independent of neuronal activity. J Neurophysiol 87:528-537.

Newcombe J, Uddin A, Dove R, Patel B, Turski L, Nishizawa Y, Smith T (2008) Glutamate receptor expression in multiple sclerosis lesions. Brain Pathol 18:52-61.

Norenberg MD, Martinez-Hernandez A (1979) Fine structural localization of glutamine synthetase in astrocytes of rat brain. Brain Research 161:303-310.

Parri HR, Gould TM, Crunelli V (2001) Spontaneous astrocytic Ca2+ oscillations in situ drive NMDAR-mediated neuronal excitation. Nat Neurosci 4:803-812.

Pascual O, Casper KB, Kubera C, Zhang J, Revilla-Sanchez R, Sul JY, Takano H, Moss SJ, McCarthy K, Haydon PG (2005) Astrocytic purinergic signaling coordinates synaptic networks. Science 310:113-116.

Pasti L, Volterra A, Pozzan T, Carmignoto G (1997) Intracellular calcium oscillations in astrocytes: a highly plastic, bidirectional form of communication between neurons and astrocytes in situ. J Neurosci 17:7817-7830.

Perea G, Araque A (2005a) Glial calcium signaling and neuron-glia communication. Cell Calcium 38:375-382.

Perea G, Araque A (2005b) Properties of synaptically evoked astrocyte calcium signal reveal synaptic information processing by astrocytes. J Neurosci 25:2192-2203.

Petravicz J, Fiacco TA, McCarthy KD (2008) Loss of IP3 receptor-dependent Ca2+ increases in hippocampal astrocytes does not affect baseline CA1 pyramidal neuron synaptic activity. J Neurosci 28:4967-4973.

Pinto L, Götz M (2007) Radial glial cell heterogeneity--The source of diverse progeny in the CNS. Progress in Neurobiology 83:2-23.

Porter JT, McCarthy KD (1995) Adenosine receptors modulate [Ca2+]i in hippocampal astrocytes in situ. Journal of neurochemistry 65:1515-1523.

Porter JT, McCarthy KD (1996) Hippocampal astrocytes in situ respond to glutamate released from synaptic terminals. J Neurosci 16:5073-5081.

Porter JT, McCarthy KD (1997) Astrocytic neurotransmitter receptors in situ and in vivo. Prog Neurobiol 51:439-455.

Pratt KG, Watt AJ, Griffith LC, Nelson SB, Turrigiano GG (2003) Activity-Dependent Remodeling of Presynaptic Inputs by Postsynaptic Expression of Activated CaMKII. Neuron 39:269-281.

Prezeau L, Gomeza J, Ahern S, Mary S, Galvez T, Bockaert J, Pin JP (1996) Changes in the carboxyl-terminal domain of metabotropic glutamate receptor 1 by alternative splicing generate receptors with differing agonist-independent activity. Mol Pharmacol 49:422-429.

Schools GP, Kimelberg HK (1999) mGluR3 and mGluR5 are the predominant metabotropic glutamate receptor mRNAs expressed in hippocampal astrocytes acutely isolated from young rats. J Neurosci Res 58:533-543.

Schummers J, Yu H, Sur M (2008) Tuned responses of astrocytes and their influence on hemodynamic signals in the visual cortex. Science 320:1638-1643.

Shigemoto R, Nakanishi S, Mizuno N (1992) Distribution of the mRNA for a metabotropic glutamate receptor (mGluR1) in the central nervous system: An in situ hybridization study in adult and developing rat. The Journal of Comparative Neurology 322:121-135.

Simard M, Arcuino G, Takano T, Liu QS, Nedergaard M (2003) Signaling at the gliovascular interface. J Neurosci 23:9254-9262.

Stevens B, Allen NJ, Vazquez LE, Howell GR, Christopherson KS, Nouri N, Micheva KD, Mehalow AK, Huberman AD, Stafford B, Sher A, Litke AM, Lambris JD, Smith SJ, John SW, Barres BA (2007) The classical complement cascade mediates CNS synapse elimination. Cell 131:1164-1178.

Stout CE, Costantin JL, Naus CC, Charles AC (2002) Intercellular calcium signaling in astrocytes via ATP release through connexin hemichannels. J Biol Chem 277:10482-10488.

Sutton MA, Wall NR, Aakalu GN, Schuman EM (2004) Regulation of dendritic protein synthesis by miniature synaptic events. Science 304:1979-1983.

Sutton MA, Ito HT, Cressy P, Kempf C, Woo JC, Schuman EM (2006) Miniature neurotransmission stabilizes synaptic function via tonic suppression of local dendritic protein synthesis. Cell 125:785-799.

Sweger EJ, Casper KB, Scearce-Levie K, Conklin BR, McCarthy KD (2007) Development of hydrocephalus in mice expressing the G(i)-coupled GPCR Ro1 RASSL receptor in astrocytes. J Neurosci 27:2309-2317.

Takano T, Tian GF, Peng W, Lou N, Libionka W, Han X, Nedergaard M (2006) Astrocyte-mediated control of cerebral blood flow. Nat Neurosci 9:260-267.

Tang F-R, Lee W-L, Yeo TT (2002) Expression of the group I metabotropic glutamate receptor in the hippocampus of patients with mesial temporal lobe epilepsy. Journal of Neurocytology 30:403-411-411.

Tran MD, Neary JT (2006) Purinergic signaling induces thrombospondin-1 expression in astrocytes. Proceedings of the National Academy of Sciences 103:9321-9326.

Tseng KY, Chambers RA, Lipska BK (2009) The neonatal ventral hippocampal lesion as a heuristic neurodevelopmental model of schizophrenia. Behav Brain Res 204:295-305.

Turrigiano G, Abbott LF, Marder E (1994) Activity-dependent changes in the intrinsic properties of cultured neurons. Science 264:974-977.

Turrigiano GG, Leslie KR, Desai NS, Rutherford LC, Nelson SB (1998) Activity-dependent scaling of quantal amplitude in neocortical neurons. Nature 391:892-896.

Ulas J, Satou T, Ivins KJ, Kesslak JP, Cotman CW, Balazs R (2000) Expression of metabotropic glutamate receptor 5 is increased in astrocytes after kainate-induced epileptic seizures. Glia 30:352-361.

Ullian EM, Christopherson KS, Barres BA (2004) Role for glia in synaptogenesis. Glia 47:209-216.

Ullian EM, Sapperstein SK, Christopherson KS, Barres BA (2001) Control of synapse number by glia. Science 291:657-661.

Van den Pol AN (1994) Metabotropic glutamate receptor mGluR1 distribution and ultrastructural localization in hypothalamus. J Comp Neurol 349:615-632.

van den Pol AN, Romano C, Ghosh P (1995) Metabotropic glutamate receptor mGluR5 subcellular distribution and developmental expression in hypothalamus. J Comp Neurol 362:134-150.

Ventura R, Harris KM (1999) Three-dimensional relationships between hippocampal synapses and astrocytes. J Neurosci 19:6897-6906.

Wang X, Lou N, Xu Q, Tian GF, Peng WG, Han X, Kang J, Takano T, Nedergaard M (2006) Astrocytic Ca2+ signaling evoked by sensory stimulation in vivo. Nat Neurosci 9:816-823.

Watt AJ, van Rossum MC, MacLeod KM, Nelson SB, Turrigiano GG (2000) Activity coregulates quantal AMPA and NMDA currents at neocortical synapses. Neuron 26:659-670.

Wierenga CJ, Ibata K, Turrigiano GG (2005) Postsynaptic expression of homeostatic plasticity at neocortical synapses. J Neurosci 25:2895-2905.

Witcher MR, Park YD, Lee MR, Sharma S, Harris KM, Kirov SA (2009) Three-dimensional relationships between perisynaptic astroglia and human hippocampal synapses. Glia.

Yang Y, Ge W, Chen Y, Zhang Z, Shen W, Wu C, Poo M, Duan S (2003) Contribution of astrocytes to hippocampal long-term potentiation through release of D-serine. Proc Natl Acad Sci U S A 100:15194-15199.

Ye ZC, Wyeth MS, Baltan-Tekkok S, Ransom BR (2003) Functional hemichannels in astrocytes: a novel mechanism of glutamate release. J Neurosci 23:3588-3596.

Zhang Z, Chen G, Zhou W, Song A, Xu T, Luo Q, Wang W, Gu X-s, Duan S (2007) Regulated ATP release from astrocytes through lysosome exocytosis. Nat Cell Biol 9:945-953.

Zonta M, Angulo MC, Gobbo S, Rosengarten B, Hossmann KA, Pozzan T, Carmignoto G (2003) Neuron-to-astrocyte signaling is central to the dynamic control of brain microcirculation. Nat Neurosci 6:43-50.

Zur Nieden R, Deitmer JW (2006) The role of metabotropic glutamate receptors for the generation of calcium oscillations in rat hippocampal astrocytes in situ. Cereb Cortex 16:676-687.

## Chapter 2: Increased astrocytic Gq GPCR signaling following 4 to 6 hour TTX-blockade of CA3-CA1 synaptic transmission

### 2.1 Abstract

In addition to synaptic communication between neurons, there is now strong evidence for neuron-to-astrocyte receptor signaling in the brain. During trains of action potentials or repetitive stimulation, neurotransmitter spills out of the synapse to activate astrocytic Gq GPCRs. To date, very little is known about the ability of astrocytic receptors to exhibit plasticity as a result of long-term changes in neuronal firing rates. Here we describe for the first time long-term plasticity of astrocytic group I mGluR signaling in acute mouse hippocampal slices on a rapid timescale following long-term blockade of neuronal synaptic transmission. Plasticity of astrocytic mGluRs was observed as: 1) an elevated percentage of astrocytes exhibiting spontaneous $Ca^{2+}$ transients in their soma and processes; 2) an elevated percentage of astrocytes responding to group I mGluR agonist; 3) faster rise times of spontaneous and evoked astrocyte $Ca^{2+}$ elevations in both astrocytic soma as well as fine processes; 4) a reduced latency of evoked astrocyte $Ca^{2+}$ elevations to group I mGluR agonist application in astrocytic processes; and 5) a significant shift in the pattern of the $Ca^{2+}$ responses to group I mGluR agonist, after 4 to 6 hours of TTX treatment. This study demonstrates that astrocytes actively detect blockade of neuronal action potentials by increasing their expression levels of group I mGluRs.

## 2.2 Introduction

Hippocampal astrocytes expresses numbers of the metabotropic receptors for known neurotransmitters and their activation is shown to be related to the local neuronal activities (Porter and McCarthy, 1995, 1996; Pasti et al., 1997; Kang et al., 1998; Araque et al., 2002; Perea and Araque, 2005; Wang et al., 2006; Navarrete and Araque, 2008). Approximately 50% of synapses in hippocampus are associated with astrocytic processes, and larger synapses are more likely to be ensheathed by perisynaptic astrocytes (Kirov et al., 1999; Bushong et al., 2002). It has been estimated that, in adult rat CA1, there are about 213 synapses per 100 $\mu m^3$ and a single astrocyte on average occupies about 66,000 $\mu m^3$ (Kirov et al., 1999; Bushong et al., 2002). Therefore, a single astrocyte occupies a volume corresponding to about 140,000 synapses (Bushong et al., 2002). Astrocytic mGluRs are extrasynaptic and their activation requires that neurotransmitters spill out of synapses in a sufficient concentration (Eroglu and Barres, 2010). Individual quanta of neurotransmitter from miniature release might not be sufficient to stimulate astrocytic mGluRs.

In pathological conditions, astrocytes up-regulate their metabotropic receptor expression and the level of metabotropic receptor mRNAs in response to large scale of the neuronal loss and in turn lack of the neurotransmitter release, although, the upregulation of receptor expression on astrocytes are usually associated with reactive astrocyte phenotypes in those conditions release (Aronica et al., 2000; Ulas et al., 2000; Ferraguti et al., 2001; Tseng et al., 2009; Drouin-Ouellet et al., 2011). It is unclear

whether astrocytic metabotropic receptor exhibit long-term plasticity in response to changes in basal level of neuronal activities without pro-inflammatory stimuli. Previous studies have shown that the prolonged timecourse of homeostatic plasticity of ionotropic glutamate receptors in postsynaptic neurons following long-term blockade of neuronal action potentials in TTX was largely due to the persistence of miniature synaptic events (Sutton et al., 2004; Sutton et al., 2006). Based on the extrasynaptic location of astrocytic mGluRs, astrocytes might be more sensitive detectors of long-term changes in neuronal firing rates and scale their receptor expression levels more rapidly.

Several pharmacological studies *in vitro* in the early- to mid-1990s examined the relationship between changes in Gq GPCR expression levels and effects on spontaneous and agonist evoked Gq GPCR $Ca^{2+}$ transients. Increased expression of functional mGluR1 in porcine kidney epithelial (LLC-PK1) or the human embryonic kidney (HEK 293) cells led to an increase in the percentage of cells in a population exhibiting spontaneous Gq GPCR activity, resulting from more coupling efficiency to G proteins (Prezeau et al., 1996). This type of spontaneous activity is agonist-independent (de Ligt et al., 2000). It is due to the constitutive activity of Gq GPCRs, which facilitates GTP/GDP exchange and activation of G-proteins in the absence of the agonist (Hermans and Challiss, 2001). Increased surface expression levels of Gq GPCRs also led to increases in the percentage of cells within a population exhibiting evoked responses to the agonist (Shao and McCarthy, 1993; Wang and Thompson, 1994), and in single cells, reduced response latencies to the agonist (Shao and McCarthy, 1993; Wang and Thompson, 1994; Ostasov et al., 2008). In the present study, functional astrocytic mGluR expression levels

were evaluated by monitoring spontaneous and evoked $Ca^{2+}$ transients following 4 to 6 hour incubation of hippocampal slices in TTX to block neuronal action potentials.

In the first part of the study, we tested whether hippocampal s.r. astrocytes exhibit scaling effects of their mGluRs signaling following decreased CA3-CA1 neuronal synaptic transmission. Specifically, we are interested in studying the potential scaling effect following changes in neuronal synaptic transmission within the physiological range. We hypothesized that mGluR mediated signaling in hippocampal s.r. astrocytes would increase in response to decreased CA3-CA1 neuronal synaptic transmission in 4 to 6 hours. Acute hippocampal slices were incubated in ACSF containing 1 μM of the $Na^{+}$ channel blocker tetrodotoxin (TTX) for 4 to 6 hours to block the neuronal synaptic transmission. We discovered that incubation of slices in TTX resulted in a significant increase in the percentage of s.r. astrocytes exhibiting spontaneous $Ca^{2+}$ activity, a significant increase in the probability of responding to group I mGluR agonist 3,4-Dihydroxyphenylglycol (DHPG), a highly significant decrease in evoked mGluR response rise times in both astrocyte somas and fine processes, and a significant decrease in evoked mGluR response latency. These changes suggest that astrocytes scale up their mGluR signaling following blockade of neuronal synaptic transmission.

## 2.3 Material and methods

### *Preparation of acute hippocampal slices.*

All mice were housed in the animal facility at the University of California, Riverside in accordance with Institutional Animal Care and Use Committee guidelines.

12- to 18-day-old C57BL/6J (Jackson Laboratory, Bar Harbor, ME) mice were anaesthetized using isoflurane and decapitated. Parasagittal hippocampal slices were prepared using a Leica VT1200s Vibratome (Bannockburn, IL). Slices were prepared in ice-cold, nominally $Ca^{2+}$-free saline containing (in mM): 125 NaCl, 3.5 KCl, 3.8 $MgCl_2$, 1.25 $NaH_2PO_4$, 26.0 $NaHCO_3$, 15 glucose, and 1.3 ascorbic acid, bubbled with 5% $CO_2$-95% $O_2$. Subsequently, slices were incubated for 45 minutes at 35°C in oxygenated ACSF containing (in mM): 125 NaCl, 3.5 KCl, 2.5 $CaCl_2$, 1.3 $MgCl_2$, 1.25 $NaH_2PO_4$, 26.0 $NaHCO_3$, 15 glucose, and 0.1 Trolox, bubbled with 5% $CO_2$-95% $O_2$. After recovery from the dissection, it has been estimated that more than 40% of the synapses are still associated with astrocyte processes (Witcher et al., 2007). Slices were then incubated 4 to 6 hours at room temperature either in standard ACSF (3.5 mM $[K^+]_o$ ACSF, control) or in standard ACSF + 1 μM TTX. Acute slices were chosen to study the scaling effect of astrocytic mGluRs because the majority of the neuronal network and neuron-to-astrocyte communication remains intact in acute slices. To block the neuronal synaptic transmission, acute hippocampal slices were incubated in ACSF containing 1 μM of the $Na^+$ channel blocker TTX for 4 to 6 hours. The same concentration of TTX blockade in primary neuronal culture led to homeostatic plasticity of postsynaptic neurons, where the expression of AMPA and NMDA receptors scaled upward in a compensatory manner in order to recover expected levels of excitatory postsynaptic activation (Watt et al., 2000; Perez-Otano and Ehlers, 2005; Wierenga et al., 2005; Ibata et al., 2008). Following the incubation period individual slices were transferred to a recording chamber and

continuously superfused with oxygenated, room temperature 3.5 mM $[K^+]_o$ ACSF + 1 µM TTX in order to isolate direct astrocyte responses to the agonist.

***CA3 neuron patch clamp and whole cell recording of spontaneous neuronal firing rates.***

Pipettes were pulled from borosilicate glass on a P-97 Flaming/Brown type horizontal micropipette puller and not fire-polished. Neuronal pipettes had resistances of 4.6–6 MΩ when filled with a solution containing the following (in mM): 145 K-gluconate, 2 $MgCl_2$, 10 HEPES, 4 Mg-ATP, 14 phosphocreatine, and 0.2 Na-GTP, pH 7.3 with KOH. Slices were constantly perfused with oxygenated room-temp ACSF with either 2.5 mM or 3.5 mM $[K^+]_o$. Whole-cell patch-clamp recording of neurons was performed using a Multiclamp 700B amplifier and PCLAMP 10.2.014 software (Axon Instruments, Union City, CA). CA3 neurons on average displayed a resting $V_m$ of ~62 mV in 2.5 mM $[K^+]_o$ ACSF and ~61 mV in 3.5 mM $[K^+]_o$ ACSF. Upon attaining the whole-cell configuration, the cell membrane potential, input resistance, and access resistance were recorded and continuously monitored during gap free recording of membrane potential. Change in any of these parameters by 20% or more was used as criteria to reject the data from further analysis. The number of spontaneous action potentials from each recording was analyzed in PCLAMP 10.2.014 software.

***Bulk-loading and bolus-loading of astrocytes with $Ca^{2+}$ indicator.***

For standard bulk-loading experiments, 10 μM Calcium Green-1 AM and 0.076% pluronic acid in dimethyl sulfoxide (DMSO, final concentration: 0.48%) were included in the ACSF during the first 45 minute incubation period. The Calcium Green-1 AM was primarily sequestered by astrocytes as observed previously for cell permeable indicators in slices from rats (Porter and McCarthy, 1996) and mice (Nett et al., 2002). For bolus-loading experiments, 1 μM sulforhodamine 101 (SR-101) was used in place of Calcium Green-1 AM during the first 45 minute incubation period to label astrocytes. A field of astrocytes in stratum radiatum was then loaded with Oregon Green BAPTA-1 (OGB-1) AM $Ca^{2+}$ indicator dye using a backpressure, bolus-loading technique (Nimmerjahn et al., 2004; Sullivan et al., 2005; Garaschuk et al., 2006).

***Astrocyte patch clamp and loading with $Ca^{2+}$ indicator.***

Pipettes were pulled from borosilicate glass on a Narishige (Tokyo, Japan) PP-10 two-stage vertical pipette puller and not fire-polished. Pipettes were filled with the following internal solution (in mM): 130 K-gluconate, 4 $MgCl_2$, 10 HEPES, 10 glucose, 1.185 Mg-ATP, 10.55 phosphocreatine, and 0.1315 mg/ml creatine phosphokinase, pH 7.3 by KOH, resistance 7-8mΩ. Also included was 200 μM of the cell-impermeant version of the $Ca^{2+}$-indicator dye Oregon green BAPTA-1 (OGB-1) (Invitrogen). In some experiments, 200 μM Alexa Fluor 488 hydrazide dye (Invitrogen) was included to image cell morphology.

Whole-cell patch-clamp recording of astrocytes performed at room temperature using a Multiclamp 700B amplifier and PCLAMP 10.2.014 software (Axon Instruments, Union City, CA). Astrocytes were patch clamped using small pipette tips for < 3 minutes as described previously (Fiacco and McCarthy, 2004) in order to limit dialysis of intracellular contents into the pipette. Astrocytes displayed a resting $V_m$ of ~80 mV in 2.5 mM $[K^+]_o$ ACSF with input resistances of < 10 MΩ, and ~75mV in 3.5 mM $[K^+]_o$ ACSF. They exhibited passive currents when the membrane was stepped from -180 mV to +80 mV in 20 mV increments. A test pulse of -5 mV was included after each voltage step in order to monitor changes in access resistance. Astrocyte current signals were low-pass filtered at 2 kHz and digitized at 100 kHz via a Digidata 1440 (Axon Instruments). A smooth, stable off-cell and formation of an outside-out patch was a strong indicator of minimal damage to the cell membrane during the patch clamp procedure.

***Confocal imaging and monitoring of astrocyte $Ca^{2+}$ activity.***

The stratum radiatum of CA1 was visualized using an Olympus BX61WI upright microscope equipped with water-immersion objectives and differential interference contrast (DIC) optics. Individual astrocytes in CA1 stratum radiatum were identified first by their location, size, and morphology. Additionally, in bulk-loaded slices astrocytes were further identified by their sequestering of $Ca^{2+}$ indicator and characteristic long-duration $Ca^{2+}$ responses. In bolus-loading experiments, overlay of the SR-101 and OGB-1 signals was used to identify bolus-loaded cells as astrocytes (Nimmerjahn et al., 2004).

In patch-clamp experiments, classification of cells as astrocytes was verified by their electrophysiological properties (Fiacco and McCarthy, 2004).

After loading with the calcium indicator, the fluorescence intensity of calcium indicator dye over time was recorded in astrocytes on a fixed focal plane. All experiments, including recordings in both control and TTX incubated slices, were performed in 1 μM TTX to eliminate the possibility of short-term TTX effects on astrocyte $Ca^{2+}$ activity. All recordings were completed within 40 minutes to reduce the possible TTX scaling effect on control slices and to limit any possible effects produced by phototoxicity. Only a single (field of) astrocyte(s) was recorded per slice to eliminate the possibility of double-sampling or changes due to multiple agonist applications. Astrocytes exhibiting at least one spontaneous $Ca^{2+}$ elevation were counted as spontaneously active cells. For patch clamping experiments, all recordings were done using 0.5% laser power to limit the potential of photosensitivity induced spontaneous $Ca^{2+}$ oscillations (see laser control experiment below) (Wang et al., 2006). The viability of astrocyte(s) in each recording was verified by bath application of an agonist cocktail (10 μM ea. of histamine, carbachol, and Na-ATP to stimulate astrocytic histamine H1 receptor [H1R], muscarinic acetylcholine receptor [mAchR], and purinergic receptor [P2YR], respectively). Astrocytes that did not respond to the agonist cocktail application were presumed dead and therefore excluded from further analysis. During astrocyte recordings, solutions were switched using an electronic valve controller (Warner Instrument, Hamden CT).

***Analysis of astrocyte Gq GPCR $Ca^{2+}$ activity and Statistics.***

Slices or single astrocytes from bolus loading and patch clamp experiments were given a numeric code and analyzed blindly. For all experiments, square-shaped regions of interest (ROIs) of a fixed size (12.3 $\mu m^2$) were placed over the cell soma and visible cellular compartments using Olympus Fluoview 1000 software. Increases in average fluorescence intensity normalized to baseline fluorescence ($\Delta F/F_0$) within each ROI were used to represent increases in $Ca^{2+}$ concentration (Takahashi et al., 1999). Such increases in $\Delta F/F_0$ values were scored as $Ca^{2+}$ elevations if the peak amplitude was greater than two standard deviations above the mean of baseline fluorescence for at least two sample points. For patch clamp experiments, within each astrocyte, microdomains were identified as compartments of astrocyte processes that exhibited spontaneous $Ca^{2+}$ elevations independently from other parts of the cell. Then in each microdomain, the ROI that corresponded to the "initiation site" of the spontaneous $Ca^{2+}$ transient was identified based on the earliest onset among all ROIs in the same microdomain, and was later used to represent this microdomain for further analysis. Spontaneous $Ca^{2+}$ transients covering $\geq$ 75% of the planar area of the astrocyte were defined as "whole cell" $Ca^{2+}$ elevations and analyzed separately.

The amplitude, frequency, and kinetics of spontaneous Gq GPCR signaling events and agonist-evoked mGluR responses were determined for each microdomain. The average baseline fluorescence intensity was calculated by averaging 30 seconds of stable baseline immediately preceding each $Ca^{2+}$ elevation. The onset of each $Ca^{2+}$ elevation

was defined as the last data point before the fluorescence intensity went one standard deviation above the mean, and the peak of the $Ca^{2+}$ elevation was defined as the first peak fluorescence intensity (in cases of "multipeak" responses the first peak was used). Rise time was defined as the difference between the response onset and the time corresponding to the peak amplitude (0% to 100%). For the agonist evoked responses, latency was calculated as the time between initiation of agonist perfusion to the peak of the response. Analysis of rise time was chosen in addition to response latency out of concern that long wash-in times of agonists in hippocampal slices vs. cultured cells would obscure potential significant differences in response latency.

For agonist evoked $Ca^{2+}$ responses, the specific response patterns were grouped into 3 categories: "single peak", "multipeak", or "plateau". Single peak responses were defined as a response with only one data point within ±10% the peak value. Plateau responses maintained the peak amplitude for at least 3.6 seconds, and usually for much longer. Therefore, the duration of single peak responses was much shorter compared to plateau $Ca^{2+}$ responses. Multi-peak responses were defined as a minimum of at least 2 single peaks in rapid succession, with $\leq$ 10.8 second gap between each single peak. Multipeak responses were defined only when the fluorescence intensity fell below 50% amplitude after the first peak prior to rising again for secondary peaks. If the second peak occurred before the first peak decayed by at least 50%, this event was defined as plateau response. Cells or microdomains that did not produce $Ca^{2+}$ elevations to group I mGluR agonist were grouped as non-responders (NR) as long as these cells were deemed viable

based on respondes to agonist cocktail. Analysis of agonist-evoked response duration and area was performed only for plateau responses for both control and treatment groups.

Analysis was done using number of astrocytes as 'n' for bulk-loading and bolus loading experiments, and number of microdomains for patch-clamp experiments. Student's independent *t*-test was used for statistical comparison of means between the control and treated groups. Pearson's chi-square test was used for comparison of the $Ca^{2+}$ activity patterns between control and treatment groups. Fisher's exact 2-tail test was used for comparison of the frequency of specific $Ca^{2+}$ activity patterns between control and treatment groups. Significance is described at the 0.05, 0.01, or 0.001 levels.

## 2.4 Results

### 2.4.1 3.5 mM extracellular potassium concentration was used as the preferred $[K^+]_o$ in the control condition based on firing rates of CA3 pyramidal neurons.

To investigate whether hippocampal astrocytic mGluRs exhibit long-term plasticity, hippocampal slices from P12-P18 mice were incubated in either 3.5 mM $[K^+]_o$ ACSF, or 3.5 mM $[K^+]_o$ ACSF containing 1 μM TTX. In previous studies on hippocampus slices, $[K^+]_o$ in ACSF typically varies between 2 mM to 5.0 mM. Historically we have been using ACSF containing 2.5 mM $[K^+]_o$. At this $[K^+]_o$, CA3 neurons on average rested at -61.7 ± 1.6 mV (n = 12; figure 2.1 B) and only very rarely fired spontaneous action potentials (0.00016 ± 8.9 E-05 Hz; n = 12; figure 2.1 A and D). In general, CA3 neurons were more hyperpolarized at the end of the 15 minute whole-

cell recording compared to the start of the recording (Vm = -64.1 ± 2.1 mV at the end of 15 minutes recording) (n = 12; figure 2.1 C). In 3.5 mM $[K^+]_o$ ACSF, CA3 neurons on average rested at -60.4 ± 1.6 mV, and slowly hyperpolarized during whole-cell recording (Vm = -63.9 ± 1.9 mV at the end of the 15 minutes recording) (n = 8; figure 2.1 B and C). On average, the membrane potential of CA3 neurons was not significantly different between neurons incubated in 2.5 mM $[K^+]_o$ vs. 3.5 mM $[K^+]_o$ ACSF. The frequency of the spontaneous action potentials of CA3 neurons was increased to 0.02 ± 0.0088 Hz (n = 8; figure 2.1 D) in 3.5 mM $[K^+]_o$. This frequency is much higher than neurons in 2.5 mM $[K^+]_o$ but was not significantly different (p = 0.054), probably due to the large variability among individual recordings (figure 2.1 E). Because of the much higher CA3 neuron basal firing frequency observed in 3.5 compared to 2.5 mM $[K^+]_o$, 3.5 mM $[K^+]_o$ was chosen as the control condition from which to determine the effects of TTX blockade of neuronal firing on astrocytic mGluR activity.

### 2.4.2 Long-term blockade of CA3-CA1 synaptic transmission leads to increased mGluR signaling in the soma of s.r. astrocytes bulk-loaded with $Ca^{2+}$ Green 1-AM

As an initial experiment to determine if astrocytes adjust their expression levels of Gq GPCRs after long-term changes in neuronal firing rates, hippocampal slices were incubated in 3.5 mM $[K^+]_o$ ACSF with 1 μM TTX for 4-6 hours. After incubation, astrocytic Gq GPCR activity was recorded in the soma of s.r. astrocytes in acute mouse hippocampal slices bulk-loaded with the $Ca^{2+}$ indicator dye Calcium Green-1 AM (Porter and McCarthy, 1996). The advantage of this approach is that spontaneous and evoked Gq

GPCR activity can be recorded from a large population of astrocytes, but at the expense of being able to record from small astrocytic compartments. After 45 minutes of incubation, s.r. astrocytes near the surface of the slice were loaded with indicator dye as shown in figure 2.2 A (Nett et al., 2002). The identity of s.r astrocytes was confirmed by their location, size, morphology, and characteristic long-duration $Ca^{2+}$ responses.

There was no difference in the distribution or basal fluorescence intensity of the astrocytes in TTX treated vs. control slices (figure 2.2 A). Regions of interest were placed on the soma of s.r. astrocytes and spontaneous somatic $Ca^{2+}$ activity monitored for 15 minutes (figure 2.2 B). The spontaneous $Ca^{2+}$ transients were observed in the soma of s.r. astrocytes (figure 2.2 B, indicated by orange ellipse). Previous studies have found that a primary target of neuron-to-astrocyte receptor communication is astrocytic group I mGluRs (Honsek et al., 2010; Porter and McCarthy, 1996; Wang et al., 2006). Therefore, after the 15 minutes baseline recording of spontaneous $Ca^{2+}$ activity, slices were perfused with 50 µM of the group I mGluR agonist DHPG to evoke group I mGluR-mediated astrocyte $Ca^{2+}$ elevations (figure 2.2 B). Astrocytes responded to 50 µM DHPG with mainly two responding patterns: multi-peak or plateau like pattern (figure 2.2 B, indicated by orange rectangles with dashed and solid outline, respectively). Very low percentage of the s.r. astrocytes responded to 50 µM DHPG with a single peak of $Ca^{2+}$ elevation, with the shape as the first peak of the multi-peak response (figure 2.4 E).

No significant differences were found between control and TTX incubated slices in the amplitude or frequency of the spontaneous astrocytic $Ca^{2+}$ elevations (control: n =

215 cells from 15 slices; TTX: n = 218 cells from 16 slices; figure 2.3 A and B). TTX incubated slices tended to have a higher percentage of spontaneously active cells (13.7% ± 3.8%) compared to control slices (7.8% ± 2.7%) ($p = 0.20$, figure 2.3 C). Also, a greater percentage of astrocytes responded to 50 µM DHPG with $Ca^{2+}$ elevations in TTX vs. control incubated slices (83.2% vs. 75.7%) (figure 2.3 D).

Consistent with the spontaneous Gq GPCR activity, there was no change in either the amplitude or duration of the DHPG-evoked group I mGluR responses in TTX treated slices compared to slices incubated in 3.5 mM $[K^+]_o$ ACSF (figure 2.4 A and B). However, a highly significant reduction in the rise time of the evoked responses was found after incubating slices in TTX ($p < 0.001$; figure 2.4 C and D). These results fit with previous reports indicating that a primary effect of changes in expression levels of Gq GPCRs were changes in $Ca^{2+}$ response latency, but not changes in response amplitudes (Shao and McCarthy, 1993; Wang and Thompson, 1994; Shao and McCarthy, 1995; Ostasov et al., 2008).

Examination of earlier work also revealed a dose-dependent effect of group I mGluR agonist concentration on the pattern of the $Ca^{2+}$ response, with lower concentrations leading to single-peak or oscillating responses while higher concentrations produced long-lasting plateau responses (Hu et al., 1999; Shelton and McCarthy, 2000; Hermans and Challiss, 2001). This may be a characteristic common to all Gq GPCRs, as we have observed the same effect in a transgenic Gq GPCR targeted to astrocytes (see chapter 4). The stepwise dose-response effect of increasing agonist concentration is

presumably the effect of stimulating a greater number of existing receptors because the probability of agonist-receptor binding will increase at higher agonist concentrations. Therefore, we reasoned that the response pattern will shift at a fixed concentration of agonist if the expression level of the receptors increases.

In TTX-treated slices, a significantly higher percentage of astrocytes elicited plateau-like DHPG responses compared to controls ($p < 0.001$), while a significantly greater percentage of astrocytes from control slices showed multi-peak responses ($p < 0.001$, figure 2.4 E). Interestingly, the area underneath the $Ca^{2+}$ responses between control and TTX incubated astrocytes was unchanged (only plateau-like responses were included in this analysis) (figure 2.4 F). These data suggest that upon group I mGluR activation, the changes in the concentration of $Ca^{2+}$ in astrocytes remains unchanged after TTX treatment. Taken together, these results provide an initial indication that astrocytic receptors, including group I mGluRs, increase their expression levels after long-term blockade of neuron-to-astrocyte receptor signaling.

### 2.4.3 Initial observations replicated using bolus-loading delivery of OGB-1 $Ca^{2+}$ indicator dye

While the initial data supported our hypothesis, we had some concern about standard bulk-loading procedures to load astrocytes with $Ca^{2+}$ indicator. Astrocytes that take up the $Ca^{2+}$ indicator tend to be within the first 0 μm to 30 μm of the slice surface, where astrocytes and their associations with synapses and cerebrovasculature may be compromised during slice preparation. Therefore, communication between neurons and

astrocytes might not be well maintained, potentially diminishing the ability of astrocytic receptors to sense changes in neuronal firing rates. To address this concern we loaded a field of s.r. astrocytes with OGB-1 AM $Ca^{2+}$ indicator dye using a backpressure, bolus-loading technique (Nimmerjahn et al., 2004; Sullivan et al., 2005; Garaschuk et al., 2006). This technique allows for improved resolution and signal-to-noise in deeper, healthier tissue compared to conventional bulk-loading protocols, while also facilitating recording of astrocytic Gq GPCR activity in both the soma as well as their larger processes. Overlay of the SR-101 and OGB-1 AM signals was used to identify bolus-loaded cells as astrocytes (figure 2.5 A). In general, TTX-treated hippocampal slices displayed more spontaneously active cells (figure 2.5 B, indicated by orange ellipse) and responded to DHPG more readily compared to astrocytes in control slices (figure 2.5 B, orange rectangle with double solid outline, solid outline, and dashed outline indicate agonist-evoked single-peak multi-peak, and plateau-like $Ca^{2+}$ elevation observed in astrocytes, respectively). These data were overall similar to the findings using the bulk-loading approach. Responses to Gq GPCR agonist cocktail consisting of 10 µM each of histamine, carbachol, and ATP, however, were the same as in control hippocampal slices, suggesting that changes in astrocyte $Ca^{2+}$ signaling are mainly due to changes in group I mGluRs.

In bolus-loaded hippocampal slices, the percentage of spontaneously active astrocytes was higher than that in bulk-loaded slices in both control slices ($p < 0.01$; bolus-loaded: 12.9% ± 5.1%; n = 40 cells/8 slices; bulk-loaded: 7.8% ± 2.7%; n = 215 cells/15 slices), and TTX treated slices ($p < 0.05$; bolus loaded: 42.1% ± 10.1%; n = 30

cells/7 slices; bulk-loaded: 13.7% ± 3.8%; n = 218 cells/16 slices) (figure 2.6 A). The percentage increase of spontaneously active astrocytes deeper in the slice suggests more intact connections among astrocyte processes and neuronal synapses exist, thereby facilitating observation of the scaling effect of long-term blockade of neuronal action potentials on astrocytic mGluRs. Analysis showed that the percentage of s.r. astrocytes exhibiting spontaneous $Ca^{2+}$ transients in both the soma and main processes was significantly higher in the TTX-treated slices compared to controls (figure 2.6 B, $p < 0.05$ in both cases; control: 12.9% ± 5.1%; n = 40 cells/8 slices; TTX: 42.1% ± 10.1%; n = 30 cells/7 slices). Within the whole population, only 10.0% of CA1 s.r. astrocytes incubated with 3.5 mM $[K^+]_o$ ACSF exhibited at least one spontaneous $Ca^{2+}$ transient in their soma, while a significant higher percentage of TTX-treated astrocytes (43.3%) exhibited somatic $Ca^{2+}$ transients ($p < 0.001$, figure 2.6 C). The main processes of astrocytes also exhibited spontaneous $Ca^{2+}$ transients that were separated from those of the cell soma. However, only 10.0% of CA1 s.r. astrocytes incubated in 3.5 mM $[K^+]_o$ ACSF exhibited spontaneous $Ca^{2+}$ transients in main processes, while 30.0% of TTX-treated astrocytes exhibited spontaneous activity in processes ($p < 0.05$, figure 2.6 C). In contrast to a previous study (Kang et al.). SR-101 alone did not seem to have a significant effect on spontaneous astrocytic Gq GPCR activity (frequency of spontaneous somatic $Ca^{2+}$ transients with SR-101: 0.0038 ± 0.0003 Hz, n = 32 cells; without SR-101: 0.0050 ± 0.0016 Hz, n = 7 cells).

No changes in the frequency of the spontaneous $Ca^{2+}$ activity either at the somatic level (figure 2.6 D) or in processes (figure 2.6 E) were observed. The frequency of

spontaneous $Ca^{2+}$ transients observed in main processes is dependent on the area of the astrocytes can be imaged. Thus, the frequency of spontaneous $Ca^{2+}$ transients in main processes has been normalized to the area of astrocytes before compared between the two groups. Consistent with observations in standard bulk-loaded astrocytes, the rise time of the spontaneous $Ca^{2+}$ transients for TTX-treated astrocytes was significantly faster compared to those of the control group (figure 2.6 F and G, $p < 0.01$).

As observed in astrocytes bulk-loaded with $Ca^{2+}$ indicator, rise times of DHPG evoked responses were significantly faster in TTX-treated vs. control astrocytes (control: n = 32 cells; TTX: n = 27 cells; figure 2.7 A; $p < 0.001$), while the amplitude and the half-width of the evoked responses remained consistent between the two groups (figure 2.7 B, control: n = 32 cells; TTX: n = 27 cells; and figure 2.7 C, control: n = 7 cells; TTX: n = 13 cells). There was no difference in the latency of DHPG evoked responses for the TTX-treated vs. control astrocytes (figure 2.7 D, control: n = 32 cells; TTX: n = 27 cells; $p = 0.13$). Several previous studies (Shao and McCarthy, 1993; Wang and Thompson, 1994; Shao and McCarthy, 1995; Ostasov et al., 2008) suggested that increased surface expression of Gq GPCRs in cultured cells led to a shorter latency of the agonist evoked response. In acute slice preparations, it takes tens of seconds for agonist to reach its working concentration in the perfusion chamber, and for a sufficient concentration of agonist to penetrate the slices and reach the cell surface. Both of these factors presumably prolonged the latency up to 60 to 70 seconds after agonist application. Therefore, we did not observe a significant difference in latency of DHPG evoked responses between TTX-treated and control astrocytes.

At the end of each experiment, a Gq GPCR agonist cocktail consisting of 10 μM each of histamine, carbachol, and ATP was applied for two main purposes: 1) as a positive control for viable astrocytes that did not respond to DHPG; and 2) to determine the specificity of changes to group I mGluRs vs. other astrocytic Gq GPCRs. Cells which failed to respond to agonist cocktail were excluded from subsequent analysis. Rise time of the agonist cocktail-evoked responses remained unchanged, suggesting that the expression levels of other Gq GPCRs were not significantly affected in s.r. astrocytes after long-term blockade of hippocampal synaptic transmission (figure 2.7 E and F; control: n = 40 cells; TTX: n = 30 cells).

To investigate in greater detail possible effects on group I mGluR evoked response patterns, DHPG was applied in two successive concentrations, 5 μM and 15 μM. In slices incubated in TTX, astrocytes tended to exhibit plateau-like responses to both concentrations of DHPG, while astrocytes from slices incubated in control ACSF exhibited a greater proportion of single-peak or multi-peak responses (figure 2.7 G). As summarized in figure 2.7 G, TTX treatment increased the percentage of astrocytes in the population responding to both 5 μM and 15 μM DHPG, and the response pattern was greatly shifted toward plateau-like responses at much lower DHPG concentrations ($p < 0.05$ for the percentage of cells showing plateau responses to 15 μM of DHPG between the two conditions; control: n = 40 cells/8 slices; TTX: n = 30 cells/7 slices). The combination of significant differences in astrocyte spontaneous and evoked $Ca^{2+}$ activity following incubation in TTX, including a greater percentage of astrocytes in the population exhibiting spontaneous Gq GPCR activity and evoked mGluR responses, a

shift toward long-lasting plateau over single peak or multi-peak oscillating responses, and faster rise times for both spontaneous and DHPG evoked $Ca^{2+}$ transients, together suggest that expression levels of astrocytic group I mGluRs significantly increase after long-term blockade of neuronal synaptic transmission.

### 2.4.4 Examination of plasticity of group I mGluR activity in astrocytic microdomains

The above experiments enabled recording of astrocyte Gq GPCR activity at the level of the soma and large processes. However, Gq GPCR activity recorded in the soma may not accurately reflect changes that may be occurring at the interface between the synapse and the astrocyte fine processes where the bulk of neuron-to-astrocyte signaling takes place. To address this issue, astrocytes were patch-clamped with an internal solution containing the cell-impermeant version of the $Ca^{2+}$ indicator OGB-1. This technique enabled us to record astrocyte $Ca^{2+}$ activity within the larger processes as well as the meshwork of fine astrocyte processes (figure 2.8 A, upper panel). Passive astrocytes in CA1 s.r. region were identified by their location, size, morphology, and were subsequently confirmed by their passive membrane properties in response to a stepwise voltage change (figure 2.8 B). Regions of interest were placed on the soma and all over the processes of the astrocyte (figure 2.8 A, middle panel). Spontaneous $Ca^{2+}$ activity in all the regions of interest was continuously monitored for 10 to 15 minutes (figure 2.8 C). Microdomains were identified as local spontaneous $Ca^{2+}$ elevations that occurred independently from other parts of the cell. Microdomains ranged considerably

in size, but if the $Ca^{2+}$ transient covered ≥ 75% of the cell area it was instead considered a whole-cell event. Spontaneous $Ca^{2+}$ transients initiating in one ROI spread through a portion of that astrocyte as a local calcium wave. The initiation site of the $Ca^{2+}$ transient of each microdomain was identified and was used in all subsequent analysis to represent the microdomain (figure 2.8 A, lower panel, figure 2.8 C).

In order to investigate astrocyte $Ca^{2+}$ activity in the fine processes of astrocytes, we first examined the distribution of OGB-1 $Ca^{2+}$ indicator dye in astrocytes. CA1 s.r. astrocytes were first loaded with OGB-1 $Ca^{2+}$ indicator dye (molecular weight: 1114.28) and loaded subsequently with Alexa Fluor 488 dye to compare differences in each dye's ability to mark the boundary of the astrocyte processes. 200 μM OGB-1 $Ca^{2+}$ indicator dye was dissolved in standard astrocyte internal solution and filled into a glass pipette. After patching and breaking into the cell, the pipette stayed on the astrocytes for about 60 seconds to allow the OGB-1 $Ca^{2+}$ indicator dye to passively diffuse into the astrocyte. Then the pipette was carefully removed from the cell and successful outside-out patch when coming off the cell indicated a smooth closure of the astrocytes membrane. During the 60 seconds loading procedure, the membrane potential of the astrocyte was measured and a stepwise voltage protocol was applied to verify the cell health and identity (figure 2.9 A left panel). After loading, astrocyte was kept in the dark for 5 minutes without any manipulation to allow the indicator dye to diffuse into its processes. A snapshot was taken afterward with standard laser power (figure 2.9 A right panels). Upon Gq GPCR agonist application (1 μM FMRFamide (Phe-Met-Arg-Phe-$NH_2$) [FMRFa], the agonist to a transgenic Gq GPCR expressed on s.r. astrocytes in this case), fluorescence intensity of

OGB-1 $Ca^{2+}$ indicator dye increased which greatly improved the signal to noise ratio at the boundary of the astrocyte processes (figure 2.9 A right panels). The same astrocyte was re-patched with an internal solution containing 200 μM Alexa Fluor 488. The membrane potential remained the same (-76.4 mV vs. -76.1 mV) and the passive membrane properties were unchanged (figure 2.9 B). After the pipette was successfully removed from the cell surface, the cell was left in the dark for 15 minutes without any manipulation to allow Alexa Fluor 488 to freely diffuse into the fine processes of the cell. Figure 2.9 C shows that the boundary of the fine processes of the astrocyte remained unchanged before and after Alexa Fluor 488 loading. Only when higher laser power was used, the signal-to-noise ratio of the cell boundary increased (figure 2.9 C). Interestingly, when the new ROIs were placed on the cell processes that were only defined under 5% laser power (figure 2.9 D), although the baseline fluencies intensities could not be distinguished from the background with either of the dye loading, $Ca^{2+}$ elevations were detected by FMRFa application from those processes (figure 2.9 E). In conclusion, we found that OGB-1 fully loaded even the finest astrocyte processes as indicated by overlay with Alexa 488 labeling.

In any imaging study there is always concern about possible artifacts created by exposure of tissue to laser light. Spontaneous $Ca^{2+}$ transients may become more frequent due to long-term imaging induced photosensitivity (Wang et al., 2006). To limit the potential influence of photosensitivity on the frequency of spontaneous $Ca^{2+}$ transients or on the responsiveness of agonist-induced $Ca^{2+}$ elevations in astrocytes, we tried to define the upper limit of laser intensity that could be safely used to image patch-clamp filled

astrocytes. This was done by monitoring the spontaneous $Ca^{2+}$ activity in microdomains of patch-clamp filled astrocytes using 5%, 4%, 3% and 2% laser output power. Spontaneous and evoked $Ca^{2+}$ activity in astrocyte processes was monitored for 30 to 40 minutes (figure 2.10 A to D). In order to gain adequate signal from the fine processes of astrocytes, the fluorescence intensity in the astrocyte soma was often saturated (shown as a straight horizontal line in representative data). Also, ROIs that represent background or unloaded astrocytes show no spontaneous or agonist cocktail evoked $Ca^{2+}$ activity (figure 2.10 A). We found that all percent laser output power used caused increased frequency of spontaneous $Ca^{2+}$ transients in astrocytes processes, and the spontaneous $Ca^{2+}$ transients in microdomains tended to synchronize after being subjected to laser light, especially after 20 minutes (figure 2.10 A to D). In some cases, the agonist cocktail failed to evoke a reliable response. Therefore, to reduce the potential artifact from laser induced photosensitivity, all patch-clamp experiments performed in this project have been done with no more than 0.5% laser power, which we considered minimal to gain adequate signal-to-noise to perform the experiment.

Consistent with previous reports, the vast majority of the spontaneous activity occurred in astrocyte processes rather than in the soma (Tian et al., 2006). Nearly 90% of astrocytes from control slices showed at least one $Ca^{2+}$ transient in their microdomains, while none of them showed any detectable $Ca^{2+}$ activity in their soma (figure 2.11 A, control: n = 10 cells). The percentage of spontaneous $Ca^{2+}$ transients in both the soma and microdomains was higher in the TTX-treated astrocytes compared to the cells from control slices (figure 2.11 A, TTX: n = 11 cells). In TTX-treated slices 72.73% of the

cells exhibited spontaneous somatic $Ca^{2+}$ transients (figure 2.11 A, $p < 0.001$), likely due to either a trend towards a greater number of microdomains per astrocyte when normalized to the surface area of individual astrocytes (figure 2.11 C; $p = 0.14$, control: n = 29 microdomains/10 cells; TTX: n = 58 microdomains/ 11 cells), and/or significantly larger areas of propagation of the spontaneous microdomain $Ca^{2+}$ signals (figure 2.11 D). The frequencies of spontaneous $Ca^{2+}$ transients remain unchanged after TTX treatment (figure 2.11 B). However the rise times of the spontaneous $Ca^{2+}$ transients were significantly faster in the microdomains of TTX incubated vs. control incubated astrocytes (figure 2.11 E and F).

Furthermore, similar to the data obtained using AM dye loading procedures, astrocytes treated with TTX had faster microdomain $Ca^{2+}$ wave initiation site rise times evoked using 50 µM DHPG compared to cells from control slices (figure 2.12 A; control: n = 28 microdomains/10 cells, TTX: n = 56 microdomains/11 cells). The amplitudes and half-widths of the DHPG evoked microdomain $Ca^{2+}$ responses remained unchanged between conditions (figure 2.12 B and C). Interestingly, a significant difference in the latency of the 50 µM DHPG evoked $Ca^{2+}$ response was observed at the microdomain level (figure 2.12 D), suggesting that the TTX-treatment scaling effect on group I mGluRs was more potent in the fine processes of astrocytes, which were more sensitive to changes in CA3-CA1 synaptic transmission.

Consistent across all experimental conditions, no significant differences were observed in rise times or amplitudes of the agonist cocktail-evoked $Ca^{2+}$ responses

between TTX-treated and control cells (figure 2.12 E and F). These data suggest that the functional expression of the group I mGluRs in astrocytes increased at the level of the astrocytic microdomains, which are anatomically close to the CA3-CA1 synapses, after inhibition of neuronal action potentials.

## 2.5 Discussion

Here evidence is provided for the first time that astrocytes actively sense long-term decreases in basal levels of neuronal synaptic transmission and respond by scaling up their group I mGluR expression levels. Previous work suggests that visible spontaneous and evoked $Ca^{2+}$ signals in passive hippocampal astrocytes are driven almost exclusively by Gq GPCR mediated release from internal stores (Carmignoto et al., 1998; Nett et al., 2002; Petravicz et al., 2008). Therefore, changes in expression levels of astrocytic Gq GPCRs were assayed by recording spontaneous and evoked astrocyte $Ca^{2+}$ transients. Data were replicated using three different, complementary approaches to load astrocytes with $Ca^{2+}$ indicator. After a 4 to 6 hour blockade of CA3-CA1 neurotransmission in acute hippocampal slices, the following changes in astrocyte $Ca^{2+}$ signaling were observed: 1) a significant increase in the percentage of astrocytes in the slice population exhibiting spontaneous $Ca^{2+}$ elevations; 2) significantly faster rise times of the spontaneous $Ca^{2+}$ transients; 3) a significant increase in response probability to the group I mGluR agonist (DHPG); 4) significantly faster rise times of evoked mGluR $Ca^{2+}$ responses; and 5) significantly shorter response latencies in astrocyte microdomains. Significant effects were observed in both astrocytic somata as well as in the fine

processes. In agreement with previous reports of all-or-none astrocytic Gq GPCR responses upon achieving a threshold agonist concentration (Shao and McCarthy, 1995) and lack of correlation of Gq GPCR density to changes in response amplitudes (Shao and McCarthy, 1993), no changes were observed in the average amplitude of either spontaneous astrocytic Gq GPCR activity or evoked astrocyte mGluR $Ca^{2+}$ elevations.

In addition to these changes, we also observed a dose-dependent shift in astrocytic responses to DHPG in TTX vs. control incubated slices. A characteristic of group I mGluRs (and likely many Gq GPCRs) is that the $Ca^{2+}$ response pattern is graded from single peak, to oscillatory ("multipeak"), to plateau as the agonist concentration is increased (Dolmetsch et al., 1998; Hu et al., 1999; Shelton and McCarthy, 1999; Hermans and Challiss, 2001). In the present study, 5 µM DHPG evoked $Ca^{2+}$ responses in only 36% of bolus-loaded astrocytes in control conditions, and only 2.6% of control incubated astrocytes exhibited plateau-like responses. In contrast, 57% of the astrocytes in TTX treated slices responded to 5 µM DHPG and 13% were already displaying plateau-like $Ca^{2+}$ elevations. A similar pattern shift was observed in 15 µM DHPG. This finding further indicated that the functional expression of group I mGluRs in astrocytes scaled upward following long-term blockade of neuronal action potentials.

Data from patch-clamp experiments in the present study indicate that the effects observed in astrocytic Gq GPCR signaling also occur at the level of astrocyte microdomains. Microdomains are loosely defined as small intracellular compartments of astrocytes that exhibit Gq GPCR signaling activity independently of other parts of the

cell (Grosche et al., 1999; Nett et al., 2002). This is significant because it suggests the possibility that plasticity of astrocytic receptors may also occur in microdomains in response to local changes in synaptic activity. The data provided here map in detail the specific changes in astrocyte $Ca^{2+}$ activity one might look for to determine microdomain plasticity of astrocytic Gq GPCRs following repetitive stimulation of a handful of the 140,000 synapses in the astrocyte domain.

Overall, our data suggest that in response to long-term decrease in neuronal activity, astrocytes exhibit increased Gq GPCR signaling, specifically, increased group I mGluR signaling in 4 to 6 hours. It is more rapid than the homeostatic plasticity of the neuronal ionotropic receptors, indicating that astrocytic mGluRs are more sensitive to the neurotransmitter release. Although, it is unclear if the changes in the receptor signaling is due to the changes in the functional expression of group I mGluRs, or the changes in the signaling pathways. The more immediate question following the current observation is whether the decrease in group I mGluR signaling is directly resulted from the decreased neuronal firing. To answer this question, neuronal activity were elevated in hippocampal slices for 4 to 6 hours in order to test of the plasticity of astrocytic receptors are bi-directional.

## 2.6 References

Araque A, Martin ED, Perea G, Arellano JI, Buno W (2002) Synaptically released acetylcholine evokes Ca2+ elevations in astrocytes in hippocampal slices. J Neurosci 22:2443-2450.

Aronica E, van Vliet EA, Mayboroda OA, Troost D, da Silva FH, Gorter JA (2000) Upregulation of metabotropic glutamate receptor subtype mGluR3 and mGluR5 in reactive astrocytes in a rat model of mesial temporal lobe epilepsy. Eur J Neurosci 12:2333-2344.

Bushong EA, Martone ME, Jones YZ, Ellisman MH (2002) Protoplasmic astrocytes in CA1 stratum radiatum occupy separate anatomical domains. J Neurosci 22:183-192.

Carmignoto G, Pasti L, Pozzan T (1998) On the role of voltage-dependent calcium channels in calcium signaling of astrocytes in situ. J Neurosci 18:4637-4645.

de Ligt RA, Kourounakis AP, AP IJ (2000) Inverse agonism at G protein-coupled receptors: (patho)physiological relevance and implications for drug discovery. British journal of pharmacology 130:1-12.

Dolmetsch RE, Xu K, Lewis RS (1998) Calcium oscillations increase the efficiency and specificity of gene expression. Nature 392:933-936.

Drouin-Ouellet J, Brownell AL, Saint-Pierre M, Fasano C, Emond V, Trudeau LE, Levesque D, Cicchetti F (2011) Neuroinflammation is associated with changes in

glial mGluR5 expression and the development of neonatal excitotoxic lesions. Glia 59:188-199.

Eroglu C, Barres BA (2010) Regulation of synaptic connectivity by glia. Nature 468:223-231.

Ferraguti F, Corti C, Valerio E, Mion S, Xuereb J (2001) Activated astrocytes in areas of kainate-induced neuronal injury upregulate the expression of the metabotropic glutamate receptors 2/3 and 5. Exp Brain Res 137:1-11.

Fiacco TA, McCarthy KD (2004) Intracellular astrocyte calcium waves in situ increase the frequency of spontaneous AMPA receptor currents in CA1 pyramidal neurons. J Neurosci 24:722-732.

Garaschuk O, Milos RI, Konnerth A (2006) Targeted bulk-loading of fluorescent indicators for two-photon brain imaging in vivo. Nat Protoc 1:380-386.

Grosche J, Matyash V, Moller T, Verkhratsky A, Reichenbach A, Kettenmann H (1999) Microdomains for neuron-glia interaction: parallel fiber signaling to Bergmann glial cells. Nat Neurosci 2:139-143.

Hermans E, Challiss RA (2001) Structural, signalling and regulatory properties of the group I metabotropic glutamate receptors: prototypic family C G-protein-coupled receptors. Biochem J 359:465-484.

Honsek SD, Walz C, Kafitz KW, Rose CR Astrocyte calcium signals at Schaffer collateral to CA1 pyramidal cell synapses correlate with the number of activated synapses but not with synaptic strength. Hippocampus.

Hu Q, Deshpande S, Irani K, Ziegelstein RC (1999) [Ca(2+)](i) oscillation frequency regulates agonist-stimulated NF-kappaB transcriptional activity. J Biol Chem 274:33995-33998.

Ibata K, Sun Q, Turrigiano GG (2008) Rapid synaptic scaling induced by changes in postsynaptic firing. Neuron 57:819-826.

Kang J, Jiang L, Goldman SA, Nedergaard M (1998) Astrocyte-mediated potentiation of inhibitory synaptic transmission. Nat Neurosci 1:683-692.

Kang J, Kang N, Yu Y, Zhang J, Petersen N, Tian GF, Nedergaard M Sulforhodamine 101 induces long-term potentiation of intrinsic excitability and synaptic efficacy in hippocampal CA1 pyramidal neurons. Neuroscience 169:1601-1609.

Kirov SA, Sorra KE, Harris KM (1999) Slices have more synapses than perfusion-fixed hippocampus from both young and mature rats. J Neurosci 19:2876-2886.

Navarrete M, Araque A (2008) Endocannabinoids mediate neuron-astrocyte communication. Neuron 57:883-893.

Nett WJ, Oloff SH, McCarthy KD (2002) Hippocampal astrocytes in situ exhibit calcium oscillations that occur independent of neuronal activity. J Neurophysiol 87:528-537.

Nimmerjahn A, Kirchhoff F, Kerr JN, Helmchen F (2004) Sulforhodamine 101 as a specific marker of astroglia in the neocortex in vivo. Nat Methods 1:31-37.

Ostasov P, Krusek J, Durchankova D, Svoboda P, Novotny J (2008) Ca2+ responses to thyrotropin-releasing hormone and angiotensin II: the role of plasma membrane integrity and effect of G11alpha protein overexpression on homologous and heterologous desensitization. Cell Biochem Funct 26:264-274.

Pasti L, Volterra A, Pozzan T, Carmignoto G (1997) Intracellular calcium oscillations in astrocytes: a highly plastic, bidirectional form of communication between neurons and astrocytes in situ. J Neurosci 17:7817-7830.

Perea G, Araque A (2005) Glial calcium signaling and neuron-glia communication. Cell Calcium 38:375-382.

Perez-Otano I, Ehlers MD (2005) Homeostatic plasticity and NMDA receptor trafficking. Trends Neurosci 28:229-238.

Petravicz J, Fiacco TA, McCarthy KD (2008) Loss of IP3 receptor-dependent Ca2+ increases in hippocampal astrocytes does not affect baseline CA1 pyramidal neuron synaptic activity. J Neurosci 28:4967-4973.

Porter JT, McCarthy KD (1995) Adenosine receptors modulate [Ca2+]i in hippocampal astrocytes in situ. Journal of neurochemistry 65:1515-1523.

Porter JT, McCarthy KD (1996) Hippocampal astrocytes in situ respond to glutamate released from synaptic terminals. J Neurosci 16:5073-5081.

Prezeau L, Gomeza J, Ahern S, Mary S, Galvez T, Bockaert J, Pin JP (1996) Changes in the carboxyl-terminal domain of metabotropic glutamate receptor 1 by alternative splicing generate receptors with differing agonist-independent activity. Mol Pharmacol 49:422-429.

Shao Y, McCarthy KD (1993) Quantitative relationship between alpha 1-adrenergic receptor density and the receptor-mediated calcium response in individual astroglial cells. Mol Pharmacol 44:247-254.

Shao Y, McCarthy KD (1995) Receptor-mediated calcium signals in astroglia: multiple receptors, common stores and all-or-nothing responses. Cell Calcium 17:187-196.

Shelton MK, McCarthy KD (1999) Mature hippocampal astrocytes exhibit functional metabotropic and ionotropic glutamate receptors in situ. Glia 26:1-11.

Shelton MK, McCarthy KD (2000) Hippocampal astrocytes exhibit Ca2+-elevating muscarinic cholinergic and histaminergic receptors in situ. Journal of neurochemistry 74:555-563.

Sullivan MR, Nimmerjahn A, Sarkisov DV, Helmchen F, Wang SS (2005) In vivo calcium imaging of circuit activity in cerebellar cortex. J Neurophysiol 94:1636-1644.

Sutton MA, Wall NR, Aakalu GN, Schuman EM (2004) Regulation of dendritic protein synthesis by miniature synaptic events. Science 304:1979-1983.

Sutton MA, Ito HT, Cressy P, Kempf C, Woo JC, Schuman EM (2006) Miniature neurotransmission stabilizes synaptic function via tonic suppression of local dendritic protein synthesis. Cell 125:785-799.

Takahashi A, Camacho P, Lechleiter JD, Herman B (1999) Measurement of intracellular calcium. Physiol Rev 79:1089-1125.

Tian GF, Takano T, Lin JH, Wang X, Bekar L, Nedergaard M (2006) Imaging of cortical astrocytes using 2-photon laser scanning microscopy in the intact mouse brain. Adv Drug Deliv Rev 58:773-787.

Tseng KY, Chambers RA, Lipska BK (2009) The neonatal ventral hippocampal lesion as a heuristic neurodevelopmental model of schizophrenia. Behav Brain Res 204:295-305.

Ulas J, Satou T, Ivins KJ, Kesslak JP, Cotman CW, Balazs R (2000) Expression of metabotropic glutamate receptor 5 is increased in astrocytes after kainate-induced epileptic seizures. Glia 30:352-361.

Wang SS, Thompson SH (1994) Measurement of changes in functional muscarinic acetylcholine receptor density in single neuroblastoma cells using calcium release kinetics. Cell Calcium 15:483-496.

Wang X, Lou N, Xu Q, Tian GF, Peng WG, Han X, Kang J, Takano T, Nedergaard M (2006) Astrocytic Ca2+ signaling evoked by sensory stimulation in vivo. Nat Neurosci 9:816-823.

Watt AJ, van Rossum MC, MacLeod KM, Nelson SB, Turrigiano GG (2000) Activity coregulates quantal AMPA and NMDA currents at neocortical synapses. Neuron 26:659-670.

Wierenga CJ, Ibata K, Turrigiano GG (2005) Postsynaptic expression of homeostatic plasticity at neocortical synapses. J Neurosci 25:2895-2905.

Witcher MR, Kirov SA, Harris KM (2007) Plasticity of perisynaptic astroglia during synaptogenesis in the mature rat hippocampus. Glia 55:13-23.

**Figure Legends**

**Figure 2.1 CA3 neurons in hippocampal slices incubated in 3.5 mM $[K^+]_o$ ACSF were slightly more depolarized and had more spontaneous action potentials compared to those incubated in 2.5 mM $[K^+]_o$ ACSF.**

(A) Whole cell recording of CA3 neuron membrane potentials indicated that CA3 neurons rarely fired spontaneous action potentials in 2.5 mM $[K^+]_o$ ACSF, while in 3.5 mM $[K^+]_o$ ACSF CA3 neurons fired occasional spontaneous action potentials (2.5 mM $[K^+]_o$: n = 12 cells; 3.5 mM $[K^+]_o$: n = 8 cells). Therefore, 3.5 mM $[K^+]_o$ ACSF was used in these experiments to increase the probability of seeing an effect of long-term incubation of slices in TTX. Scale bar: 20 mV/5 sec.

(B) There was no significant difference in membrane potential between CA3 neurons incubated in 2.5 mM $[K^+]_o$ ACSF and those incubated in 3.5 mM $[K^+]_o$ ACSF ($p = 0.64$) (2.5 mM $[K^+]_o$: n = 12 cells; 3.5 mM $[K^+]_o$: n = 8 cells). Error bars represent S.E.M.

(C) CA3 neurons were hyperpolarized during the 15 minutes whole-cell recording. There was no significant difference in membrane potential of CA3 neurons after whole-cell recordings between the neurons incubated in 2.5 mM $[K^+]_o$ ACSF and 3.5 mM $[K^+]_o$ ACSF ($p = 0.11$) (2.5 mM $[K^+]_o$: n = 12 cells; 3.5 mM $[K^+]_o$: n = 8 cells). Error bars represent S.E.M.

(D) CA3 neurons incubated in 3.5 mM $[K^+]_o$ ACSF tended to have more spontaneous action potentials than those incubated in 2.5 mM $[K^+]_o$ ACSF ($p = 0.054$) (2.5 mM $[K^+]_o$: n = 12 cells; 3.5 mM $[K^+]_o$: n = 8 cells). Error bars represent S.E.M.

(E) The distribution of frequency of spontaneous action potentials from individual CA3 neurons tested (2.5 mM $[K^+]_o$: n = 12 cells; 3.5 mM $[K^+]_o$: n = 8 cells). In general, CA3 neurons incubated in 3.5 mM $[K^+]_o$ ACSF had more frequent spontaneous action potentials compared to those incubated in 2.5 mM $[K^+]_o$ ACSF, but there was a large variation among individual cells incubated in 3.5 mM $[K^+]_o$. Error bars represent S.E.M.

**Figure 2.2 Representative data of $Ca^{2+}$ imaging on s.r. astrocytes in the CA1 region of acute hippocampal slices using traditional bulk-loading.**

(A) No difference in dye loading was observed between control and TTX incubated hippocampal slices. Numbered ROIs were placed over the astrocyte somata to record spontaneous and 50 μM DHPG evoked astrocyte $Ca^{2+}$ transients.

(B) Representative traces of astrocyte $Ca^{2+}$ activity over time. Each trace indicates the average fluorescence intensity within each ROI over individual astrocyte somata. Orange ellipse indicates the spontaneous $Ca^{2+}$ transient observed in astrocytes. Orange rectangle with solid outline indicates agonist-evoked multi-peak $Ca^{2+}$ elevation observed in astrocytes. Orange rectangle with dashed outline indicates agonist-evoked plateau-like $Ca^{2+}$ elevation observed in astrocytes. Scale bar: 100% $\Delta F/F_0$/100 sec.

**Figure 2.3 Long-term blockade of neuronal action potentials in TTX significantly altered spontaneous $Ca^{2+}$ transients in astrocytes bulk-loaded with $Ca^{2+}$ indicator.**

(A) There was no significant difference in amplitude of the spontaneous astrocyte $Ca^{2+}$ transients between control and TTX-treated astrocytes (control: n = 24 cells, TTX, n = 36 cells). Error bars represent S.E.M.

(B) There was no significant difference in frequency of the spontaneous astrocyte $Ca^{2+}$ transients between control and TTX-treated astrocytes (control: n = 24 cells, TTX, n = 36 cells). Frequency was shown as number of events per 100 seconds. Error bars represent S.E.M.

(C) There was a nonsignificant trend toward a higher percentage of astrocytes in the population to exhibit spontaneous activity compared to controls (control: n = 215 cells/15 slices; TTX, n = 218 cells/16 slices; p = 0.20). Error bars represent S.E.M.

(D) A higher percentage of TTX treated cells responded to 50 μM DHPG with $Ca^{2+}$ elevations in their soma (83.2%) compared to control cells (75.7%).

**Figure 2.4 Long-term blockade of neuronal action potentials in TTX significantly altered DHPG evoked mGluR astrocyte $Ca^{2+}$ responses in astrocytes bulk-loaded with $Ca^{2+}$ indicator.**

(A) No change in the amplitudes of DHPG-evoked $Ca^{2+}$ responses were found between control and TTX incubated astrocytes (control: n = 215 cells/15 slices; TTX, n = 218 cells/16 slices). Error bars represent S.E.M.

(B) No change in the duration of DHPG-evoked $Ca^{2+}$ responses were found between control and TTX incubated astrocytes (control: n = 215 cells/15 slices; TTX, n = 218 cells/16 slices). Error bars represent S.E.M.

(C) Representative traces of the rising phase of DHPG-evoked $Ca^{2+}$ responses from astrocytes incubated with either 3.5 mM $[K^+]_o$ ACSF or 3.5 mM $[K^+]_o$ ACSF + 1 µM TTX. Arrows indicate onset and the peak of the responses (onset defined as the last data point before + 1 S.D. over mean of baseline noise; event was defined by peak being = 2 S.D. over mean of baseline noise).

(D) TTX-treated astrocytes had significantly faster rise times of their DHPG-evoked $Ca^{2+}$ responses (control: n = 215 cells/15 slices; TTX, n = 218 cells/16 slices). Error bars represent S.E.M.

(E) Astrocytes incubated in TTX displayed a significant shift toward plateau-like evoked $Ca^{2+}$ responses to bath application of 50 µM DHPG compared to astrocyte responses in control conditions ($p < 0.001$; control: n = 215 cells/15 slices; TTX, n = 218 cells/16 slices). Significant differences were found in the percentage of multi-peak and plateau responses between control and TTX treated cells ($p < 0.001$ in both cases).

(F) There was no change in area under DHPG-evoked $Ca^{2+}$ responses between control and TTX incubated astrocytes (control: n = 215 cells/15 slices; TTX, n = 218 cells/16 slices). Error bars represent S.E.M.

**Figure 2.5 Representative data of $Ca^{2+}$ imaging on s.r. astrocytes in CA1 region of acute hippocampal slices using the newer bolus-loading technique.**

(A) A group of s.r. astrocytes bolus-loaded with OGB-1 AM $Ca^{2+}$ indicator dye and the astrocyte marker SR-101 in a control (upper panels) and TTX-incubated (lower panels) slice. Numbered ROIs match $Ca^{2+}$ traces in (B).

(B) Representative astrocyte $Ca^{2+}$ activity in astrocyte somata over time in control (upper) and TTX-incubated (lower) slice shown in (A). Orange ellipse indicates the spontaneous $Ca^{2+}$ transient observed in astrocytes. Orange rectangle with double solid outline indicates agonist-evoked single-peak $Ca^{2+}$ elevation observed in astrocytes. Orange rectangle with solid outline indicates agonist-evoked multi-peak $Ca^{2+}$ elevation observed in astrocytes. Orange rectangle with dashed outline indicates agonist-evoked plateau-like $Ca^{2+}$ elevation observed in astrocytes. TTX-treated astrocytes were more likely to exhibit spontaneous somatic $Ca^{2+}$ transients. They also exhibited marked differences in their DHPG evoked responses, including a greater percentage of responding cells, and a shift toward a plateau-like pattern even at low doses. This is summarized in figure 2.7 G (control: n = 40 cells/8 slices; TTX: n = 30 cells/7 slices). Note that the amplitude of the astrocyte $Ca^{2+}$ responses was unaffected. Scale bar: 100% $\Delta F/F_0$/100 sec.

**Figure 2.6 Long-term effects of TTX incubation on astrocyte spontaneous Gq GPCR activity occurred in soma and main processes of astrocytes filled with indicator dye by bolus-loading.**

(A) The percentage of spontaneously active cells in slices loaded by bolus-loading were significant higher than those loaded by bulk-loading (Control bolus-loaded: 12.9% ± 5.1%; n = 40 cells/8 slices; Control bulk-loaded: 7.8% ± 2.7%; n = 215 cells/15 slices; TTX bolus-loaded: 42.1% ± 10.1%; n = 30 cells/7 slices; TTX bulk-loaded: 13.7% ± 3.8%; n = 218 cells/16 slices), suggesting that astrocytes in deeper, healthier tissue exhibit more $Ca^{2+}$ activity compared to injured astrocytes near the slice surface.

(B) The percentage of spontaneously active astrocytes was significantly higher in TTX treated vs. control slices (control: n = 40 cells/8 slices; TTX: n = 30 cells/7 slices; $p < 0.05$ in both cases). Error bars represent S.E.M.

(C) The percentage of astrocytes in the population exhibiting spontaneous $Ca^{2+}$ transients in the soma and major processes was significantly increased following TTX treatment ($p < 0.001$ between the percentage of active cells in soma, $p < 0.05$ between the percentage of active cells in processes; control: n = 40 cells; TTX: n = 30 cells).

(D) The frequency of the spontaneous $Ca^{2+}$ transients in the cell soma was similar between control and TTX treated groups (control: n = 4 cells; TTX: n = 13 cells). Error bars represent S.E.M.

(E) The overall frequency of the spontaneous $Ca^{2+}$ transients in astrocyte processes normalized to the area of astrocytes was similar between groups (control: n = 4 cells; TTX: n = 9 cells). Error bars represent S.E.M.

(F) Representative traces of the rising phase of the spontaneous $Ca^{2+}$ transients in both control and TTX cells. Arrows indicate the onsets and the peaks (onset defined as the last data point before + 1 S.D. over mean of baseline noise; event was defined by peak being = 2 S.D. over mean of baseline noise).

(G) Rise times of the spontaneous $Ca^{2+}$ transients were significantly faster in the TTX incubated group ($p < 0.01$; control: n = 40 cells; TTX: n = 30 cells). Error bars represent S.E.M.

**Figure 2.7 Long-term effects of TTX incubation on DHPG-evoked $Ca^{2+}$ responses on astrocytes filled with indicator dye by bolus-loading.**

(A) TTX-treated cells had faster rise times of their evoked $Ca^{2+}$ responses to 15 µM DHPG ($p < 0.001$; control: n = 32 cells; TTX: n = 27 cells). Left panel shows the representative traces of the rising phase of the spontaneous $Ca^{2+}$ transients in both control and TTX cells. Arrows indicate the onsets and the peaks (onset defined as the last data point before + 1 S.D. over mean of baseline noise; event was defined by peak being = 2 S.D. over mean of baseline noise). Error bars represent S.E.M.

(B) The amplitude of $Ca^{2+}$ responses to 15 µM DHPG was unaffected by TTX treatment (control: n = 32 cells; TTX: n = 27 cells). Error bars represent S.E.M.

(C) The half width of $Ca^{2+}$ responses to 15 µM DHPG was unaffected by TTX treatment (control: n = 7 cells; TTX: n = 13 cells; $p = 0.14$). Error bars represent S.E.M.

(D) The latency of $Ca^{2+}$ responses to 15 μM DHPG was unaffected by TTX treatment ($p = 0.13$; control: n = 32 cells; TTX: n = 27 cells). Error bars represent S.E.M.

(E) The rise times of $Ca^{2+}$ responses to agonist cocktail was unaffected by TTX treatment (control: n = 40 cells; TTX: n = 30 cells). Error bars represent S.E.M.

(F) The amplitude of $Ca^{2+}$ responses to agonist cocktail was unaffected by TTX treatment (control: n = 40 cells; TTX: n = 30 cells). Error bars represent S.E.M.

(G) Summary of the pattern of DHPG evoked astrocyte $Ca^{2+}$ responses in control and TTX-incubated slices. TTX-treated astrocytes exhibited marked differences in their DHPG evoked responses, including a greater percentage of responding cells, and shift toward a plateau-like pattern even at low doses compare to control astrocytes (control: n = 40 cells/8 slices; TTX: n = 30 cells/7 slices; $p < 0.05$ for the percentages of plateau-like responses to 15 μM DHPG application between the two groups).

**Figure 2.8 Representative data of $Ca^{2+}$ imaging on s.r. astrocytes in CA1 region of acute hippocampal slices following patch-clamp loading with $Ca^{2+}$ indicator dye OGB-1.**

(A) A single astrocyte patch clamped with OGB-1 $Ca^{2+}$ indicator dye in a control incubated hippocampal slice. Colored ROIs in the right panel indicate individual microdomains and match colored boxes in (C). Equal sized boxes of 3.6 μm per side (12.3 $\mu m^2$) were placed over even the smallest astrocyte processes to study microdomain Gq GPCR activity (right panel) and match corresponding $Ca^{2+}$ traces in (C).

(B) The same astrocyte exhibited passive currents when the membrane was stepped from -180 mV to +80 mV in 20 mV increments. A test pulse of -5 mV was included after each voltage step in order to monitor changes in access resistance (scale bar: 2 nA or 60 mV/10 msec).

(C) Traces of spontaneous microdomain $Ca^{2+}$ activity and DHPG evoked $Ca^{2+}$ responses from cell in (A). Each microdomain in this cell is highlighted using a different colored ROI (5 in total). Scale bar: 100% $\Delta F/F_0$/100 sec.

**Figure 2.9 OGB-1 $Ca^{2+}$ indicator dye is sufficient to mark the border of CA1 s.r. passive astrocytes.**

(A) Patch-clamped astrocytes exhibited passive currents when the membrane was stepped from -180 mV to +80 mV in 20 mV increments (scale bar: 2 nA or 60 mV/10 msec). The same astrocyte was visualized 5 minutes after patch-camping with OGB-1 $Ca^{2+}$ indicator dye (left panel). The astrocyte showed elevated fluorescence signal in response to 1 µM FMRFa application to activate the astrocytic MrgA1 receptors. ROIs were placed on the cell based on the OGB-1 loading. Scale bar: 10 µm.

(B) The same astrocyte was patch-clamped a second time with Alexa Fluor 488 tracer dye and exhibited similar passive currents when the membrane was stepped from -180 mV to +80 mV in 20 mV increments.

(C) 15 minutes after patch clamp delivery of Alex Fluor 488 (upper right panel). Signal-to-noise ratio of the same astrocyte processes improved only with increased laser

intensity, but at the same laser intensity Alexa Fluor 488 did not improve signal-to-noise over OGB-1 $Ca^{2+}$ indicator. Scale bar: 10 μm.

(D) New ROIs (in total 12) were placed on the astrocyte processes which can only be imaged under 5% laser power.

(E) The $Ca^{2+}$ elevations were detected by FMRF application from the new ROIs, which indicated OGB-1 $Ca^{2+}$ indicator fully loaded into the finest astrocyte processes.

**Figure 2.10 Laser power-induced artifacts on spontaneous and evoked $Ca^{2+}$ activity in astrocyte processes.**

(A) Spontaneous $Ca^{2+}$ activity during a 30 minute recording in processes of astrocytes patch clamp loaded with OGB-1 $Ca^{2+}$ indicator dye using 5% laser power. The fluorescence signal from soma was saturated and shown as a flat horizontal line. Increased and synchronized spontaneous $Ca^{2+}$ transients among microdomains can be seen in regions within the dashed line. ROI number 13 indicates the background fluorescence in the hippocampal slice. The number of synchronized activities among microdomains (more than 50% of the microdomains exhibit microdomain activity at the same time) in every 10 minutes (I: the first 10 minutes, II: the second 10 minutes; III: the third 10 minutes; evoked activities were not taken count) were counted and displayed in the bar graph on right. Arrows indicates the time agonist cocktail was applied. Scale bar: 100% $\Delta F/F_0$/100 sec.

(B) to (D) Spontaneous and evoked $Ca^{2+}$ activity during a 40 minute recording in processes of an astrocyte patch clamped with OGB-1 $Ca^{2+}$ indicator dye using 4%, 3%, 2% laser power, respectively. All ROIs numbered '1' present the fluorescence signal in the soma of astrocytes, while the ROIs with the highest numbers (15, 17 and 17 in B to D, respectively) present fluorescence of background in hippocampal slices. Increased and synchronized spontaneous $Ca^{2+}$ transients among microdomains are indicated in regions within the dashed line. The number of synchronized activities among microdomains (more than 50% of the microdomains exhibit microdomain activity at the same time) in every 10 minutes (I: the first 10 minutes, II: the second 10 minutes; III: the third 10 minutes; evoked activities were not taken count) were counted and displayed in the bar graph on right. Arrows indicates the time agonist cocktail was applied. Scale bar: 100% $\Delta F/F_0$/100 sec.

**Figure 2.11 Long-term effects of TTX incubation on astrocyte spontaneous Gq GPCR activity occurred in astrocyte microdomains.**

(A) TTX-treated s.r. astrocytes showed a higher percentage of spontaneous activity at the soma level ($p < 0.001$) of s.r. astrocytes while most of the s.r. astrocytes exhibit spontaneous $Ca^{2+}$ activities at the microdomain level (control: n = 10 cells; TTX: n = 11 cells).

(B) There was no significant change in frequency of spontaneous microdomain $Ca^{2+}$ transients normalized to the area of astrocytes between the TTX treated astrocytes

compared to the controls ( p = 0.92; control: n = 29 microdomains/10 cells; TTX: n = 58 microdomains/11 cells). Error bars represent S.E.M.

(C) TTX treated astrocytes exhibited a trend toward a greater number of microdomains per cell when normalized to the area of astrocytes compared to controls (p = 0.14; control: n = 29 microdomains/10 cells; TTX: n = 58 microdomains/11 cells; p = 0.14). Error bars represent S.E.M.

(D) Spontaneous microdomain $Ca^{2+}$ transients had significantly larger areas of propagation compared to controls ($p < 0.01$; control: n = 29 microdomains/10 cells; TTX: n = 58 microdomains/11 cells). Error bars represent S.E.M.

(E) Representative rise times for microdomain activity from TTX-treated and control cells, with arrows indicating the onset and the peak (onset defined as the last data point before + 1 S.D. over mean of baseline noise; event was defined by peak being = 2 S.D. over mean of baseline noise). Error bars represent S.E.M.

(F) Spontaneous microdomain $Ca^{2+}$ transients had significantly faster rise times compared to controls (control: n = 29 microdomains/10 cells; TTX: n = 58 microdomains/11 cells).

**Figure 2.12 Long-term effects of TTX incubation on astrocyte evoked group I mGluR responses occurred in astrocyte microdomains.**

(A) Evoked responses to 50 μM DHPG analyzed in microdomains revealed significantly faster rise times in the TTX vs. control group ($p < 0.01$, control: n = 28 microdomains/10 cells; TTX: n = 56 microdomains/11 cells). Error bars represent S.E.M.

(B) Evoked responses to 50 μM DHPG analyzed in microdomains revealed no change in amplitude in the TTX vs. control group (control: n = 28 microdomains/10 cells; TTX: n = 56 microdomains/11 cells). Error bars represent S.E.M.

(C) Evoked responses to 50 μM DHPG analyzed in microdomains revealed no change in half width in the TTX vs. control group (control: n = 28 microdomains/10 cells; TTX: n = 56 microdomains/11 cells). Error bars represent S.E.M.

(D) Evoked responses to 50 μM DHPG analyzed in microdomains revealed significantly shorter response latencies in the TTX vs. control group (control: n = 28 microdomains/10 cells; TTX: n = 56 microdomains/11 cells). Error bars represent S.E.M.

(E) Evoked responses to agonist cocktail analyzed in microdomains showed a trend but no significant changes in rise times of $Ca^{2+}$ responses in the TTX treatment group vs. control group (control: n = 40 cells; TTX: n = 30 cells). Error bars represent S.E.M.

(F) Evoked responses to the agonist cocktail analyzed in microdomains revealed no changes in amplitudes of $Ca^{2+}$ responses in the TTX treatment group vs. control group (control: n = 12 microdomains/6 cells; TTX: n = 28 microdomains/6 cells). Error bars represent S.E.M.

Figure 2.1 Comparison of neuronal activity between CA3 neurons incubated in 2.5 mM $[K^+]_o$ and 3.5 mM $[K^+]_o$ ACSF

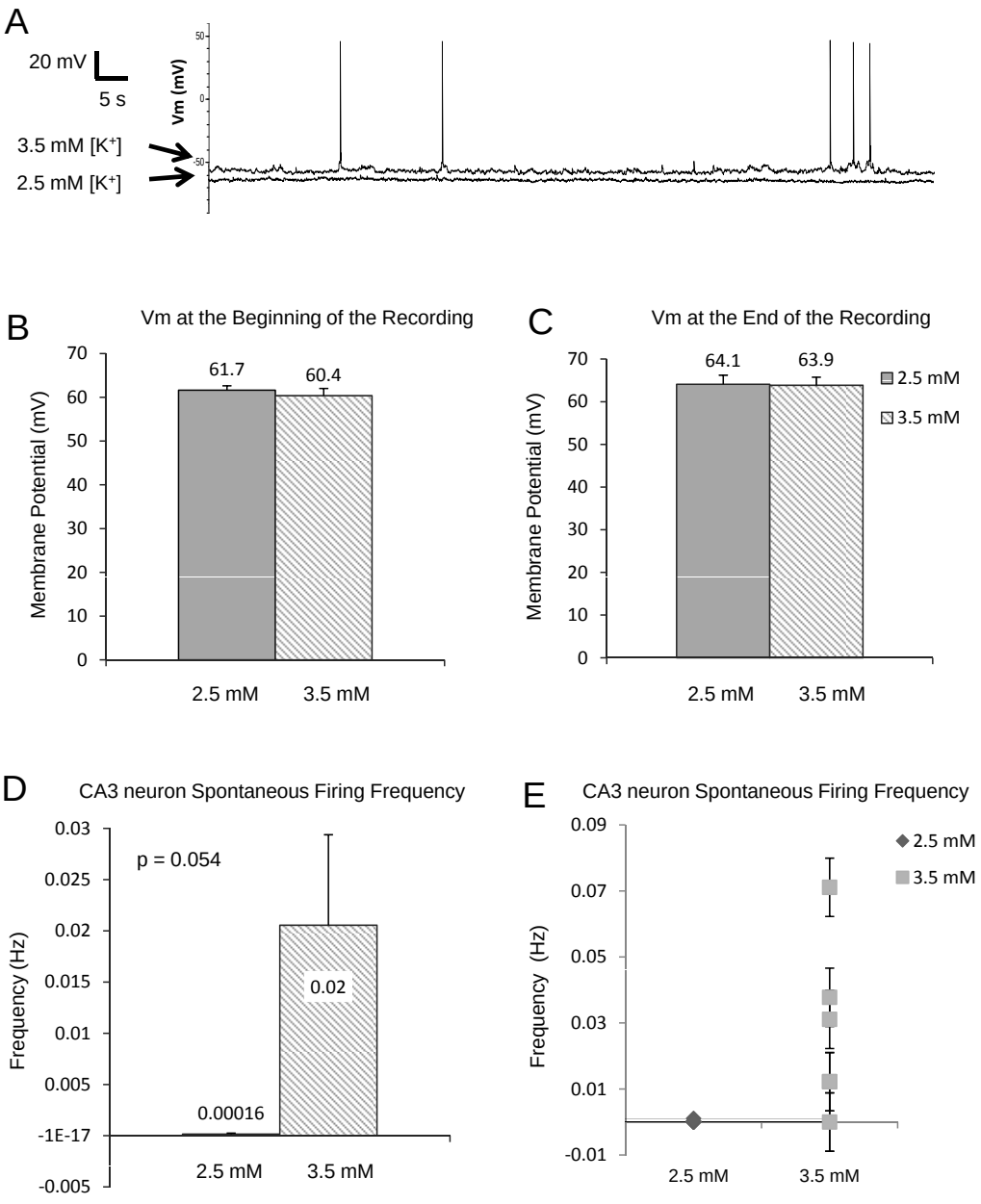

Figure 2.2 $Ca^{2+}$ imaging on s.r. astrocytes using traditional bulk-loading

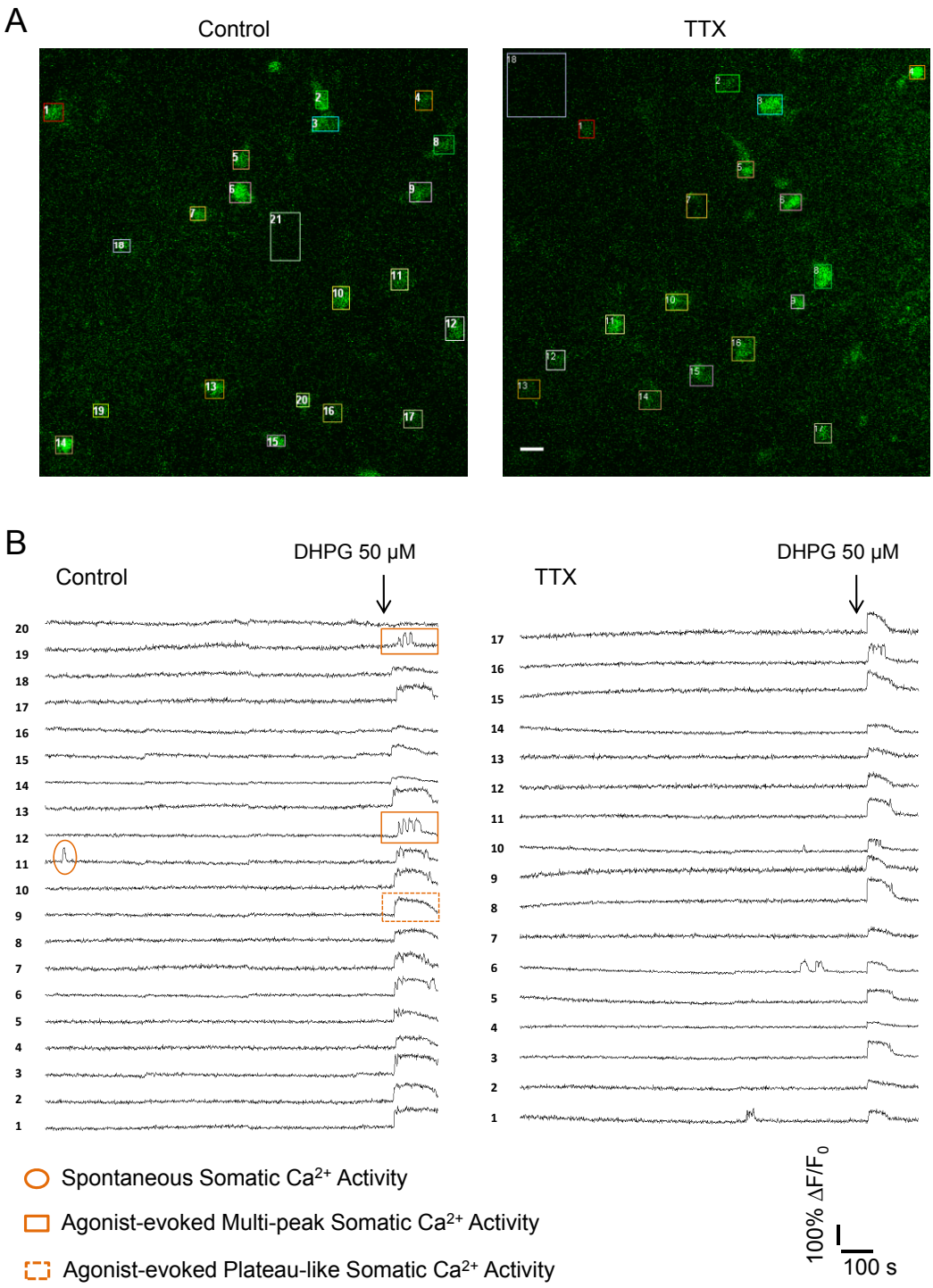

Figure 2.3 Long-term effects on spontaneous $Ca^{2+}$ transients in astrocytes bulk-loaded with $Ca^{2+}$ indicator

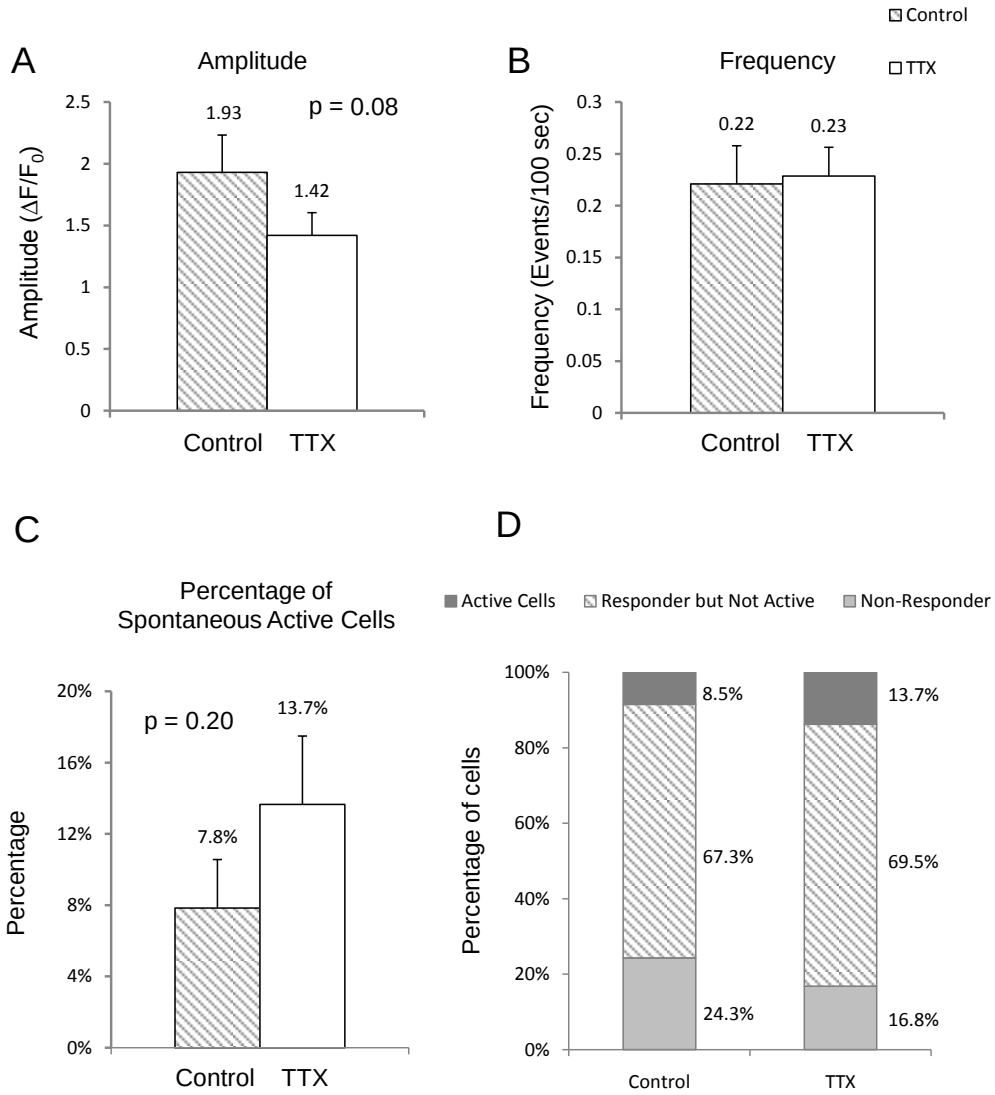

Figure 2.4 Long-term effects on DHPG evoked $Ca^{2+}$ responses in astrocytes bulk-loaded with $Ca^{2+}$ indicator

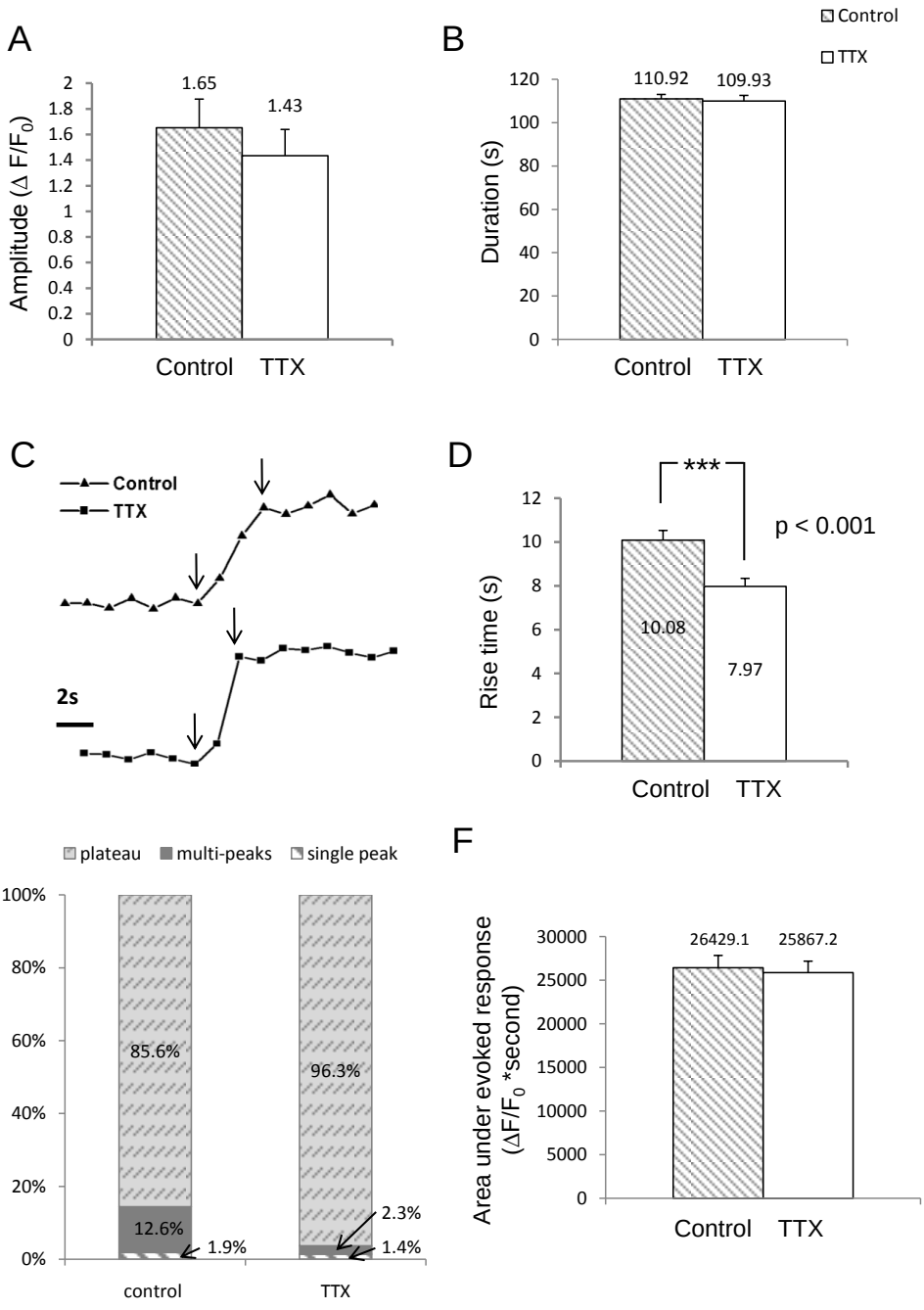

Figure 2.5 $Ca^{2+}$ imaging on s.r. astrocytes using the newer bolus-loading

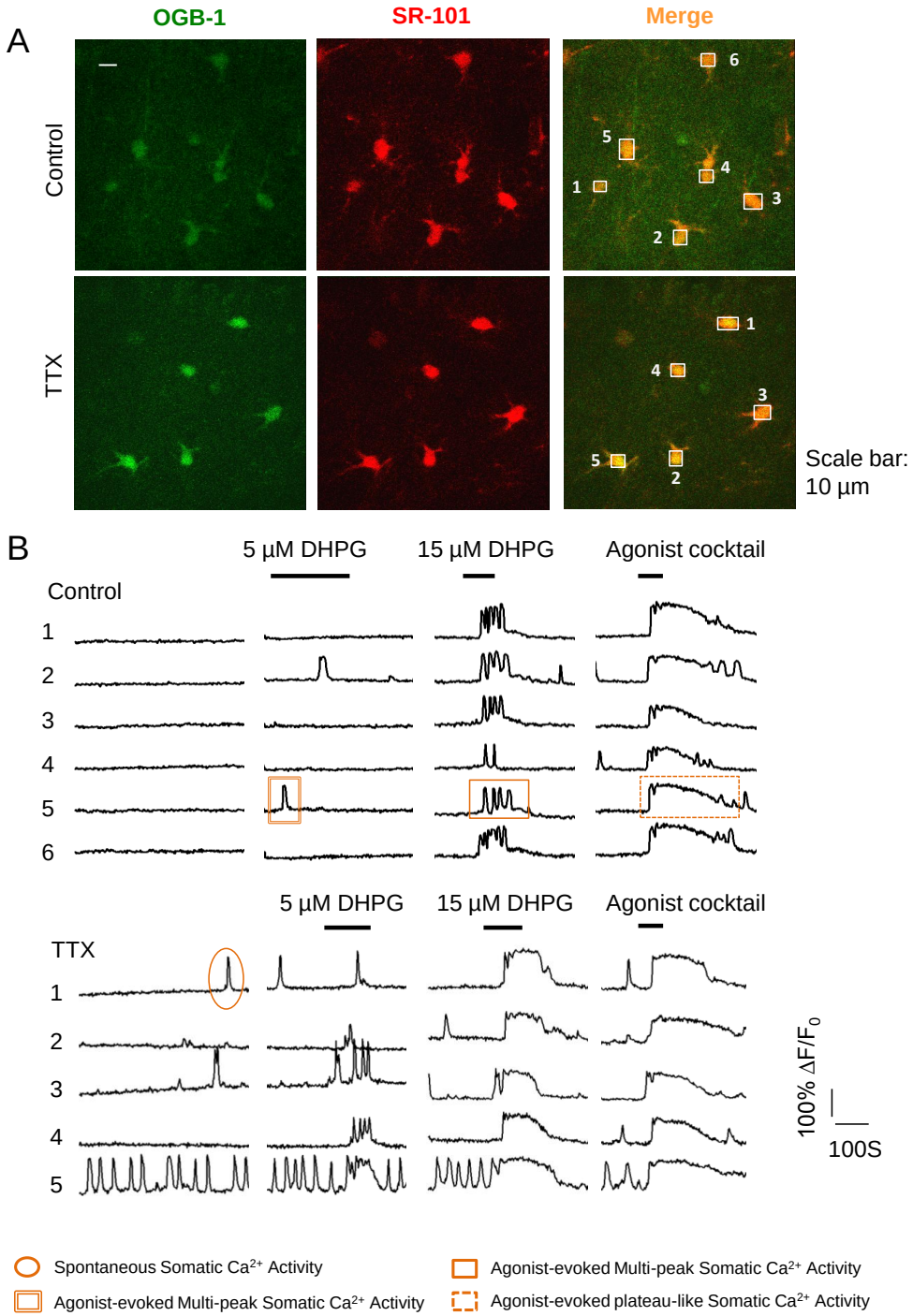

Figure 2.6 Long-term effects on spontaneous $Ca^{2+}$ activity occurred in soma and main processes of astrocytes by using bolus-loading

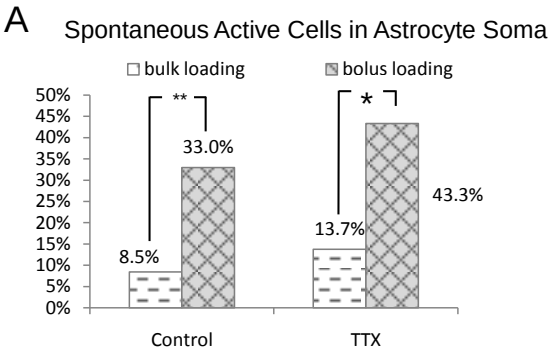


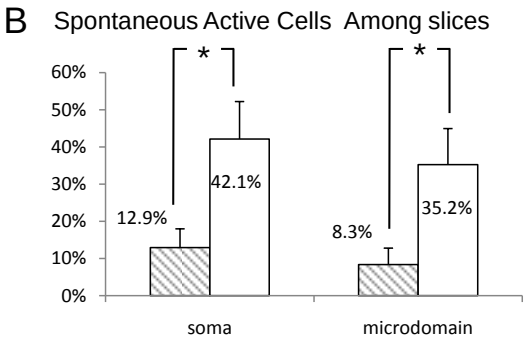


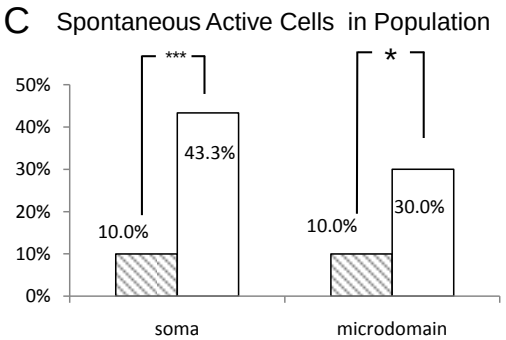


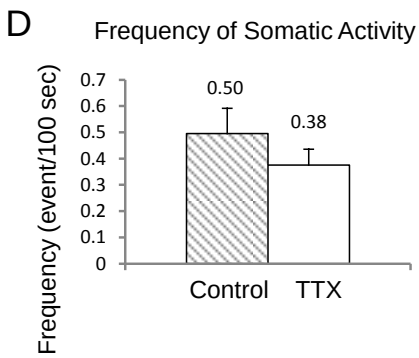


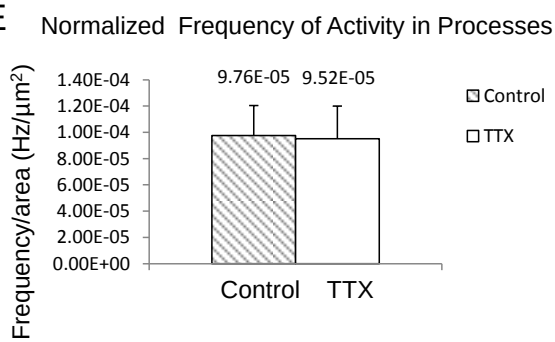


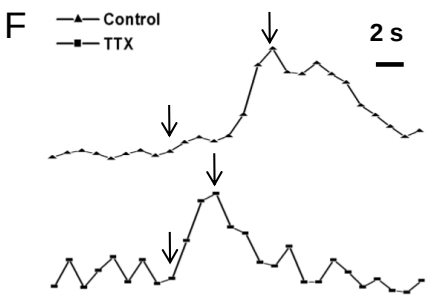


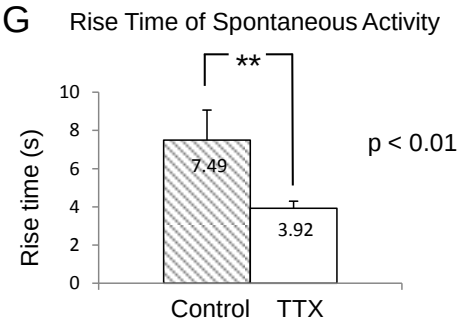

Figure 2.7 Long-term effects on DHPG-evoked $Ca^{2+}$ responses on astrocytes filled by bolus-loading

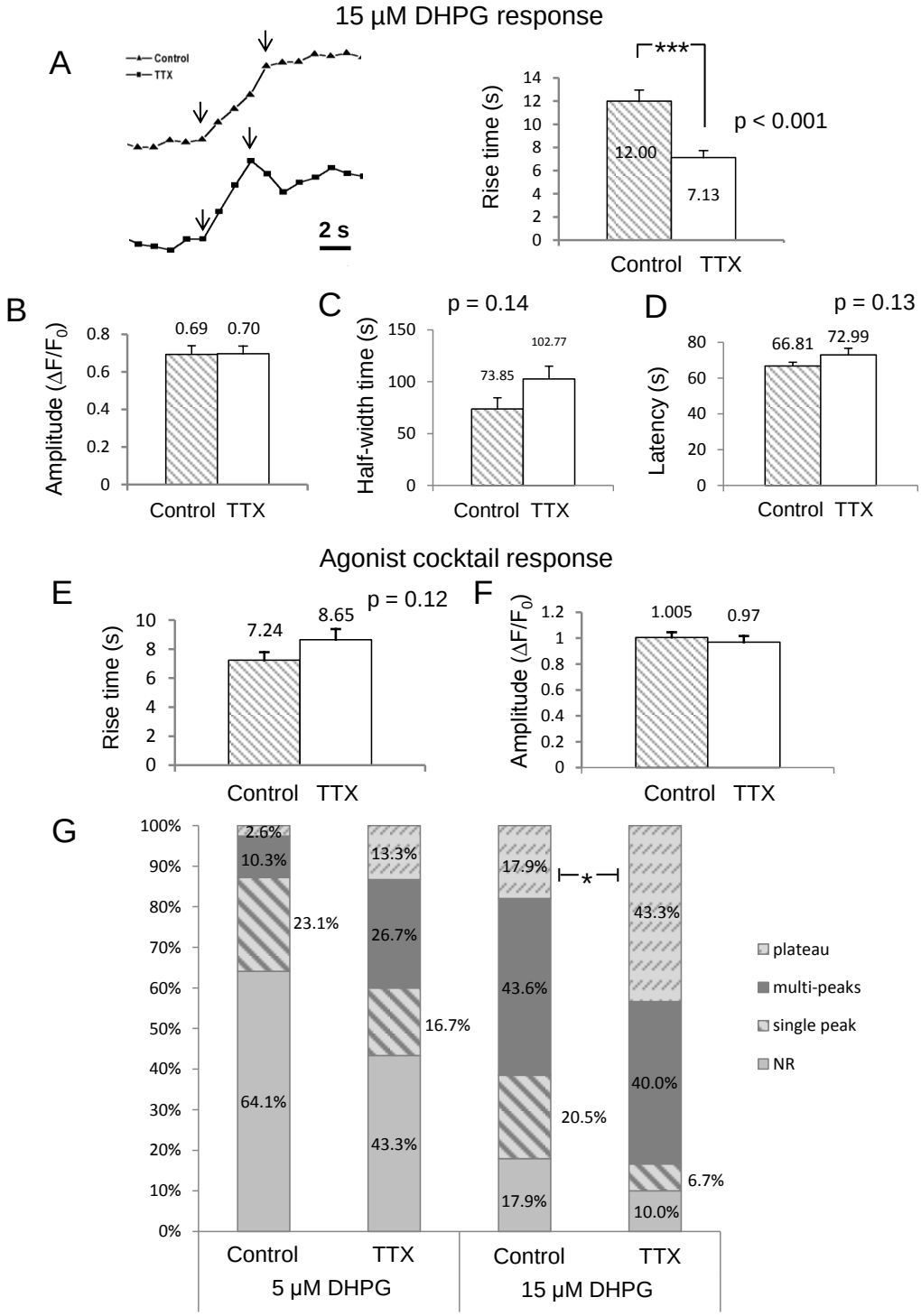

Figure 2.8 $Ca^{2+}$ imaging on a single s.r. astrocyte loaded by patch clamp technique

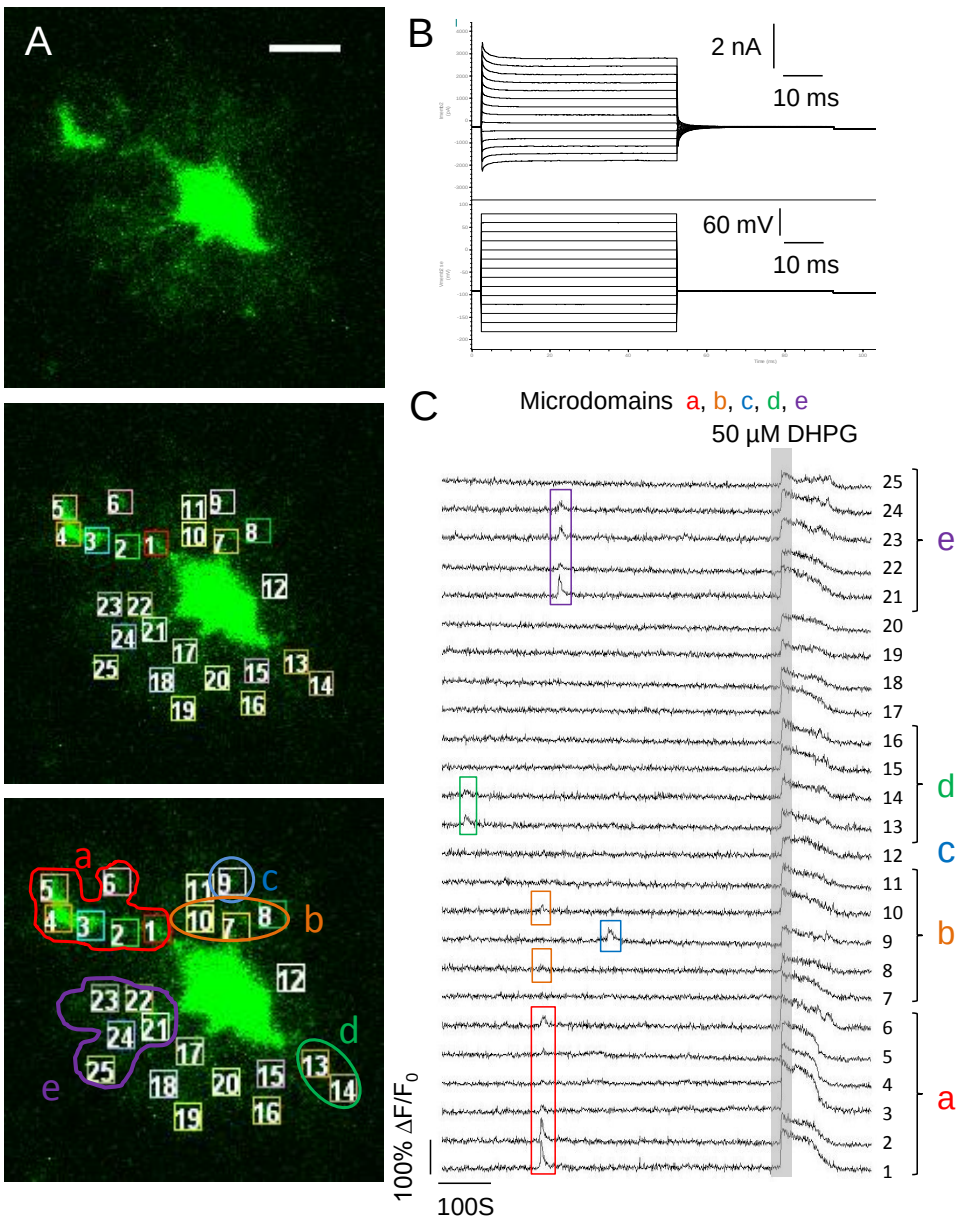

Figure 2.9 Comparison of dye loading between OGB-1 and Alexa 488 dye

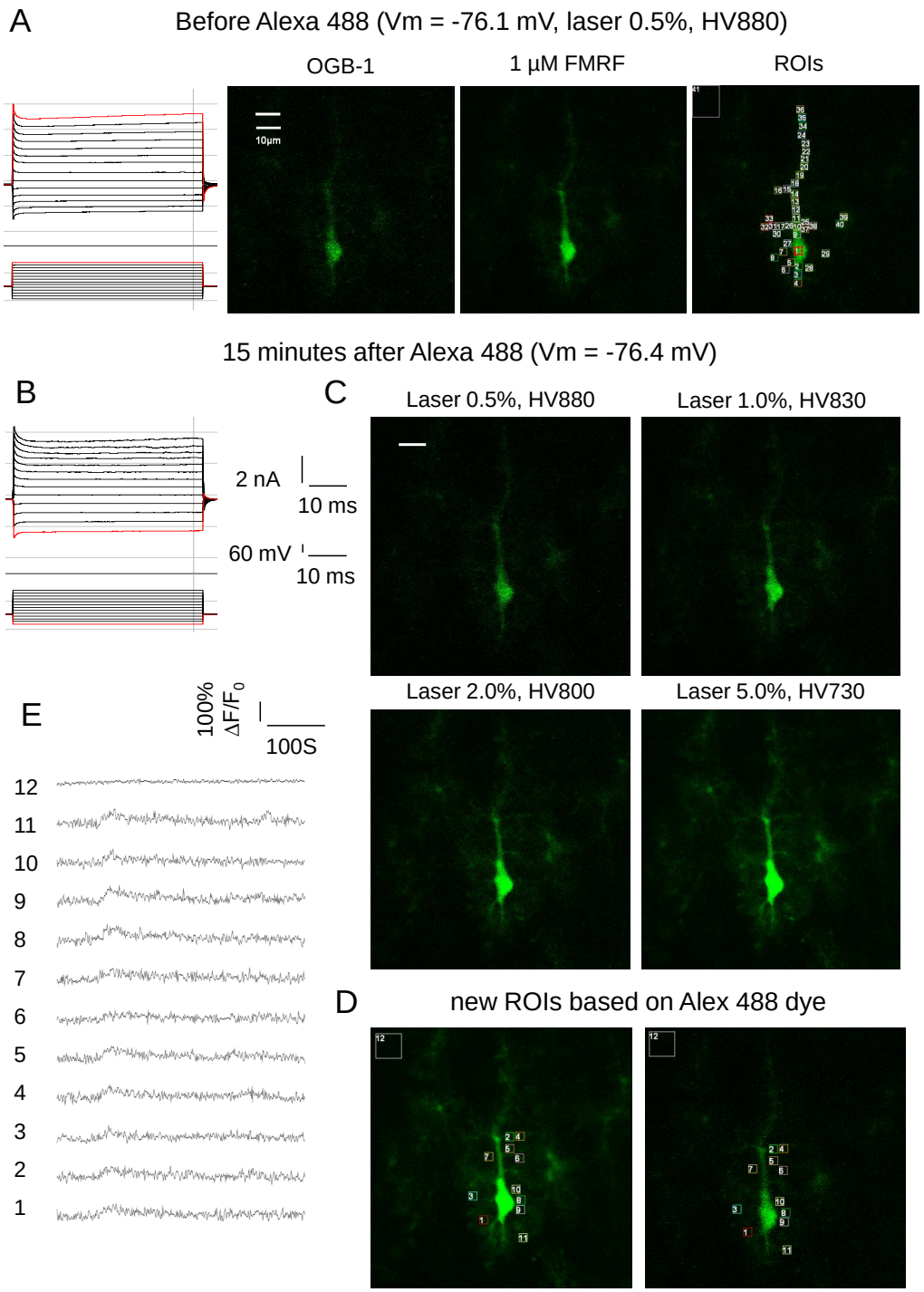

Figure 2.10 Exposure to high laser power induced increase in spontaneous $Ca^{2+}$ activity in astrocyte processes

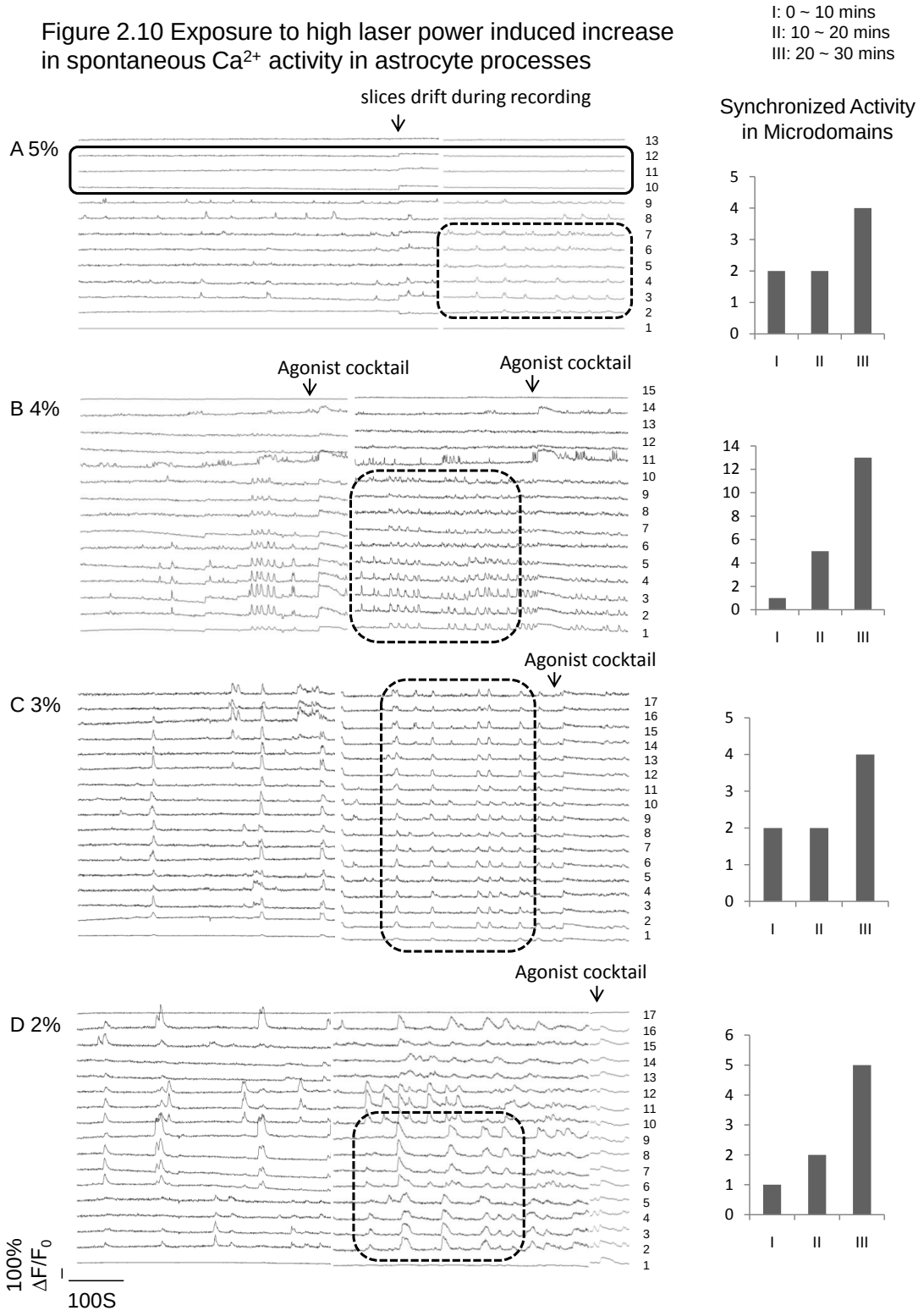

Figure 2.11 Long-term effects on spontaneous $Ca^{2+}$ activity in microdomains

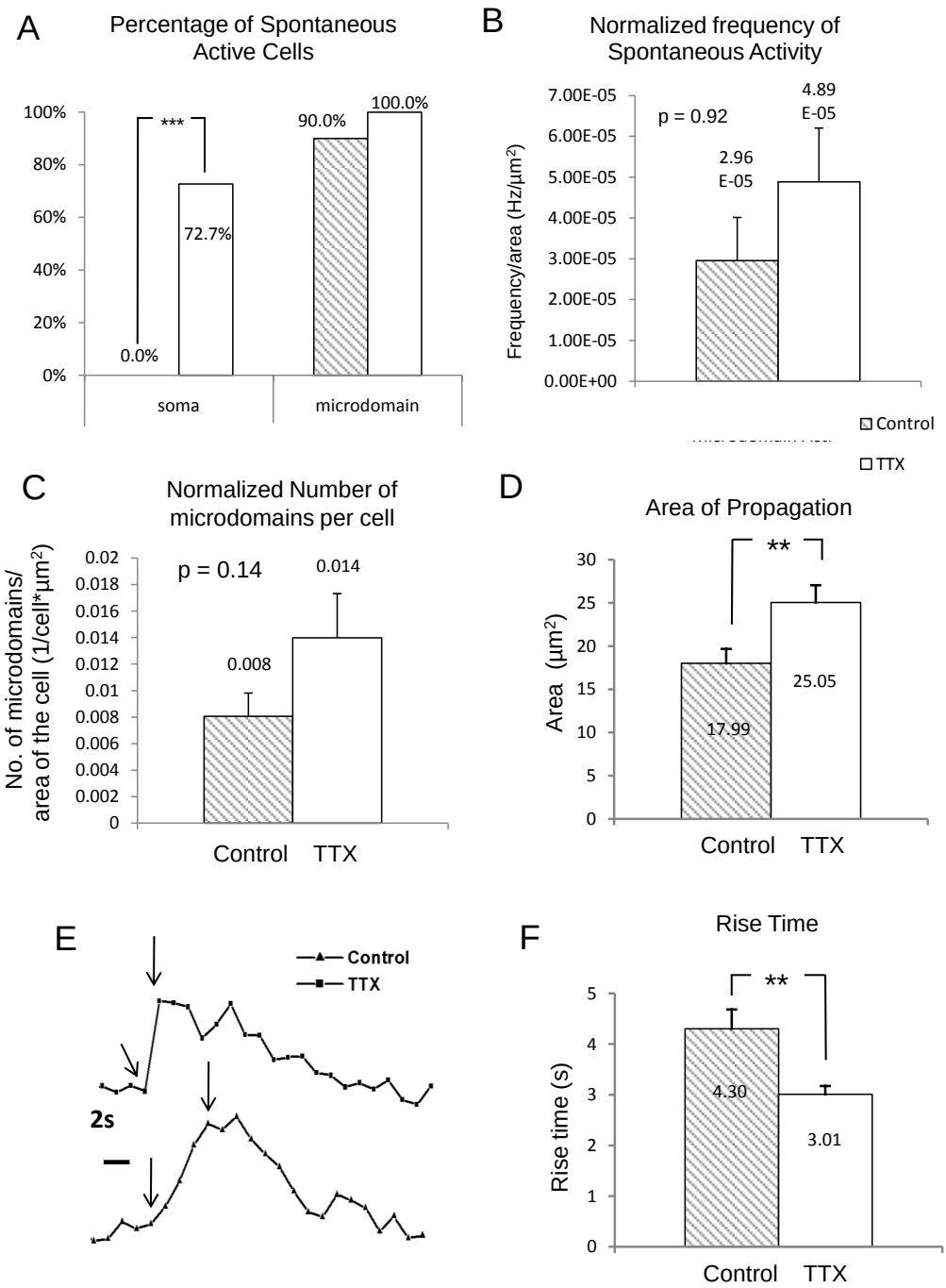

Figure 2.12 Long-term effects on evoked $Ca^{2+}$ responses occurred in microdomains

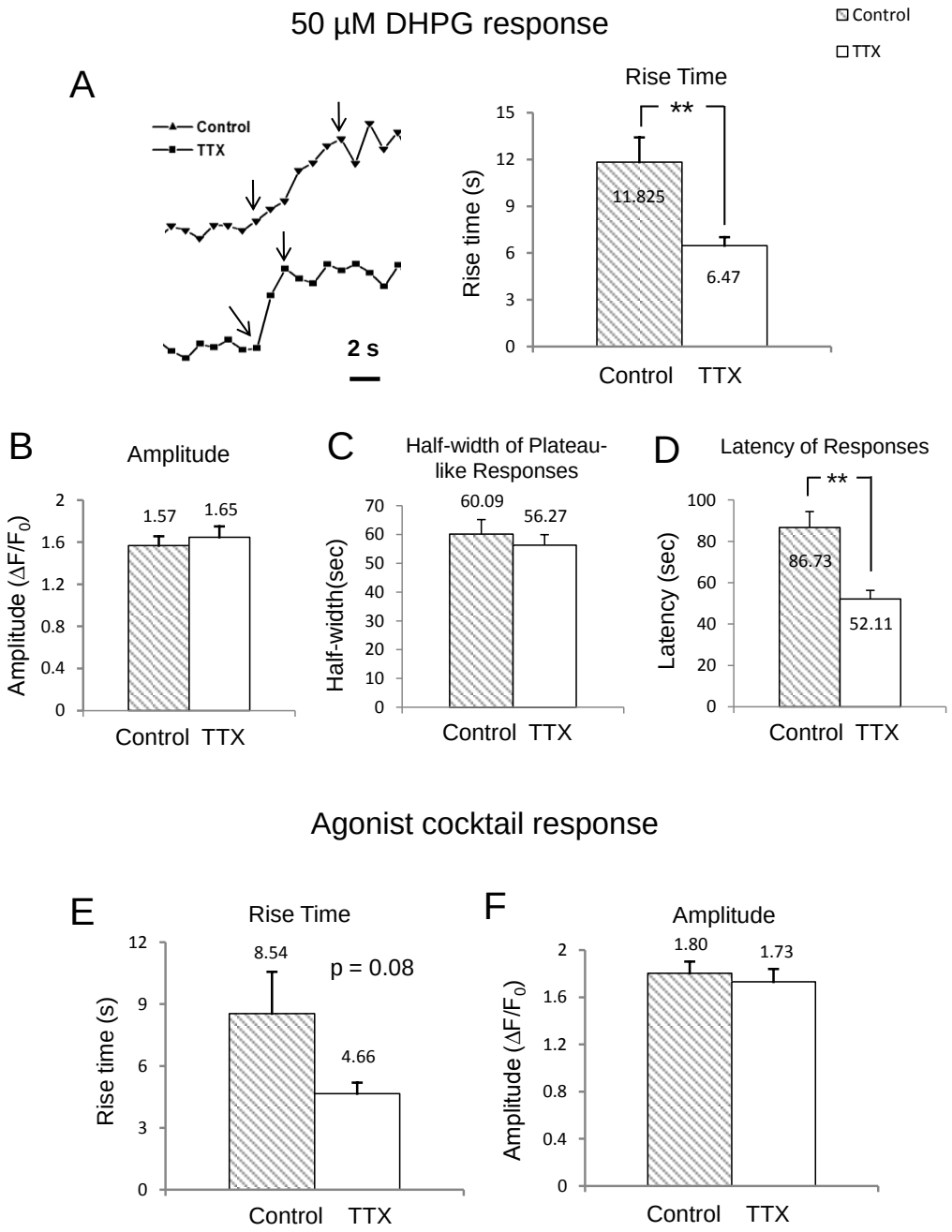

## Chapter 3: Decreased astrocytic Gq GPCR signaling following 4 to 6 hour elevation of CA3-CA1 synaptic transmission by 5.0 mM $[K^+]_o$

### 3.1 Abstract

In a previous chapter, we have provided evidence suggesting that hippocampal s.r. astrocytes exhibit long-term plasticity of their group I mGluR signaling activity after long-term blockade of CA3 to CA1 neuronal synaptic transmission. In this chapter, the goal is to determine if *increasing* the basal level of neuronal synaptic transmission *reduces* spontaneous and evoked group I mGluR signaling activity. To this end, acute hippocampal slices were incubated in 5.0 mM $[K^+]_o$ ACSF and the astrocytic group I mGluR activity compared to slices incubated in 2.5 mM $[K^+]_o$ ACSF. We find that s.r. astrocytes incubated in 5.0 mM $[K^+]_o$ ACSF for 4 to 6 hours showed: 1) a lower percentage of cells in the population exhibiting spontaneous Gq GPCR activity; 2) a lower percentage of cells within the population exhibiting spontaneous Gq GPCR activity; 3) a lower percentage of microdomains in the same cells exhibiting evoked responses to group I mGluR agonist; 4) slower rise times of the spontaneous and evoked $Ca^{2+}$ elevations in both astrocyte soma and fine processes; 5) prolonged latencies of $Ca^{2+}$ responses to bath application of group I mGluR agonist; and, 5) a significant shift in the pattern of $Ca^{2+}$ responses toward single peak vs. multipeak or plateau responses to group I mGluR agonist. These data are in the exact opposite direction as the findings after blockade of neuronal activity and strongly suggest that the scaling effect on astrocytic group I mGluRs occurs bidirectionally depending upon the direction of signaling,

specifically, the group I mGluR signaling in astrocytes in response to long-term changes of neuronal synaptic transmission.

## 3.2 Introduction

In Chapter 1, experimental data is provided to suggest that hippocampal s.r. astrocytes increase their group I mGluR signaling capability after long-term blockade of CA3 to CA1 neuronal synaptic transmission. If the observed changes in astrocytic Gq GPCR activity occur as a direct consequence of a reduction in neuronal action potentials, then the effect should be reversible when neuronal action potential frequency is significantly elevated. To test this, we compared spontaneous and evoked astrocyte Gq GPCR activity between acute hippocampal slices incubated in 5.0 mM $[K^+]_o$ ACSF to slices incubated in 2.5 mM $[K^+]_o$ ACSF (control). The 2.5 mM $[K^+]_o$ condition was chosen as the control as evidence was provided in Chapter 1 that neurons only very rarely fire spontaneous action potentials in these conditions. Therefore, 2.5 mM $[K^+]_o$ provides an ideal basal neuronal firing rate to determine if elevating neuronal activity using 5 mM $[K^+]_o$ leads to long-term depression of astrocytic Gq GPCR activity. As in the previous chapter, 300 μm hippocampal slices from P12 to P18 mice were used. After recovery from the dissection, acute hippocampal slices were incubated in ACSF containing either 2.5 mM or 5.0 mM $[K^+]_o$ ACSF for 4 to 6 hours. We hypothesized that Gq GPCR activity in hippocampal s.r. astrocytes would change in a direction suggesting a long-term reduction in surface receptor expression levels.

Functional astrocytic mGluR expression levels were evaluated by monitoring the spontaneous and evoked $Ca^{2+}$ transients following the 4 to 6 hour incubation in control or elevated $[K^+]_o$ ACSF. Based on the pharmacological studies *in vitro* on the relationship

between changes in Gq GPCR expression levels and effects on spontaneous and agonist evoked Gq GPCR $Ca^{2+}$ transients, we expected that s.r. astrocytes incubated in 5.0 mM $[K^+]_o$ ACSF for 4 to 6 hours would show: 1) a lower percentage of cells in a population exhibiting spontaneous Gq GPCR activity; 2) a lower percentage of cells within a population exhibiting evoked responses to agonist; and, 3) prolonged response latencies or rise times to the agonist (Shao and McCarthy, 1993; Wang and Thompson, 1994; de Ligt et al., 2000; Hermans and Challiss, 2001; Ostasov et al., 2008).

Using two different dye delivery techniques to study spontaneous and evoked $Ca^{2+}$ activity in both microdomains and cell bodies of s.r. astrocytes, we discovered that incubation of slices in 5 mM $[K^+]_o$ caused a significant decrease in the percentage of s.r. astrocytes exhibiting spontaneous $Ca^{2+}$ activity, a significant decrease in the probability of responding to the group I mGluR agonist DHPG, a highly significant increase in evoked mGluR response rise times in both astrocyte soma and microdomains, and a significant increase in evoked mGluR response latency in microdomains. These changes suggest that astrocytes scale down their group I mGluR signaling following increases in neuronal synaptic transmission.

## 3.3 Material and methods

### *Preparation of acute hippocampal slices.*

All mice were housed in the animal facility at the University of California, Riverside in accordance with Institutional Animal Care and Use Committee guidelines. 12- to 18-day-old C57BL/6J (Jackson Laboratory, Bar Harbor, ME) mice were

anaesthetized using isoflurane and decapitated. Parasagittal hippocampal slices were prepared using a Leica VT1200s Vibratome (Bannockburn, IL). Slices were prepared in ice-cold, oxygenated $Ca^{2+}$-free saline (see chapter 1). Subsequently, slices were incubated for 45 minutes at 35°C in oxygenated ACSF (see Chapter 1). Slices were incubated in either 2.5 mM $[K^+]_o$ ACSF (control) or in ACSF containing 5.0 mM $[K^+]_o$. Following the incubation period individual slices were transferred to a recording chamber and continuously superfused with oxygenated, room temperature ACSF of the same $[K^+]_o$ that they were incubated in. During recording, 1 μM TTX was added to the ACSF in order to isolate direct astrocyte responses to agonist.

***Whole cell recording of CA3 neuron spontaneous firing rate.***

Neuronal pipettes were prepared then filled with an internal solution as previous described (see Chapter 1). Slices were constantly perfused with oxygenated room-temp ACSF with in either 2.5 mM or 5.0 mM $[K^+]_o$. Whole-cell patch-clamp recording of neurons was performed by using a Multiclamp 700B amplifier and PCLAMP 10.2.014 software (Axon Instruments, Union City, CA). CA3 neurons on average displayed a resting $V_m$ of ~60.6 mV in 2.5 mM $[K^+]_o$ ACSF and ~50.5 mV in 5.0 mM $[K^+]_o$ ACSF. Upon attaining the whole-cell configuration, the cell membrane potential, input resistance, and access resistance were recorded and continuously monitored during gap free recording of membrane potential. Data obtained from neurons with any parameters changed by more than 20% were excluded. Numbers of spontaneous action potentials from each recording were analyzed in PCLAMP 10.2.014 software.

***Astrocyte patch clamp and loading with $Ca^{2+}$ indicator.***

Astrocyte pipettes were made and filled with an internal solution as previous described (see chapter 1). The internal solution also included was 200 μM of the cell-impermeant version of the $Ca^{2+}$ indicator dye OGB-1 (Invitrogen). Whole-cell patch-clamp recordings of astrocytes were performed as precious described (see Chapter 1). Astrocytes displayed a resting $V_m$ of ~77.8 mV in 2.5 mM $[K^+]_o$ standard ACSF and a resting $V_m$ of ~69.7 mV in 5.0 mM $[K^+]_o$ ACSF. Voltage step protocol and test pulses of -5 mV were used to verify the identity of passive astrocytes. A smooth, stable off-cell and formation of an outside-out patch was a strong indicator of minimal damage to the cell membrane during the patch clamp procedure.

***Bolus-loading of astrocytes with $Ca^{2+}$ indicator.***

For bolus-loading experiments, 1 μM SR-101 was used in place of OGB-1 during the first 45 minute incubation period for to label astrocytes. A field of s.r. astrocytes in was then loaded with OGB-1 AM $Ca^{2+}$ indicator dye using a backpressure, bolus-loading technique (Nimmerjahn et al., 2004; Sullivan et al., 2005; Garaschuk et al., 2006).

***Confocal imaging and monitoring of astrocyte $Ca^{2+}$ activity.***

Stratum radiatum of CA1 was visualized and individual s.r. astrocytes were identified as previous described (see Chapter 1). After loading with the calcium indicator, the fluorescence intensity of calcium indicator dye over time was recorded in astrocytes on a fixed focal plane. In all experiments, only a single (field of) astrocyte(s) was

recorded per slice to eliminate the possibility of double-sampling or changes due to multiple agonist applications. Astrocytes exhibiting at least one spontaneous $Ca^{2+}$ elevation were counted as spontaneously active cells. All recordings were completed within 40 minutes to reduce the possible TTX scaling effect on control slices and to limit possible phototoxicity. The viability of astrocyte(s) in each recording was verified by bath application of agonist cocktail (see Chapter 1). Astrocytes not responding to the agonist cocktail application were excluded from analysis.

***Analysis of astrocyte Gq GPCR $Ca^{2+}$ activity and Statistics.***

Slices or single astrocytes from patch clamp experiments were given a numeric code and analyzed as previous described (see Chapter 1). The amplitudes, frequencies and kinetics of the spontaneous Gq GPCR signaling events and agonist-evoked mGluR responses were compared between treatment groups. Spontaneous $Ca^{2+}$ transients covering over $\geq$ 75% of the planar area of the cell were defined as whole cell $Ca^{2+}$ elevations and analyzed separately. Analysis was done using number of astrocytes as 'n' for bulk-loading and bolus loading experiments, and number of microdomains for patch-clamp experiments. Student's independent *t*-test was used for statistical comparison of means between the control and treated groups. Pearson's chi-square test was used for comparison of the $Ca^{2+}$ activity patterns between control and treatment groups. Fisher's exact 2-tail test was used for comparison of the frequency of specific $Ca^{2+}$ activity pattern between control and treatment groups. Significance is described at the 0.05, 0.01, or 0.001 levels.

## 3.4 Results

### 3.4.1 5.0 mM extracellular potassium concentration was used in order to elevate the frequency of CA3-CA1 synaptic transmission

To test if astrocytic Gq GPCR activity changes as a direct consequence of an increase in neuronal action potentials, we compared spontaneous and evoked astrocyte Gq GPCR activity between acute hippocampal slices incubated in 5.0 mM $[K^+]_o$ ACSF to slices incubated in 2.5 mM $[K^+]_o$ ACSF (control). 2.5 mM $[K^+]_o$ was used as the control condition in these experiments because neurons very rarely fire spontaneous action potentials in these conditions (figure 3.1 A). Incubation in 5.0 mM $[K^+]_o$ resulted in a 10 mV depolarizing shift in resting membrane potential (figure 3.1 B). On average, CA3 neurons rested at -50.51 mV after incubated in 5.0 mM $[K^+]_o$ and CA3 neurons incubated in 2.5 mM $[K^+]_o$ ACSF rested around -60.60 mV.

In general, CA3 neurons gradually hyperpolarized during the 15 minute whole-cell recording. At the end of the recording, the CA3 neurons incubated in 5.0 mM $[K^+]_o$ ACSF rested at -52.96 mV and CA3 neurons incubated in control ACSF rested around -64.1 mV. There was still a significant difference in the membrane potentials between the two groups (figure 3.1 C). Because CA3 pyramidal neurons were depolarized in 5.0 mM $[K^+]_o$ ACSF, they exhibited a significantly higher rate of spontaneous action potentials compared to CA3 neurons in control incubated slices (figure 3.1 D and E).

### 3.4.2 Decreased astrocytic mGluR spontaneous and evoked activity follows increased CA3-CA1 synaptic transmission using bolus-loading delivery of OGB-1 $Ca^{2+}$ indicator dye

We also tested fields of astrocytes bolus-loaded with $Ca^{2+}$ indicator dye for their spontaneous somatic Gq GPCR activity and responsivity to group I mGluR agonist, DHPG. A field of s.r. astrocytes was loaded with Oregon Green BAPTA-1 (OGB-1) AM $Ca^{2+}$ indicator dye using a backpressure, bolus-loading technique (Nimmerjahn et al., 2004; Sullivan et al., 2005; Garaschuk et al., 2006). This technique allows study of a large population of hippocampal s.r. astrocytes within 30 - 50 μm deep into the slice, where astrocytes and their associations with synapses and cerebrovasculature are well maintained. Another advantage of this technique is that multiple concentrations of DHPG can be applied to further investigate the pattern shift of the agonist $Ca^{2+}$ response. Overlay of the SR-101 and OGB-1 AM signals was used to identify bolus-loaded cells as astrocytes (figure 3.2 A). In general, astrocytes incubated in 5.0 mM $[K^+]_o$ had fewer spontaneous $Ca^{2+}$ transients and weak DHPG-evoked $Ca^{2+}$ responses. However, these same astrocytes responded to Gq GPCR agonist cocktail consisting of 10 μM each of histamine, carbachol, and ATP in the same manner as astrocytes incubated in 2.5 mM $[K^+]_o$ (figure 3.2 B).

In 5.0 mM $[K^+]_o$ incubated slices, there was a significantly lower percentage of spontaneously active astrocytes (24.88% ± 7.80%) compared to control slices (59.08% ± 12.43%) for $Ca^{2+}$ activity recorded in the cell soma (figure 3.3 A, $p < 0.05$). In the whole

population, there was also a significantly lower percentage of spontaneously active astrocytes in 5.0 mM $[K^+]_o$ treated cells (25.49%) compared to untreated cells (57.69%) in the soma (figure 3.3 B, $p < 0.01$). Among all spontaneously active astrocytes, there was no difference in the frequency or the amplitude of the spontaneous $Ca^{2+}$ activity in the soma in 5.0 mM $[K^+]_o$ vs. control incubated slices (figure 3.3 C and D). Contrary to what we observed when slices were incubated in TTX, spontaneous somatic $Ca^{2+}$ elevations had slower rise times in astrocytes incubated in 5.0 mM $[K^+]_o$ compared to controls (figure 3.3 E).

Three successive concentrations of DHPG (15 μM, 30 μM and 50 μM) were applied to the same slices to investigate the percentage of responding astrocytes to DHPG in the population as well as to compare the pattern of response to DHPG between control and 5.0 mM $[K^+]_o$ incubated slices. There were at least 5 minutes intervals in between DHPG application to avoid receptor desensitization of group I mGluRs. As the concentration of DHPG was increased, the percentage of the astrocytes that responded increased, as expected (figure 3.4, 2.5 mM $[K^+]_o$: n = 52 cells/10 slices; 5.0 mM $[K^+]_o$: n = 51 cells/10 slices). At all DHPG concentrations tested, 5.0 mM $[K^+]_o$ treated astrocytes were less likely to respond to DHPG, and the pattern of their responses shifted toward the weaker, single peak phenotype compared to astrocytes incubated in 2.5 mM $[K^+]_o$ ACSF (figure 3.4).

There were also changes in the rise times of group I mGluR mediated $Ca^{2+}$ responses to the different concentrations of DHPG tested. There was a trend toward

longer rise times in 15 μM DHPG in the 5.0 mM $[K^+]_o$ condition (figure 3.5 A, $p = 0.17$, 2.5 mM $[K^+]_o$: n = 19 cells; 5.0 mM $[K^+]_o$: n = 11 cells). When 30 μM and 50 μM DHPG were applied to hippocampal slices, s.r. astrocytes incubated in 5.0 mM $[K^+]_o$ for 4 to 6 hours had significantly slower rise times compared to cells in control slices (figure 3.5 A, to 30 μM DHPG: $p < 0.05$; to 50 μM DHPG: $p < 0.01$, 2.5 mM $[K^+]_o$: n = 29 cells; 5.0 mM $[K^+]_o$: n = 26 cells). There was no difference in the rise times of somatic $Ca^{2+}$ responses to agonist cocktail, which suggests that the scaling effect is primarily due to decreased functional expression of group I mGluRs specifically (figure 3.5 A, $p = 0.45$, 2.5 mM $[K^+]_o$: n = 52 cells; 5.0 mM $[K^+]_o$: n = 51 cells). There was no difference in the amplitude of somatic $Ca^{2+}$ responses at any concentration of DHPG or to agonist cocktail in 5.0 mM $[K^+]_o$ treated vs. control slices (figure 3.5 B). There was also no significant difference in the latency of the $Ca^{2+}$ response to DHPG or agonist cocktail between the two groups (figure 3.5 C).

### 3.4.3 Long-term elevation of CA3-CA1 synaptic transmission led to deceased spontaneous Gq GPCR signaling in astrocytic microdomains

To test if the changes in group I mGluR signaling after 5.0 mM $[K^+]_o$ treatment in microdomains, OGB-1 $Ca^{2+}$ indicator dye was delivered into astrocytes via patch clamp, and the $Ca^{2+}$ activity monitored in both microdomains and soma. As we discussed in the previous chapter, most of the hippocampal s.r. astrocytes exhibited spontaneous $Ca^{2+}$ transients in microdomains. Such spontaneous $Ca^{2+}$ transients remained local and hardly propagated to other parts of the cell. Even though 100% of the cells exhibited

spontaneous $Ca^{2+}$ transients at least once in microdomain(s), only 16.7% of astrocytes in control ACSF showed detectable spontaneous $Ca^{2+}$ transients in their soma. After incubation in 5.0 mM $[K^+]_o$ ACSF for 4 to 6 hours, a lower percentage of s.r. astrocytes exhibited spontaneous $Ca^{2+}$ transients in their soma (9.1%; figure 3.6 A). Also, s.r. astrocytes from slices incubated in 5.0 mM $[K^+]_o$ ACSF exhibited a shift toward fewer spontaneous microdomains per cell ($p = 0.32$, figure 3.6 B). Among each microdomain that showed spontaneous $Ca^{2+}$ transients, the frequency, area of propagation and rise time of the spontaneous activity was compared between the two groups (2.5 mM $[K^+]_o$: n = 71 microdomains/12 cells; 5.0 mM $[K^+]_o$: n = 51 microdomains/11 cells). There was a trend toward a lower frequency of spontaneous $Ca^{2+}$ transients in microdomains from 5.0 mM $[K^+]_o$ treated s.r. astrocytes compared to control cells (figure 3.6 C). This might be due to the smaller number of microdomains per astrocyte incubated in 5.0 mM $[K^+]_o$. Area of microdomain propagation remained unchanged in the 5.0 mM $[K^+]_o$ treatment group (figure 3.6 D).

As predicted, rise time of microdomain spontaneous $Ca^{2+}$ transients in 5.0 mM $[K^+]_o$ treated astrocytes was significantly slower than rise times in control cells ($p < 0.01$ figure 3.6 E). The decreased number of microdomains per cell and the prolonged rise time of spontaneous microdomain activity after long-term 5.0 mM $[K^+]_o$ incubation suggests that the scaling effect on astrocytic Gq GPCR signaling in response to long-term changes in neuronal synaptic transmission is bi-directional.

To test if the group I mGluR signaling was decreased in response to elevation of neuronal synaptic transmission, 50 μM DHPG, the group I mGluR specific agonist, was applied to the bath. Consistent with our previous observations, group I mGluR-mediated $Ca^{2+}$ responses evoked by 50 μM DHPG exhibited no difference in amplitude or half width following incubation in 5 mM $[K^+]_o$ compared to the control group (figure 3.7 A and B, 2.5 mM $[K^+]_o$: n = 69 microdomains in 12 cells; 5.0 mM $[K^+]_o$: n = 37 microdomains in 11 cells). But there was a significantly slower DHPG evoked rise time following incubation in 5 mM $[K^+]_o$ compared to the control group (figure 3.7 C, $p < 0.05$). Also, as seen after TTX treatment, the latency to group I mGluR-mediated $Ca^{2+}$ responses evoked by 50 μM DHPG increased significantly after incubation in 5 mM $[K^+]_o$ compared to the control group (figure 3.7 D, $p < 0.001$). These data suggest that elevated levels of neuronal synaptic transmission reduce the functional expression of astrocytic group I mGluRs, and that scaling of astrocytic group I mGluRs is therefore bidirectional.

At the end of the recordings, the agonist cocktail was applied to the cell to verify the responsiveness of all the microdomains. Consistent with the specificity of the TTX treatment-induced effect to group I mGluRs, there was no change in either the amplitude (figure 3.7 F) or rise time of the agonist cocktail-evoked responses after incubation in 5 mM $[K^+]_o$ (figure 3.7 G, $p = 0.18$), suggesting that group I mGluRs are the main astrocytic receptor type affected by changes in basal neuronal synaptic transmission (2.5 mM $[K^+]_o$: n = 69 microdomains in 12 cells; 5.0 mM $[K^+]_o$: n = 37 microdomains in 11 cells).

Application of agonist cocktail also showed that almost all microdomains that exhibited spontaneous $Ca^{2+}$ transients also responded to agonist cocktail. Interestingly, only a certain percentage of those microdomains responded to 50 μM DHPG after 5.0 mM $[K^+]_o$ incubation. 50 μM DHPG normally evokes a $Ca^{2+}$ response that incorporates the entire visible area of the astrocyte, but after a long-term increase in neuronal action potentials, only about 68.6% of all the microdomains responded to 50 μM DHPG ($p < 0.001$). Thus, about 31.4% of the spontaneously active microdomains in 5.0 mM $[K^+]_o$ ACSF incubated slices failed to respond to 50 μM DHPG application. In comparison, in control astrocytes 100% of the microdomains that were spontaneously active also responded to the 50 μM DHPG (figure 3.8 A; 2.5 mM $[K^+]_o$: n = 69 microdomains in 12 cells; 5.0 mM $[K^+]_o$: n = 51 microdomains in 11 cells).

Microdomains from astrocytes treated in 5 mM $[K^+]_o$ ACSF also exhibited a significant shift in the pattern of their $Ca^{2+}$ responses evoked by 50 μM DHPG. There was a shift towards the weaker single-peak evoked microdomain responses in 5.0 mM $[K^+]_o$ treated cells compared to control cells (figure 3.8 A, $p < 0.01$ for the percentage of plateau responses between the two groups). At the somatic level, the same decrease in responsiveness and pattern shift to 50 μm DHPG was observed. There were 27.3% of the astrocytes that failed to show any detectable response to 50 μM DHPG in the soma (figure 3.8 B, $p < 0.05$ for the percentage of non-responders), while 100% of the control cells responded, 70% with a plateau–like long-lasting $Ca^{2+}$ elevations. These data are exactly opposite to what we observed when slices were incubated in TTX and is a strong

indication that the functional expression of astrocytic mGluRs scale down in response to long-term increase in neuronal firing rates.

### 3.5 Discussion

Overall our data suggest that astrocytes actively sense long-term increases in basal neuronal firing rates with a decrease in functional expression of their group I mGluRs. Taken together with data obtained in Chapter 2, the findings suggest that astrocytic group I mGluRs exhibit long-term plasticity that is bi-directional depending upon the direction of long-term changes in neuronal synaptic transmission. Data were replicated using both patch clamp and bolus-loading approaches to load astrocytes with $Ca^{2+}$ indicator. After CA3-CA1 neurotransmission in hippocampal slices was elevated for 4 to 6 hours using 5.0 mM $[K^+]_o$ to depolarize neurons and increase their basal firing rates, the following changes in astrocyte $Ca^{2+}$ signaling were observed: 1) a significant decrease in the percentage of astrocytes exhibiting spontaneous $Ca^{2+}$ elevations; 2) significantly slower rise times of the spontaneous $Ca^{2+}$ transients; 3) a significant decrease in response probability to the group I mGluR agonist DHPG; and, 4) significantly slower rise times of evoked mGluR $Ca^{2+}$ responses. These changes were observed in both astrocytic somata as well as in microdomains. In agreement with previous reports of all-or-none astrocytic Gq GPCR responses upon achieving a threshold agonist concentration (Shao and McCarthy, 1995) and lack of correlation of Gq GPCR density to changes in response amplitudes (Shao and McCarthy, 1993), no changes were observed in average amplitude of either spontaneous astrocytic Gq GPCR activity or

evoked astrocyte mGluR $Ca^{2+}$ elevations. These data suggest that there is significant neuronal signaling to astrocytes taking place during basal levels of neuronal synaptic transmission, and provide a compelling indication of the sensitivity of active neuron-to-astrocyte communication in the brain.

We also observed a significantly longer latency in the evoked group I mGluR $Ca^{2+}$ responses in astrocyte microdomains after long-term 5.0 mM $[K^+]_o$ incubation. But there was no significant difference in the latency of somatic $Ca^{2+}$ responses to any of the DHPG concentrations used between the two groups (figure 3.5 C). As we observed in the TTX treatment condition, the difference in the latency was seen at the level of astrocyte microdomains, but not in the cell somata. It might be due to the different origins of responses in microdomains vs. the cell soma. $Ca^{2+}$ responses in microdomains initiate locally within the microdomains, in small astrocyte processes adjacent to neuronal synapses where the group I mGluRs are concentrated. Calcium responses to agonist in astrocyte somata often result from intracellular propagation of the $Ca^{2+}$ elevation that originated in the microdomain, and often result from integration of many $Ca^{2+}$ microdomains. The time it takes for $Ca^{2+}$ elevations in microdomains to successfully evoke a somatic $Ca^{2+}$ response varies between cells and this variation might contribute to the inability to detect a significant difference somatic $Ca^{2+}$ response latencies.

In addition to these changes, we also observed a dose-dependent shift in astrocytic $Ca^{2+}$ responses to DHPG in 5.0 mM $[K^+]_o$ vs. 2.5 mM $[K^+]_o$ (control) incubated slices. As discussed in the previous chapter, a characteristic of group I mGluRs is that the $Ca^{2+}$

response pattern is graded from single peak, to oscillatory ("multipeak"), to plateau as the agonist concentration is increased (Dolmetsch et al., 1998; Hu et al., 1999; Shelton and McCarthy, 1999; Hermans and Challiss, 2001). Bath application of 15 μM DHPG evoked $Ca^{2+}$ responses in 37% of bolus-loaded astrocytes in control conditions. In contrast, only 22% of the astrocytes in 5.0 mM $[K^+]_o$ treated slices responded to 15 μM DHPG. When 30 μM DHPG was applied to control slices, 56% of astrocytes responded while only 34% of the cells from 5.0 mM $[K^+]_o$ treated slices responded to the same concentration of DHPG ($p < 0.05$). Finally, 60% of astrocytes from control slices responded to 50 μM DHPG while only 50% cells from 5.0 mM $[K^+]_o$ treated slices responded to 50 μM DHPG. These differences in the percentage of responding cells in the population suggest a decrease on the agonist-receptor binding probability, indicating lower level of functional receptor expression in 5.0 mM $[K^+]_o$ treated cells.

A similar pattern shift was observed in astrocyte microdomains when 50 μM DHPG was applied to astrocytes filled with $Ca^{2+}$ indicator dye via patch clamp. All identified spontaneous microdomains from both groups of astrocytes readily responded to agonist cocktail. Actually, there were about 6% of microdomains in control astrocytes that did not respond to agonist cocktail, while all of the microdomains in 5.0 mM $[K^+]_o$ treated cells showed a detectable $Ca^{2+}$ response to agonist cocktail. When 50 μM DHPG was applied to control astrocytes, 97% of the microdomains from all the cells responded to DHPG, the agonist of group I mGluRs. These data suggested that mGluRs were expressed in almost all of the microdomains in control astrocytes. When hippocampal slices were incubated in 5.0 mM $[K^+]_o$ for 4 to 6 hours, 32% of the microdomains that

exhibited spontaneous activity and evoked responses to agonist cocktail failed to respond to 50 μM DHPG. This was a startling finding that suggests that the functional expression of group I mGluRs in microdomains scaled downward following long-term increase in neuronal action potential frequency, while the expression level and constitutive activity of other Gq GPCRs remained unaltered. The data from microdomains suggests the possibility that bi-directional plasticity of astrocytic receptors also occurs in microdomains in response to long-term changes in synaptic activity.

### 3.6 References

de Ligt RA, Kourounakis AP, AP IJ (2000) Inverse agonism at G protein-coupled receptors: (patho)physiological relevance and implications for drug discovery. British journal of pharmacology 130:1-12.

Dolmetsch RE, Xu K, Lewis RS (1998) Calcium oscillations increase the efficiency and specificity of gene expression. Nature 392:933-936.

Garaschuk O, Milos RI, Konnerth A (2006) Targeted bulk-loading of fluorescent indicators for two-photon brain imaging in vivo. Nat Protoc 1:380-386.

Hermans E, Challiss RA (2001) Structural, signalling and regulatory properties of the group I metabotropic glutamate receptors: prototypic family C G-protein-coupled receptors. Biochem J 359:465-484.

Hu Q, Deshpande S, Irani K, Ziegelstein RC (1999) [Ca(2+)](i) oscillation frequency regulates agonist-stimulated NF-kappaB transcriptional activity. J Biol Chem 274:33995-33998.

Nimmerjahn A, Kirchhoff F, Kerr JN, Helmchen F (2004) Sulforhodamine 101 as a specific marker of astroglia in the neocortex in vivo. Nat Methods 1:31-37.

Ostasov P, Krusek J, Durchankova D, Svoboda P, Novotny J (2008) Ca2+ responses to thyrotropin-releasing hormone and angiotensin II: the role of plasma membrane integrity and effect of G11alpha protein overexpression on homologous and heterologous desensitization. Cell Biochem Funct 26:264-274.

Shao Y, McCarthy KD (1993) Quantitative relationship between alpha 1-adrenergic receptor density and the receptor-mediated calcium response in individual astroglial cells. Mol Pharmacol 44:247-254.

Shao Y, McCarthy KD (1995) Receptor-mediated calcium signals in astroglia: multiple receptors, common stores and all-or-nothing responses. Cell Calcium 17:187-196.

Shelton MK, McCarthy KD (1999) Mature hippocampal astrocytes exhibit functional metabotropic and ionotropic glutamate receptors in situ. Glia 26:1-11.

Sullivan MR, Nimmerjahn A, Sarkisov DV, Helmchen F, Wang SS (2005) In vivo calcium imaging of circuit activity in cerebellar cortex. J Neurophysiol 94:1636-1644.

Wang SS, Thompson SH (1994) Measurement of changes in functional muscarinic acetylcholine receptor density in single neuroblastoma cells using calcium release kinetics. Cell Calcium 15:483-496.

**Figure Legends**

**Figure 3.1 CA3 pyramidal neurons incubated in 5.0 mM $[K^+]_o$ ACSF are significantly depolarized with increased spontaneous firing rates.**

(A) Whole cell recording of CA3 pyramidal neurons incubated in either 2.5 mM or 5.0 mM $[K^+]_o$ ACSF. CA3 neurons were significantly depolarized in 5 mM $[K^+]_o$ ACSF and regularly fired action potentials (2.5 mM $[K^+]_o$: n = 12 cells; 5.0 mM $[K^+]_o$: n = 14 cells). Scale bar: 20 mV/ 5 sec.

(B) CA3 neurons incubated in 5.0 mM $[K^+]_o$ ACSF had significantly depolarized resting membrane potentials compared to CA3 neurons incubated in 2.5 mM $[K^+]_o$ ACSF (2.5 mM $[K^+]_o$: n = 12 cells; 5.0 mM $[K^+]_o$: n = 14 cells; $p< 0.001$). Error bars represent S.E.M.

(C) CA3 neurons gradually hyperpolarized during the 15 minute whole-cell recording. At the end of recording, CA3 neurons incubated in 5.0 mM $[K^+]_o$ ACSF had significantly depolarized resting membrane potentials compared to CA3 neurons incubated in 2.5 mM $[K^+]_o$ ACSF (2.5 mM $[K^+]_o$: n = 12 cells; 5.0 mM $[K^+]_o$: n = 14 cells; $p < 0.001$). Error bars represent S.E.M.

(D) CA3 neurons incubated in 5.0 mM $[K^+]_o$ ACSF had significantly elevated spontaneous firing rates compared to those incubated in 2.5 mM $[K^+]_o$ ACSF (2.5 mM $[K^+]_o$: n = 12 cells; 5.0 mM $[K^+]_o$: n = 14 cells; $p < 0.01$). Error bars represent S.E.M.

(E) The distribution of the frequency of spontaneous action potentials from individual CA3 neurons tested (2.5 mM $[K^+]_o$: n = 12 cells; 5.0 mM $[K^+]_o$: n = 14 cells). Error bars represent S.E.M.

**Figure 3.2 Representative data of s.r. astrocytes in CA1 region of acute hippocampal slices bolus-loaded with $Ca^{2+}$ indicator.**

(A) s.r. astrocytes bolus-loaded with OGB-1 AM $Ca^{2+}$ indicator dye and the astrocyte-specific marker SR-101 in a 2.5 mM $[K^+]_o$ incubated (upper panels) and 5.0 mM $[K^+]_o$ incubated (lower panels) slice. Numbered ROIs match $Ca^{2+}$ traces in (B). Scale bar: 10 μm.

(B) Representative astrocyte $Ca^{2+}$ activity in astrocyte somata over time in the 2.5 mM $[K^+]_o$ incubated (upper) and 5.0 mM $[K^+]_o$ incubated (lower) slice shown in (A). 5.0 mM $[K^+]_o$ treated astrocytes were less likely to exhibit spontaneous somatic $Ca^{2+}$ transients. They also showed marked differences in their DHPG evoked responses, including a smaller percentage of responding cells, and a shift away from the plateau-like pattern at all the DHPG concentrations tested. This is summarized in figure 3.8 (2.5 mM $[K^+]_o$: n = 52 cells/10 slices; 5.0 mM $[K^+]_o$: n = 51 cells/10 slices). Note that the amplitude of the astrocyte $Ca^{2+}$ responses was unaffected. Scale bar: 100% $\Delta F/F_0$/100 seconds.

**Figure 3.3 Astrocyte soma exhibit changes in spontaneous astrocyte $Ca^{2+}$ transients following incubation in 5.0 mM $[K^+]_o$ ACSF.**

(A) The percentage of spontaneously active astrocytes was significantly lower in 5.0 mM $[K^+]_o$ ACSF treated vs. control slices (2.5 mM $[K^+]_o$: n = 52 cells/10 slices; 5.0 mM $[K^+]_o$: n = 51 cells/10 slices). Error bars represent S.E.M.

(B) The percentage of astrocytes in the population exhibiting spontaneous $Ca^{2+}$ transients in their soma was significantly lower following 5.0 mM $[K^+]_o$ ACSF treatment ($p < 0.01$, 2.5 mM $[K^+]_o$: n = 52 cells/10 slices; 5.0 mM $[K^+]_o$: n = 51 cells/10 slices).

(C) The frequency of somatic spontaneous $Ca^{2+}$ transients was similar between the groups (2.5 mM $[K^+]_o$: n = 30 cells; 5.0 mM $[K^+]_o$: n = 13 cells). Error bars represent S.E.M.

(D) Rise times of somatic spontaneous $Ca^{2+}$ transients in 5.0 mM $[K^+]_o$ treated astrocytes were significantly slower compared to the control group (2.5 mM $[K^+]_o$: n = 30 cells; 5.0 mM $[K^+]_o$: n = 13 cells; $p < 0.05$). Error bars represent S.E.M.

(E) Amplitude of somatic spontaneous $Ca^{2+}$ transients remained unchanged after 5.0 mM $[K^+]_o$ treatment (2.5 mM $[K^+]_o$: n = 30 cells; 5.0 mM $[K^+]_o$: n = 13 cells). Error bars represent S.E.M.

**Figure 3.4 Summary of the pattern of evoked astrocyte somatic $Ca^{2+}$ responses to 15 µM, 30 µM, 50 µM DHPG and agonist cocktail in 2.5 mM $[K^+]_o$ and 5.0 mM $[K^+]_o$ incubated slices.**

In all DHPG concentrations tested, there was a lower percentage of 5.0 mM $[K^+]_o$ treated astrocytes that responded to DHPG, and a shift away from plateau-like responses toward

the weaker single-peak phenotype, compared to astrocytes incubated in 2.5 mM $[K^+]_o$ (2.5 mM $[K^+]_o$: n = 52 cells/10 slices; 5.0 mM $[K^+]_o$: n = 51 cells/10 slices). To 30 μM DHPG, the percentage of non-responding cells and the percentage of the cells exhibit plateau-like responses are significant different between the two groups ($p < 0.05$).

**Figure 3.5 Summary of effects of elevating neuronal action potentials in 5.0 mM $[K^+]_o$ ACSF on DHPG evoked somatic astrocyte $Ca^{2+}$ responses.**

(A) 5.0 mM $[K^+]_o$ treated astrocytes had slower rise times of their evoked $Ca^{2+}$ responses to different concentrations of DHPG. There was a significant difference between the control and 5.0 mM $[K^+]_o$ incubated groups in the rise time of somatic evoked $Ca^{2+}$ responses to 30 μM and 50 μM DHPG (to 15 μM DHPG: $p = 0.17$, 2.5 mM $[K^+]_o$: n = 19 cells; 5.0 mM $[K^+]_o$: n = 11 cells; to 30 μM DHPG: $p < 0.05$, 2.5 mM $[K^+]_o$: n = 28 cells; 5.0 mM $[K^+]_o$: n = 17 cells; to 50 μM DHPG: $p < 0.01$, 2.5 mM $[K^+]_o$: n = 29 cells; 5.0 mM $[K^+]_o$: n = 26 cells). There was no difference in agonist cocktail-evoked rise times between 5.0 mM $[K^+]_o$ treated and control cells ($p= 0.45$, 2.5 mM $[K^+]_o$: n = 52 cells; 5.0 mM $[K^+]_o$: n = 51 cells). Error bars represent S.E.M.

(B) There was no difference in the amplitude of somatic astrocyte $Ca^{2+}$ responses at all concentrations of DHPG or agonist cocktail tested between the two groups (to 15 μM DHPG: 2.5 mM $[K^+]_o$: n = 19 cells; 5.0 mM $[K^+]_o$: n = 11 cells; to 30 μM DHPG: 2.5 mM $[K^+]_o$: n = 28 cells; 5.0 mM $[K^+]_o$: n = 17 cells; to 50 μM DHPG: 2.5 mM $[K^+]_o$: n = 29 cells; 5.0 mM $[K^+]_o$: n = 26 cells; to agonist cocktail: 2.5 mM $[K^+]_o$: n = 52 cells; 5.0 mM $[K^+]_o$: n = 51 cells). Error bars represent S.E.M.

(C) There was no difference in the latency of somatic astrocyte $Ca^{2+}$ responses at all concentrations of DHPG or agonist cocktail tested between the two groups (to 15 μM DHPG: 2.5 mM $[K^+]_o$: n = 19 cells; 5.0 mM $[K^+]_o$: n = 11 cells; to 30 μM DHPG: 2.5 mM $[K^+]_o$: n = 28 cells; 5.0 mM $[K^+]_o$: n = 17 cells; to 50 μM DHPG: 2.5 mM $[K^+]_o$: n = 29 cells; 5.0 mM $[K^+]_o$: n = 26 cells; to agonist cocktail: 2.5 mM $[K^+]_o$: n = 52 cells; 5.0 mM $[K^+]_o$: n = 51 cells). Error bars represent S.E.M.

**Figure 3.6 Decreased spontaneous Gq GPCR activity in astrocyte microdomains after 4 to 6 hr incubation in 5.0 mM $[K^+]_o$ ACSF .**

(A) Spontaneous $Ca^{2+}$ transients occurred in microdomains of all s.r. astrocytes, but astrocytes incubated in 5.0 mM $[K^+]_o$ ACSF had a lower percentage of spontaneous activity in the soma compared to control astrocytes (2.5 mM $[K^+]_o$: n = 12 cells; 5.0 mM $[K^+]_o$: n = 14 cells).

(B) 5.0 mM $[K^+]_o$ treated astrocytes exhibited a trend toward a lower number of microdomains per cell compared to the controls (2.5 mM $[K^+]_o$: n = 71 microdomains in 12 cells; 5.0 mM $[K^+]_o$: n = 51 microdomains in 11 cells; p = 0.32). Error bars represent S.E.M.

(C) There was no significant change in the frequency of spontaneous microdomain $Ca^{2+}$ transients between the 5.0 mM $[K^+]_o$ treated astrocytes compared to the controls (2.5 mM $[K^+]_o$: n = 12 cells; 5.0 mM $[K^+]_o$: n = 11 cells). Error bars represent S.E.M.

(D) There was no significant difference in the areas of propagation of spontaneous microdomain $Ca^{2+}$ transients between 5.0 mM $[K^+]_o$ treated astrocytes and control cells (2.5 mM $[K^+]_o$: n = 71 microdomains in 12 cells; 5.0 mM $[K^+]_o$: n = 51 microdomains in 11 cells). Error bars represent S.E.M.

(E) Spontaneous microdomain $Ca^{2+}$ transients in 5.0 mM $[K^+]_o$ treated cells had significantly slower rise times compared to controls (2.5 mM $[K^+]_o$: n = 71 microdomains in 12 cells; 5.0 mM $[K^+]_o$: n = 51 microdomains in 11 cells; $p < 0.01$). Error bars represent S.E.M.

**Figure 3.7 Astrocyte microdomains in slices incubated in 5.0 mM $[K^+]_o$ had significantly slower rise times compared to control incubated astrocytes.**

(A) There was no change in amplitude of 50 μM DHPG evoked $Ca^{2+}$ responses between 5.0 mM $[K^+]_o$ treated astrocytes and control cells (2.5 mM $[K^+]_o$: n = 69 microdomains in 12 cells; 5.0 mM $[K^+]_o$: n = 37 microdomains in 11 cells). Error bars represent S.E.M.

(B) There was no change in half width of 50 μM DHPG evoked $Ca^{2+}$ responses between 5.0 mM $[K^+]_o$ vs. 2.5 mM $[K^+]_o$ treated astrocytes (2.5 mM $[K^+]_o$: n = 49 microdomains in 12 cells; 5.0 mM $[K^+]_o$: n = 13 microdomains in 11 cells). Only plateau type responses were included in this analysis. Error bars represent S.E.M.

(C) Rise times of evoked responses to 50 μM DHPG analyzed in microdomains were significantly slower in astrocytes incubated in 5.0 mM $[K^+]_o$ vs. 2.5 mM $[K^+]_o$ ACSF (2.5

mM $[K^+]_o$: n = 69 microdomains in 12 cells; 5.0 mM $[K^+]_o$: n = 37 microdomains in 11 cells; $p < 0.05$). Error bars represent S.E.M.

(D) Latency of the evoked responses to 50 μM DHPG analyzed in microdomains was significantly longer in the astrocytes incubated in 5.0 mM $[K^+]_o$ vs. 2.5 mM $[K^+]_o$ ACSF (2.5 mM $[K^+]_o$: n = 69 microdomains in 12 cells; 5.0 mM $[K^+]_o$: n = 37 microdomains in 11 cells; $p < 0.001$). Error bars represent S.E.M.

(E) Rise time of evoked responses to the agonist cocktail in microdomains remained unchanged (2.5 mM $[K^+]_o$: n = 69 microdomains in 12 cells; 5.0 mM $[K^+]_o$: n = 51 microdomains in 11 cells; $p = 0.18$). Error bars represent S.E.M.

(F) There was no change in the amplitude of evoked responses to the agonist cocktail in microdomains between 5.0 mM $[K^+]_o$ treated astrocytes vs. controls (2.5 mM $[K^+]_o$: n = 69 microdomains in 12 cells; 5.0 mM $[K^+]_o$: n = 51 microdomains in 11 cells). Error bars represent S.E.M.

**Figure 3.8 Summary of the pattern of evoked $Ca^{2+}$ responses in astrocyte microdomains to 50 μM DHPG and agonist cocktail in control and 5.0 mM $[K^+]_o$ incubated slices.**

(A) Summary of the evoked response pattern in microdomains. 31.4% of microdomains in 5.0 mM $[K^+]_o$ treated astrocytes did not respond to 50 μM DHPG ($p < 0.001$), while only 2.8% of microdomains in 2.5 mM $[K^+]_o$ treated astrocytes did not respond. There was also a significant shift away from the plateau-like responses in the microdomains

after incubation in 5.0 mM $[K^+]_o$ toward the weaker, single-peak phenotype ($p < 0.01$, 2.5 mM $[K^+]_o$: n = 71 microdomains in 12 cells; 5.0 mM $[K^+]_o$: n = 51 microdomains in 11 cells). All the microdomains in 5.0 mM $[K^+]_o$ treated astrocytes and most of the microdomains in control astrocytes responded to agonist cocktail (2.5 mM $[K^+]_o$: n = 71 microdomains in 12 cells; 5.0 mM $[K^+]_o$: n = 51 microdomains in 11 cells).

(B) Summary of the evoked response pattern for somatic $Ca^{2+}$ responses., 27.3% of the astrocytes incubated in 5.0 mM $[K^+]_o$ did not respond to 50 μM DHPG ($p < 0.05$), and the ones that responded exhibited a shift away from the plateau-like response toward the weaker single-peak phenotype (2.5 mM: $[K^+]_o$: n = 12 cells; 5.0 mM $[K^+]_o$: n = 11 cells). All astrocytes from both groups responded to the agonist cocktail (2.5 mM: $[K^+]_o$: n = 12 cells; 5.0 mM $[K^+]_o$: n = 11 cells).

Figure 3.1 Comparison of neuronal activity between CA3 neurons incubated in 2.5mM $[K^+]_o$ and 5.0 mM $[K^+]_o$ ACSF

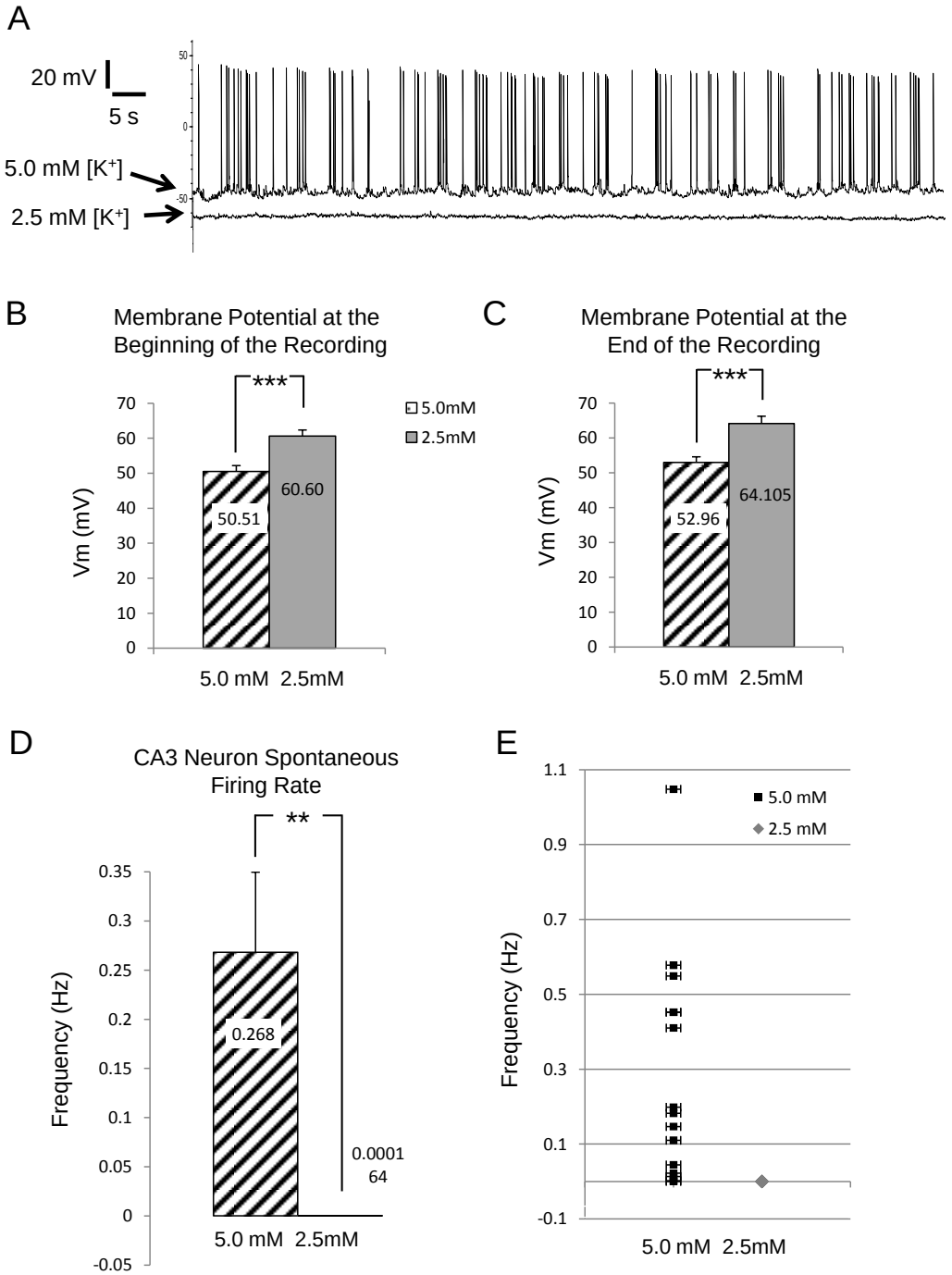

Figure 3.2 $Ca^{2+}$ imaging from slices bolus-loaded with $Ca^{2+}$ indicator

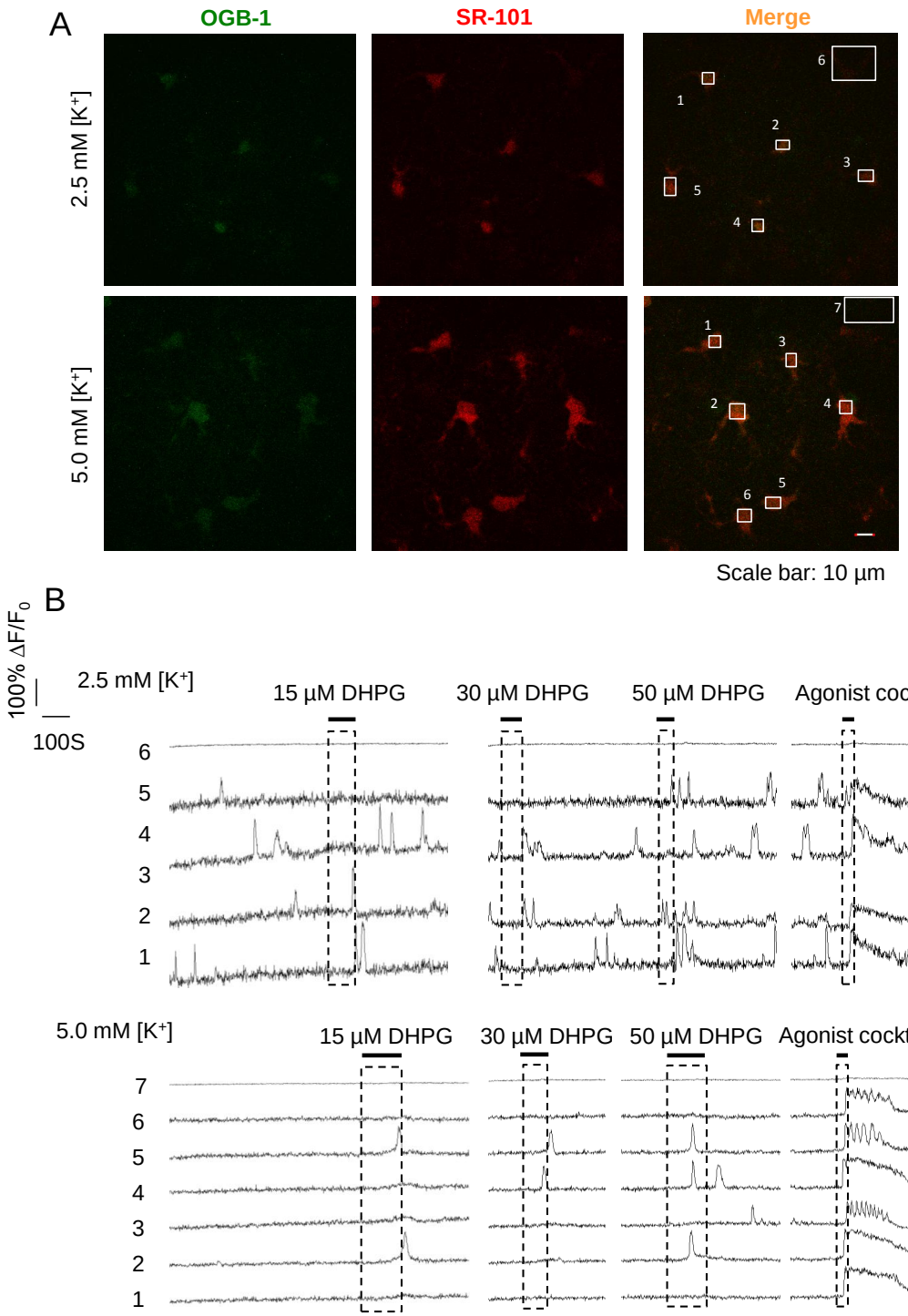

Figure 3.3 Changes in spontaneous $Ca^{2+}$ transients following incubation in 5.0 mM $[K^+]_o$ ACSF

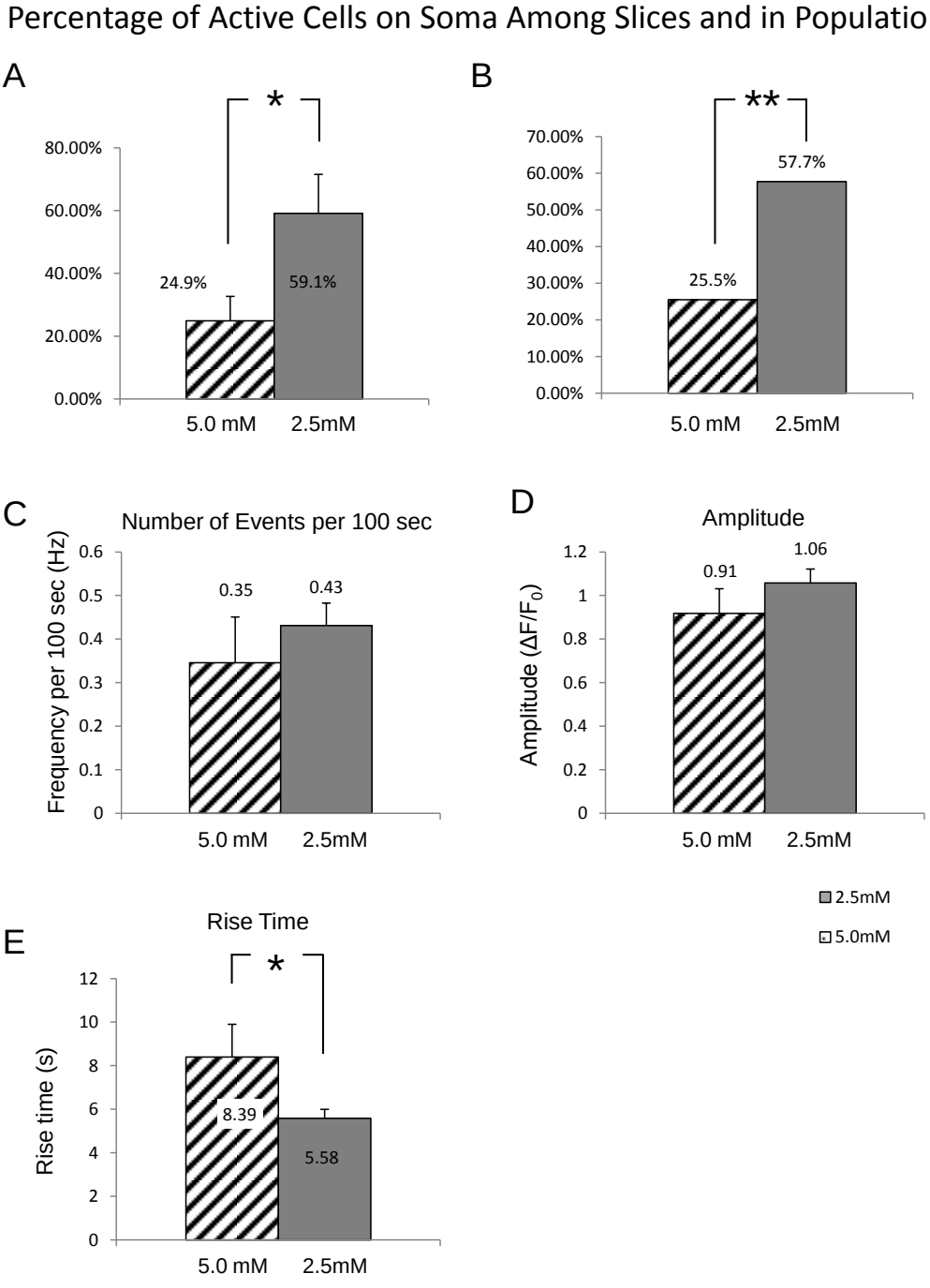

Figure 3.4 Summary of the pattern of evoked somatic $Ca^{2+}$ responses in bolus-loaded slices

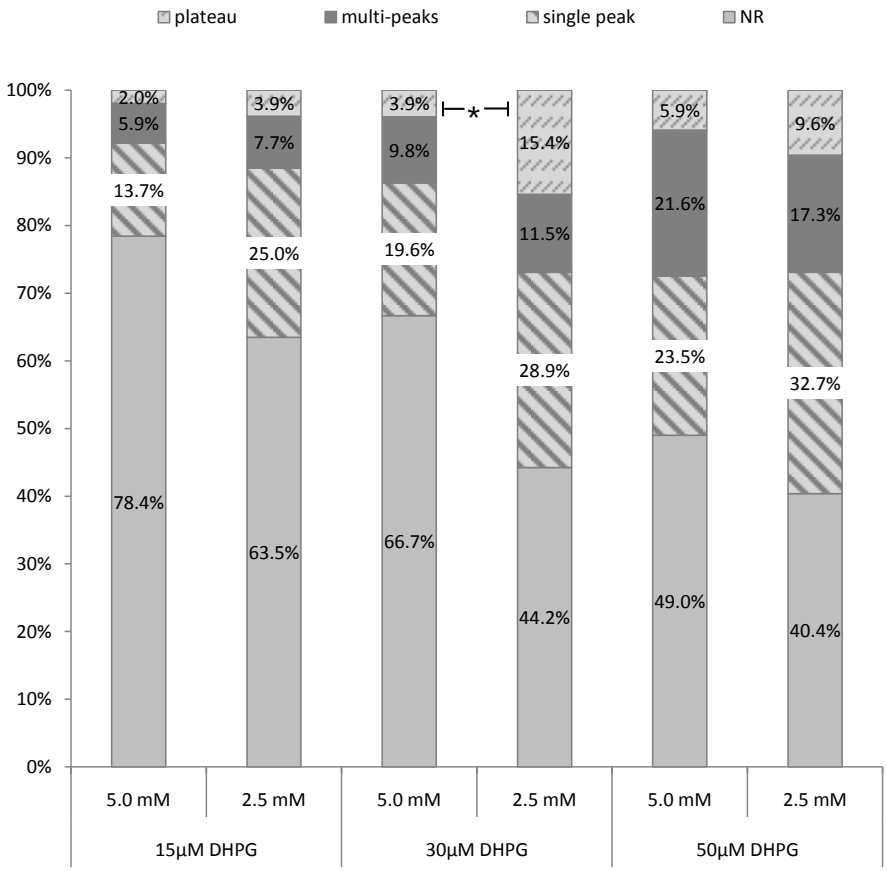

Figure 3.5 Effects on agonist-evoked somatic $Ca^{2+}$ responses

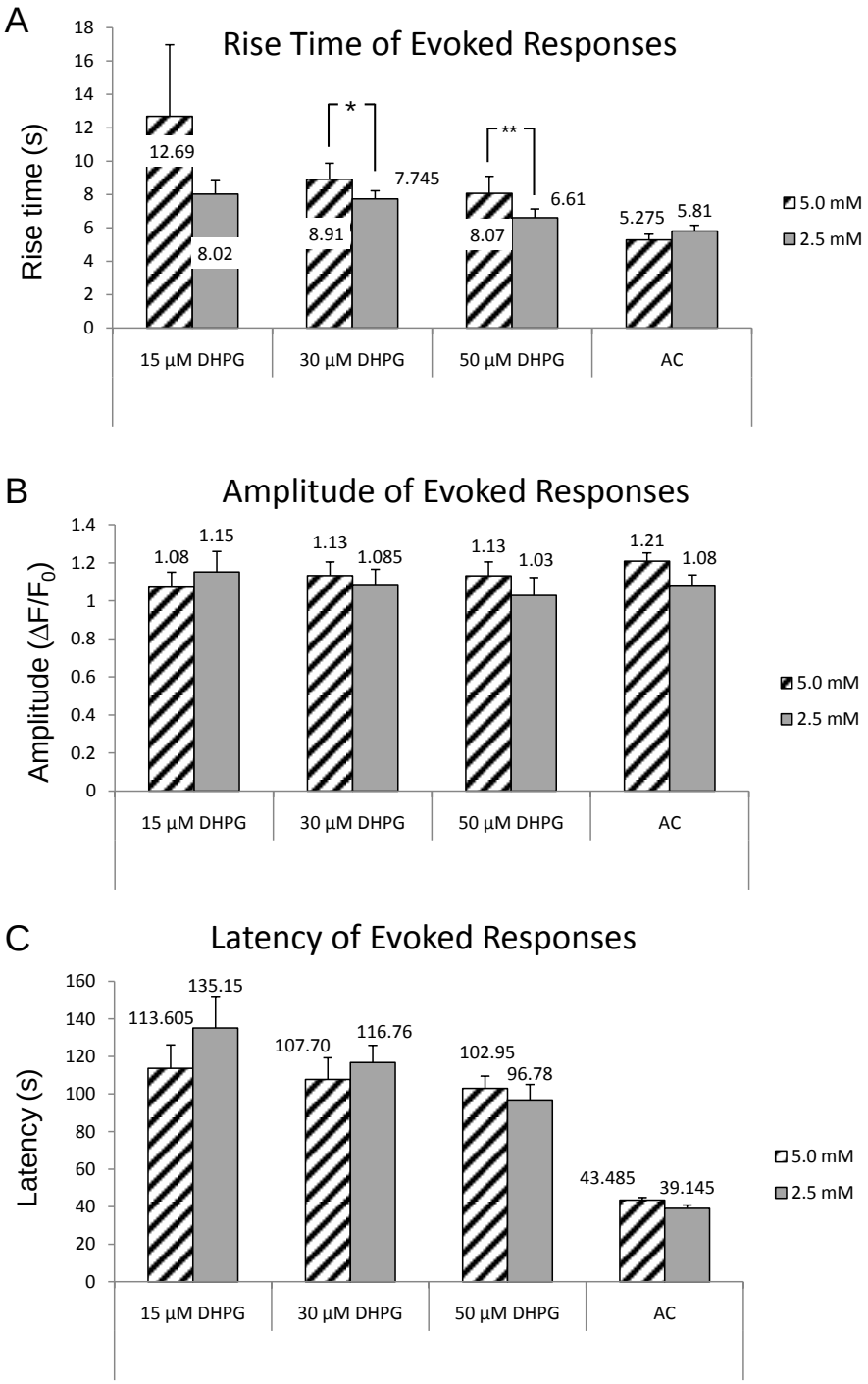

Figure 3.6 Effects on spontaneous activity in microdomains after 4 to 6 hr incubation in 5.0 mM $[K^+]_o$ ACSF

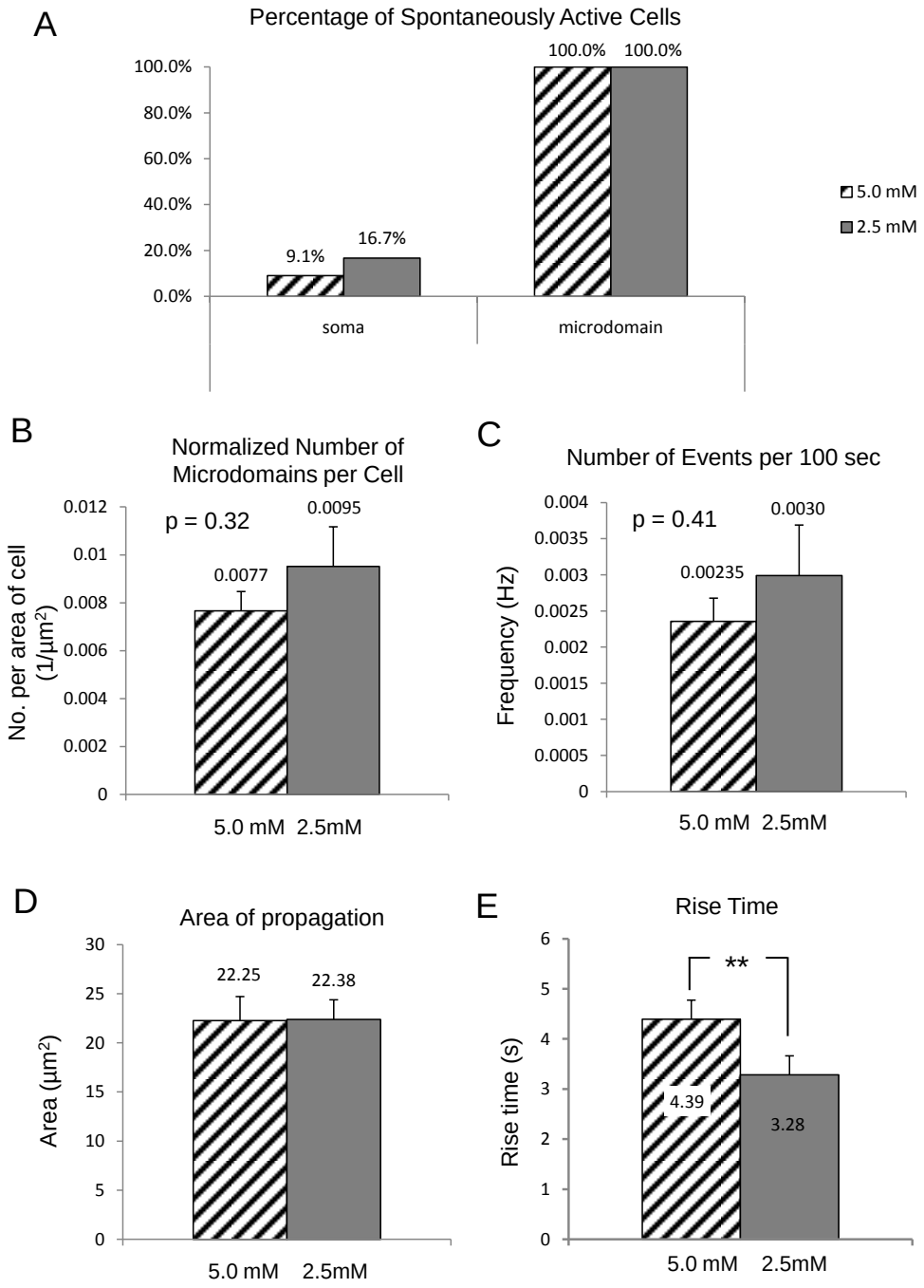

Figure 3.7 Effects on agonist evoked activity in microdomains after 4 to 6 hr incubation in in 5.0 mM $[K^+]_o$ ACSF

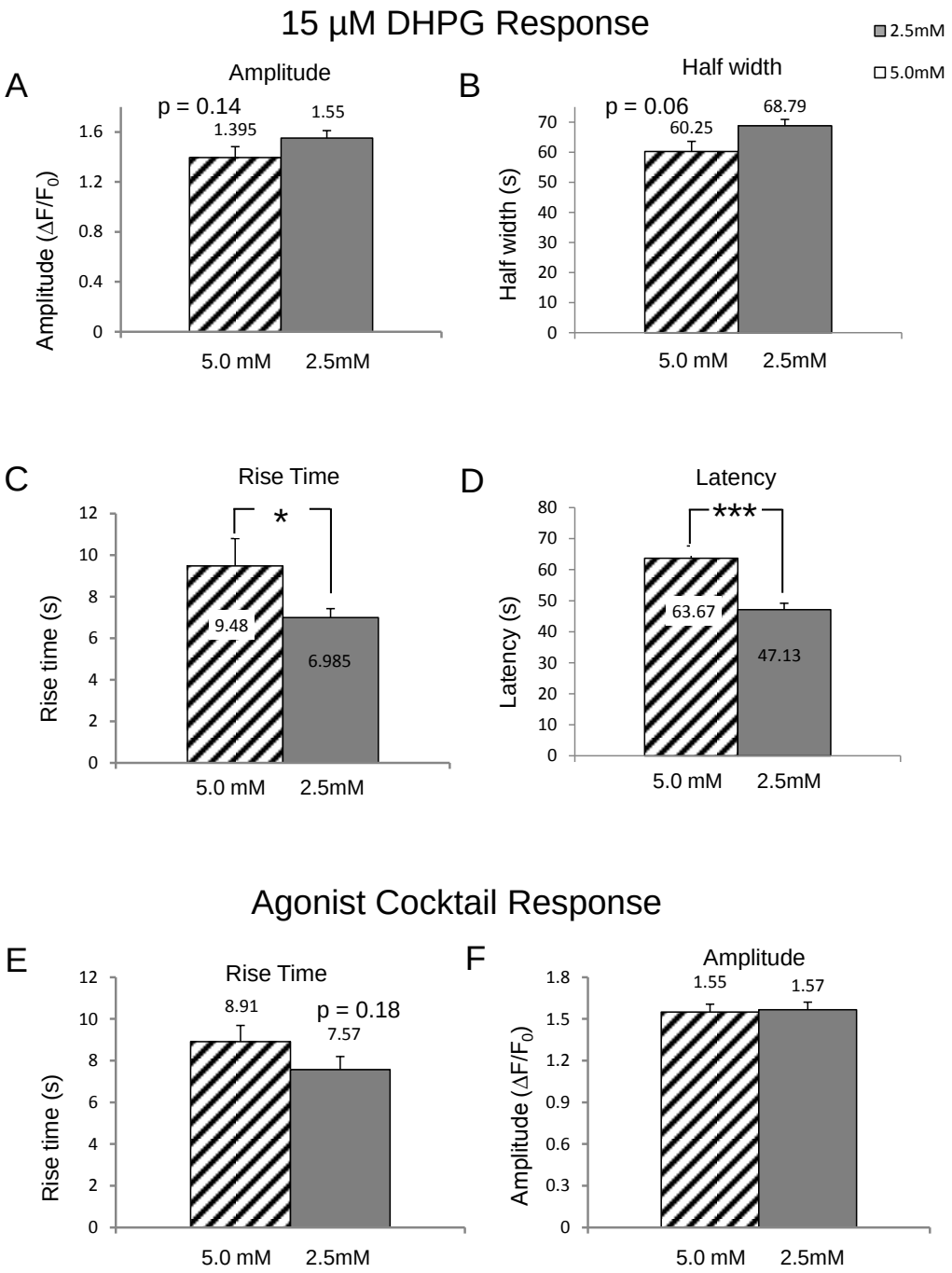

Figure 3.8 Summary of the pattern of agonist-evoked $Ca^{2+}$ responses in microdomains

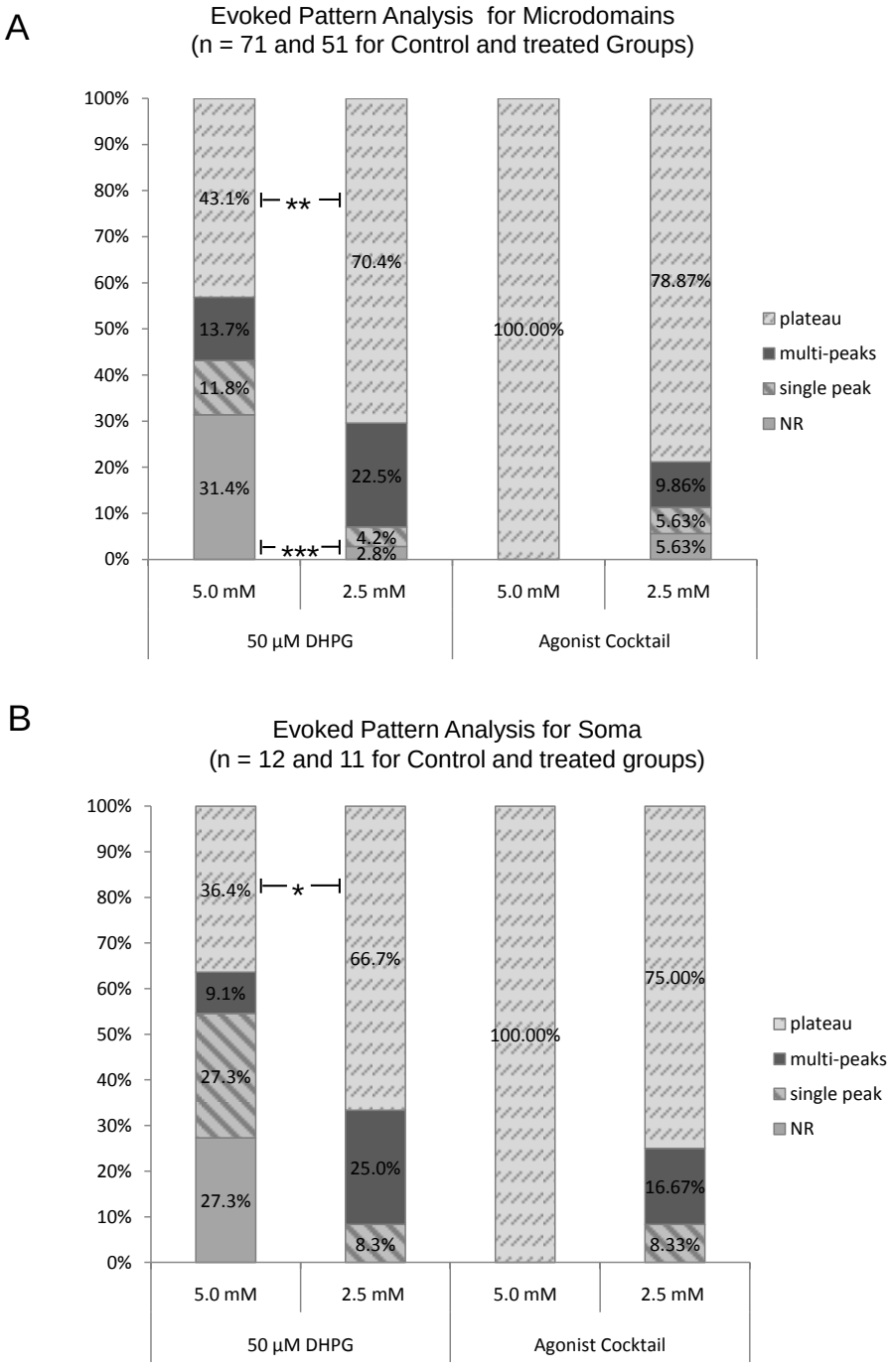

## Chapter 4: The changes in astrocytic group I mGluR signaling are largely due to the change in the functional receptor expression

### 4.1 Abstract

Results from Chapters 2 and 3 suggest that hippocampal s.r. astrocytes exhibit bidirectional long-term plasticity of their group I mGluR signaling in response to changes in CA3 to CA1 neuronal synaptic transmission. Next we wanted to test to what extent this plasticity occurs at the level of the mGluRs themselves as opposed to any number of intracellular Gq GPCR signaling molecules between activation of the receptor and release of $Ca^{2+}$ from internal stores. Brain slices from transgenic mice expressing a novel Gq GPCR (the MrgA1R) only in astrocytes were utilized in this study. The rationale is that because the MrgA1R is not native to brain and therefore not activated by endogenously released neurotransmitter, its functional expression will not change in response to changes in neuronal synaptic transmission. To this end, $Ca^{2+}$ responses evoked by the endogenous mGluR activation were compared to those evoked by novel Gq GPCR activation in the same astrocytes after 4 to 6 hours incubation in TTX to block neuronal action potentials. Data suggest that hippocampal s.r. astrocytes from transgenic $MrgA1R^{+}$ mice exhibit the same potentiation of endogenous mGluR signaling, evident by the faster rise times of tACPD evoked $Ca^{2+}$ responses. However, there was no change in the $Ca^{2+}$ responses evoked by the agonist to the novel Gq GPCR. These data suggest that the changes measured in $Ca^{2+}$ signaling after long-term incubation in TTX, including faster rise times, shift in pattern toward more robust DHPG evoked responses, and increased

probability of responding to agonist in the population, are due to increased expression of the group I mGluRs themselves. To begin to assay for the possible physiological significance of these changes, CA1 neuron AMPA receptor mediated mEPSCs were compared between slices incubated in 3.5 mM $[K^+]_o$ ACSF, 3.5 mM $[K^+]_o$ ACSF with TTX, and 5.0 mM $[K^+]_o$ ACSF to determine if neuronal AMPA receptor scaling is occurring alongside the long-term changes in astrocytic receptors.

## 4.2 Introduction

In previous chapters, we have provided evidence to suggest that long-term changes in CA3-CA1 synaptic transmission leads to changes in astrocytic Gq GPCR signaling that are likely specific to group I mGluRs. In response to 4 to 6 hour blockade of CA3 neuronal firing, a significant increase in the population of s.r. astrocytes exhibited spontaneous $Ca^{2+}$ transients with faster rise times in both the somata and the microdomains. In addition, a greater percentage of s.r. astrocytes and more microdomains per astrocyte responded to group I mGluR agonist with shorter response latencies and faster rise times. When CA3 neuronal firing was elevated by 5.0 mM $[K^+]_o$ for 4 to 6 hours, a smaller percentage of astrocytes in the population exhibited spontaneous $Ca^{2+}$ transients and these had slower rise times compared to controls. Additionally, a smaller percentage of astrocytes in the population and a smaller number of microdomains per cell responded to group I mGluR agonist with longer latencies and slower rise times after long-term increase in neuronal firing rates. These data strongly suggest that hippocampal astrocytes exhibit bi-directional plasticity of their mGluR signaling in response to long-term changes in action potential driven neurotransmitter release.

Our data suggest that such plasticity is due to, at least partially, the changes in functional expression of astrocytic group I mGluRs. We found that s. r. astrocytes from hippocampal slices treated with either TTX or 5.0 mM $[K^+]_o$ responded to group I mGluR agonist with different patterns of $Ca^{2+}$ elevations in both astrocyte soma and microdomains. Based on previous pharmacological studies, which showed a strong

correlation between expression levels of Gq GPCRs and the latency to Gq GPCR mediated $Ca^{2+}$ responses in cultured cells (Shao and McCarthy, 1993; Wang and Thompson, 1994; Ostasov et al., 2008), we hypothesize that the long-term plasticity of group I mGluR mediated $Ca^{2+}$ responses we observe is largely, if not exclusively, due to changes in functional expression of group I mGluRs in astrocytes.

This is the first report of long-term plasticity in astrocytic receptors in a non-pathological system, and this plasticity very much resembles the homeostatic plasticity in neurons. It has been demonstrated that homeostatic scaling in neurons is mainly due to changes in functional expression of ionotropic glutamate receptors on postsynaptic neurons. Activity blockade progressively increased postsynaptic accumulation of synaptic AMPA receptors over 2 days in primary neuronal culture, while the ratio between glutamate receptor 1 (GluR1) and GluR2 AMPA receptor subunits remained unchanged. This increase in AMPA receptor expression affected the entire population of imaged synapses in the culture, with more than 2-fold increases in the strength of synaptic connections between pyramidal neurons. In addition, the changes in synaptic strength did not affect short-term depression or the coefficient of variation of the postsynaptic responses (Wierenga et al., 2005), indicating that neuronal homeostatic scaling does not influence plasticity at a specific synapse, as suggested by Hebb's rule. This accumulation of AMPA receptor subunits can be observed as early as 4 hours after activity blockade (Ibata et al., 2008), suggesting that active gene transcription and new protein synthesis can likely contribute to plasticity on a relatively rapid timescale. In addition, NMDA receptors have been shown to be co-regulated during activity blockade

induced scaling on postsynaptic neurons. The ratio between AMPA receptor- vs. NMDA receptor-evoked EPSC remains unchanged (Watt et al., 2000).

Based on our observation of changes in group I mGluR signaling in astrocytes and previous studies on neuronal homeostatic plasticity, we hypothesize that the increased group I mGluR signaling is largely, if not exclusively, due to increased expression of the surface receptors on s.r. astrocytes. To test this hypothesis, an estimate of the expression level of group I mGluRs and the production of several key players in the Gq GPCR signaling pathway is required. However, many signaling molecules including PLC, $PIP_2$, $IP_3$, and $IP_3$ receptors are also expressed by other cell types in hippocampus. It is clear that mGluR1 and mGluR5 are expressed by pyramidal neurons, and a recent study has shown that mGluR5 is highly expressed in primary microglial cultures and actively regulates the pro-inflammatory phenotype in microglia (Loane et al., 2009).

To test the locus of the scaling effect of group I mGluR $Ca^{2+}$ signaling in astrocytes, we chose to use a strain of transgenic mice that express a novel Gq coupled metabotropic receptor only in astrocytes. Mas-related gene A1 (MrgA1) receptor is normally expressed only in a specific subset of dorsal root ganglion nociceptive sensory neurons in the spinal cord of mice and humans (Dong et al., 2001; Lembo et al., 2002). In the transgenic mice (C57BL/6J background), the MrgA1 receptor was targeted to astrocytes using the inducible tet-off system (Figure 4.1 A). In this system, the tetracycline transactivator (tTA) is targeted to astrocytes using the human glial fibrillary

acidic protein (hGFAP) promoter (Gossen and Bujard, 2002) while a green fluorescent protein (GFP)-tagged MrgA1 receptor, is driven by the tetracycline minimal promoter (tetO). In the absence of doxycycline (dox), tTA binds to tetO and drives expression of the MrgA1-GFP construct (Figure 4.1 A). This results in astrocyte-specific expression of the MrgA1 receptor and GFP in the brain. Dox can also be administered to the offspring in order to control the expression of MrgA1. In the rest of this chapter, hGFAP-tTA:: tetO-MrgA1 mice are referred to as $MrgA1^+$ for simplicity.

The $MrgA1^+$ transgenic mice appeared normal and healthy compared to single transgenic littermates and C57BL/6J mice. In hippocampus, the MrgA1 receptor can be detected in approximately 80% to 90% of astrocytes in both the soma and the processes as indicated by co-localization of GFAP and GFP (Fiacco et al., 2007). In addition, it has been demonstrated that this receptor is not expressed in the neuronal population nor by $NG2^+$ glia in the brain (Fiacco et al., 2007).

The MrgA1 receptor can be activated by RF amide neuropeptides which results in $Ca^{2+}$ release from internal stores (Dong et al., 2001). Figure 4.1 C shows the $Ca^{2+}$ response in hippocampal s.r. astrocytes, induced by bath-application of FMRFa and FLRFa. FMRFa and FLRFa can reliably activate $Ca^{2+}$ responses in astrocytes in the microdomains and somata in the same fashion as those evoked by endogenous receptor activation (Fiacco et al., 2007). It has been shown that MrgA1 receptor mediated $Ca^{2+}$ responses mirror endogenous mGluR responses, as $Ca^{2+}$ elevated first in a particular compartment(s) with similar amplitude (Fiacco et al., 2007). These data suggest that the

MrgA1 receptor activates the same localized signaling molecules as those activated by endogenous group I mGluRs.

More importantly, the ligands for the MrgA1 receptor do not activate endogenous receptors in the brain. It has been shown that stimulation of the MrgA1 receptor in astrocytes does not result in neuronal $Ca^{2+}$ elevations, nor does it result in changes in neuronal activity through $Ca^{2+}$ elevations in astrocytes (Fiacco et al., 2007). To our knowledge, there is no endogenous ligand or agonist present in the brain that can activate the MrgA1 receptor. Thus, the $MrgA1^{+}$ transgenic mouse is a very useful tool for studying to what extent the scaling effect on astrocytic group 1 mGluRs is due to changes in the Gq GPCR signaling pathway. Since there are no changes in the activation of this receptor in the absence of its own agonist, our manipulation of neuronal activity is not expected to cause changes in MrgA1 receptor mediated $Ca^{2+}$ activity. By manipulating CA3-CA1 synaptic transmission in hippocampal slices from $MrgA1^{+}$ transgenic mice and by comparing $Ca^{2+}$ responses evoked by agonists to endogenous group I mGluRs and to MrgA1 receptors, we can determine if the scaling effect as measured by changes in $Ca^{2+}$ signaling is occurring at the level of the surface group I mGluRs or if changes extend into the intracellular signaling cascade.

An important question remains as to the physiological significance of this form of plasticity in astrocytes. We have initiated a series of experiments to test the functional significance of the scaling effect on astrocytic receptors. Previous studies suggest that astrocytic group I mGluRs contribute to NMDA receptor mediated slow inward currents

(SICs) in neurons (Parri et al., 2001; Angulo et al., 2004; Fellin et al., 2004; Fiacco and McCarthy, 2004). Astrocytes are highly secretory cells (Cahoy et al., 2008) and play a primary role in controlling the extracellular microenvironment to support neuron and brain homeostasis. Therefore, long-term changes in astrocytic group I mGluR signaling may contribute to astrocytic release of neurotransmitters in an attempt to "recover" levels of synaptic activity in the absence of neuronal action potentials. To investigate the potential influence of astrocytic receptor scaling on neuronal activity, we plan to compare levels of ambient glutamate and evoked SICs in CA1 neurons from control and TTX-treated slices. Previous studies have shown that new AMPA receptor insertion could be detected as early as 1 to 2 hours after TTX blockade (Ibata et al., 2008), while there was no indication that NMDA receptor scaling occurred over such a rapid time course. As a first experiment in this line of studies, we evaluated whether neuronal scaling of AMPA and NMDA receptors occurred in CA1 neurons after 4 to 6 hours blockade of neuronal action potentials.

## 4.3 Material and methods

### *Preparation of hippocampal slices*

All mice were housed in the animal facility at the University of California, Riverside in accordance with Institutional Animal Care and Use Committee guidelines. 12- to 18-day-old C57BL/6J (Jackson Laboratory, Bar Harbor, ME) mice were anaesthetized using isoflurane and decapitated. Parasagittal hippocampal slices were prepared using a Leica VT1200s Vibratome (Bannockburn, IL). Slices were prepared in

ice-cold, oxygenated $Ca^{2+}$-free saline (see Chapter 1). Subsequently, slices were incubated for 45 minutes at 35°C in oxygenated ACSF (see Chapter 1). Slices were incubated in either 2.5 mM $[K^+]_o$ ACSF (control) or in ACSF containing 5.0 mM $[K^+]_o$. Following the incubation period individual slices were transferred to a recording chamber and continuously superfused with oxygenated, room temperature ACSF of the same $[K^+]_o$ that they were incubated in. During recording, 1 μM TTX was added to the ACSF in order to isolate direct astrocyte responses to agonist.

***Astrocyte patch clamp and loading with $Ca^{2+}$ indicator.***

Astrocyte pipettes were made and filled with an internal solution as previous described (see Chapter 1). The internal solution also included was 200 μM of the cell-impermeant version of the $Ca^{2+}$-indicator dye OGB-1 (Invitrogen). Whole-cell patch-clamp recordings of astrocytes were performed as precious described (see Chapter 1). Astrocytes displayed a resting $V_m$ of ~75 mV in 3.5 mM $[K^+]_o$ standard ACSF. Voltage step protocol and test pulses of -5 mV were used to verify the identity of passive astrocytes. A smooth, stable off-cell and formation of an outside-out patch was a strong indicator of minimal damage to the cell membrane during the patch clamp procedure.

***Confocal imaging and monitoring of astrocyte $Ca^{2+}$ activity.***

Stratum radiatum of CA1 was visualized and individual s.r. astrocytes were identified as previous described (see Chapter 1). After loading with the calcium indicator, the fluorescence intensity of calcium indicator dye over time was recorded in astrocytes on a fixed focal plane. In all experiments, only a single (field of) astrocyte(s) was

recorded per slice to eliminate the possibility of double-sampling or changes due to multiple agonist applications. Astrocytes exhibiting at least one spontaneous $Ca^{2+}$ elevation were counted as spontaneously active cells. All recordings were completed within 40 minutes to reduce the possible TTX scaling effect on control slices and to limit possible phototoxicity. In experiments performed using Gq GPCR agonist, including group I and II mGluR agonist tACPD, MrgA1 receptor agonist peptide FMRFa, and an agonist cocktail (See Chapter 1), agonists were applied for 30 to 50 seconds depending upon the delay to the initiation of the astrocyte $Ca^{2+}$ response. The viability of astrocyte(s) in each recording was verified by bath application of the agonist cocktail. Astrocytes not responding to the agonist cocktail application were excluded from analysis.

***Analysis of astrocyte Gq GPCR $Ca^{2+}$ activity and Statistics.***

Slices or single astrocytes from patch clamp experiments were given a numeric code and analyzed as previous described (see Chapter 1). The amplitudes, frequencies and kinetics of the spontaneous Gq GPCR signaling events and agonist-evoked mGluR responses were compared between treatment groups. Spontaneous $Ca^{2+}$ transients covering over $\geq$ 75% of the planar area of the cell were defined as whole cell $Ca^{2+}$ elevations and analyzed separately. Analysis was done using number of astrocytes as 'n' for bulk-loading and bolus loading experiments, and number of microdomains for patch-clamp experiments. Student's independent *t*-test was used for statistical comparison of means between the control and treated groups.

***Estimation of mGluR5 expression in brain cells by flow cytometry analysis***

12- to 18-day-old MrgA1$^{+}$ transgenic mice and littermate control animals were anaesthetized using isoflurane and decapitated. Whole brains were extracted and parasagittal brain slices were prepared using a Leica VT1200s Vibratome (Bannockburn, IL). Slices were prepared in ice-cold, nominally $Ca^{2+}$-free saline containing (in mM): 125 NaCl, 3.5 KCl, 3.8 $MgCl_2$, 1.25 $NaH_2PO_4$, 26.0 $NaHCO_3$, 15 glucose, and 1.3 ascorbic acid, bubbled with 5% $CO_2$-95% $O_2$. Subsequently, slices were incubated for 45 minutes at 35°C in oxygenated ACSF (see Chapter 1). Slices were then incubated 4 to 6 hours at room temperature either in standard ACSF (3.5 mM $[K^+]_o$ ACSF, control) or in standard ACSF + 1 μM TTX. Following the incubation period, all the slices incubated in the same condition were transferred into ice-cold RPMI complete (10% fetal calf serum [FCS], 1% penicillin/streptomycin, 1% glutamine, 1% sodium pyruvate, 1% nonessential amino acids, 0.1% β-mercaptoethanol). Slices were washed in RPMI to remove excess blood and dissociated in a petri-dish with 1.5 ml RPMI. A single-cell suspension was prepared from whole brain slices by passing cells through a 5 ¾ inch Pasteur glass pipet (Fisher Scientific). 4 ml of 0.25% Trypsin was added to the suspension and the suspension was transferred into a 50ml conical tube with Pasteur glass pipet, and then incubated for 30 minutes at 37 degrees centigrade. Cell suspension was passed through a Pasteur glass pipet every 5 minutes to prevent clumping. After 30 minutes of incubation, 10 ml pre-chilled 20% FCS RPMI was added to stop the effect of Trypsin. Cell suspension was centrifuged and resuspended in RPMI 1% FCS. Cell suspensions were purified using a density gradient composed of 70% and 30% solutions of Percoll (GE

Healthcare). Following washes, the cells were counted and resuspended in fluorescence-activated cell sorter (FACS) buffer (PBS containing 1% bovine serum albumin [BSA], 0.1 mM ethylenediaminetetraacetic acid [EDTA]) for incubation with FcBlock and antibodies against cell surface markers. For intracellular staining, cells were then fixed in 4% PFA (EMS) in PBS, permeabilized with 0.3% saponin in PBS, and incubated with either purified rabbit anti-human mGluR5 (GenScript) or isotype IgG control. Secondary antibodies to rabbit IgG conjugated to Alexa FluorH 647 (Invitrogen) were used for detection. The cells were washed with FACS buffer and analyzed using the BD FACSCanto II flow cytometer and FlowJo analysis software v.8.7.3.

***Recording miniature synaptic events in CA1 pyramidal neurons***

Neuronal pipettes had resistances of 4.6–6 MΩ when filled with a solution containing the following (in mM): 145 K-gluconate, 2 $MgCl_2$, 10 HEPES, 4 Mg-ATP, 14 phosphocreatine, and 0.2 Na-GTP, pH 7.3 with KOH. Slices were constantly perfused with oxygenated room temperature 3.5 mM $[K^+]_o$ ACSF, 3.5 mM $[K^+]_o$ ACSF containing 1 μM TTX, or 5.0 mM $[K^+]_o$ ACSF. Neurons were patch-clamped in ACSF containing 1 μM TTX with the same $[K^+]_o$ as the ACSF they were incubated in. Whole-cell patch-clamp recording of neurons was performed using a Multiclamp 700B amplifier and PCLAMP 10.2.014 software (Axon Instruments, Union City, CA). In some experiments the external solution was the same as described above with the addition of 10 mM 2,3-dihydroxy-6-nitro-7-sulfamoyl-benzo[f]quinoxaline-2,3-dione (NBQX) to block AMPA receptor-mediated mEPSCs. Upon attaining the whole-cell configuration,

cell membrane potential, input resistance, and access resistance were recorded, and the access resistances were monitored during the recording. Neurons with access resistances changing ≥ 20% were excluded from the analysis.

***Analysis of miniature synaptic events in CA1 pyramidal neurons***

Neuronal currents were analyzed using PCLAMP 10.2.014 software (Axon Instruments). A template intrinsic to each recording was created by averaging five individual mEPSCs together which was then used to detect individual events within the same recording. A separate template was created for each recording. Only events erroneously counted twice by the analysis software were rejected; otherwise, every event selected by the template was included in subsequent analyses. Currents were not curve-fitted, and event statistics were taken for individual currents and then averaged, rather than taking the parameters from the averaged trace. Amplitude and frequency were analyzed. Error bars in all graphs presented are SEM. Student's t test was used to test for statistical significance of individual current parameters between events in different groups. Significance is described at the 0.05, 0.01, or 0.001 levels.

## 4.4 Results

### 4.4.1 MrgA1 receptor signaling did not change after long-term blockade of neuronal firing

To assay for possible changes in astrocytic MrgA1R signaling, hippocampal slices dissected from MrgA1$^+$ mice were incubated in either 3.5 mM $[K^+]_o$ ACSF or 3.5

mM $[K^+]_o$ ACSF containing 1 μM TTX to block neuronal action potentials for 4 to 6 hours. After the incubation period, s.r. astrocytes were patch clamped and filled with OGB-1 $Ca^{2+}$ indicator dye. Spontaneous $Ca^{2+}$ activity in astrocytic somata and microdomains were monitored for 10 minutes prior to bath application of agonists to MrgA1Rs and endogenous Gq GPCRs. In general, s.r. astrocytes had spontaneous $Ca^{2+}$ activity mostly in microdomains and responded to 1 μM FMRFa, 4 μM FMRFa, 50 μM tACPD and agonist cocktail (10 μM ea. of histamine, carbachol, and Na-ATP) with whole-cell $Ca^{2+}$ elevations (figure 4.2). The rise times of all the Gq GPCR agonist responses were measured as a barometer of long-term changes in Gq GPCR signaling activity. Consistent with previous observations, TTX-treated s.r. astrocytes had significantly faster rise times of their $Ca^{2+}$ responses to 50 μM tACPD, a group 1/group 2 specific mGluR agonist, compared to those of control cells ($p < 0.05$, figure 4.3 A). The $Ca^{2+}$ response was considered to be predominatly due to activation of group I mGluRs by tACPD since group II mGluRs are not Gq GPCRs. These data suggest that 4 to 6 hr TTX blockade of neuronal activity successfully led to the same scaling effect on group I mGluRs in $MrgA1^+$ astrocytes as previously observed in astrocytes from wild type hippocampal slices. There was no difference in rise times of $Ca^{2+}$ responses evoked by either 1 μM FMRFa or 4 μM FMRFa, suggesting that the MrgA1 Gq GPCR signaling pathway is not sensitive to long-term changes in neuronal synaptic activity. Since previous data suggest that MrgA1 receptors and endogenous group I mGluRs engage the same Gq GPCR signaling molecules (Fiacco et al., 2007), the current data provide compelling evidence that the changes observed in group I mGluR $Ca^{2+}$ signaling are due

to long-term changes in surface expression of the group I mGluRs themselves and not downstream signaling molecules.

In addition to lack of an effect of TTX incubation on rise times of evoked MrgA1R responses, there was also no difference in the response patterns to 1 μM or 4 μM FMRFa. Two out of 8 control and 2 out of 10 TTX-treated cells responded to 1 μM FMRFa with single peak responses, and 1 cell from each group responded to 1 μM FMRFa with multi peak responses. The rest of the cells (5 out of 8 in control cells, 7 out of 10 TTX cells) had plateau-like responses to 1 μM FMRFa. All control and TTX treated cells responded to 4 μM FMRFa with plateau-like responses. Consistent with previous observations, there was no difference in rise time of agonist cocktail evoked $Ca^{2+}$ responses in TTX-treated vs. control astrocytes. The amplitudes of the $Ca^{2+}$ responses evoked by all agonists tested also remained unchanged between control and TTX treated slices (figure 4.3 B). There were also no differences observed in the latencies of all agonist evoked responses (figure 4.3 C). These data were consistent with previous observations of the effects of long-term action potential blockade on evoked somatic astrocyte $Ca^{2+}$ responses.

Overall, the data show that there were no differences in percentage of responding cells, responding patterns, or rise times of the MrgA1-mediated $Ca^{2+}$ responses after 4-6 hr TTX treatment, while the changes in group I mGluR signaling were still observed in the same astrocytes. It is strongly suggested that the changes in the group I mGluR signaling is largely due to the changes in the functional expression level of those

receptors, but not the changes in the expression level of the key molecules in the Gq GPCR signaling pathway. The next question is whether the change in functional receptor expression is due to the change in whole protein expression in astrocytes. Direct measurement of the mGluR5 protein expression level of group I mGluRs was performed next to further address this question.

### 4.4.2 Direct measurement of mGluR5 expression levels in TTX and control incubated astrocytes by flow cytometry

So far, through use of pharmacological and transgenic approaches and monitoring of spontaneous and evoked $Ca^{2+}$ activity in astrocytes, substantial evidence has been provided that astrocytes respond to long-term changes in neuronal firing rates with long term changes in expression of group 1 mGluRs. We next wanted to directly assay for changes in mGluR5 expression levels in astrocytes following long-term blockade of action potential-mediated neuronal synaptic transmission. The mGluR5 polyclonal antibodies used here were designed to target the intracellular C-terminus of the 7-transmembrane mGluR5 receptor in rodent and human tissues. Thus, the expression level of mGluR5 protein measured using this approach is the whole protein expression in astrocytes, not just the surface receptor expression. In this experiment brain slices from $MrgA1^{+}$ transgenic mice were used in order to take advantage of the super-GFP tag fused to the MrgA1 transcript in order to differentiate the astrocyte population from other cell types present in the tissue. Our previous experiments clearly indicate that MrgA1/GFP expression does not interfere with group I mGluRs scaling in astrocytes. As shown in

figure 4.4, $GFP^+$ cells were clearly detected from single cell suspension after whole brain slices were incubated with 3.5 mM $[K^+]_o$ ACSF for 4 to 6 hours (lower panels). Almost no $GFP^+$ cells could be detected in littermate control brain (upper panels). However, there was no detectable level of mGluR5 signal from any cells in the single cell suspension from $MrgA1^+$ brain tissue, indicating failure of the mGluR5 antibody to label the c-terminus of mGluR5 (figure 4.5). Future experiments are planned to further study mGluR5 expression levels in astrocytes using flow cytometry analysis.

### 4.4.3 Rapid homeostatic plasticity observed in neuronal AMPA receptors

In order to test the hypothesis that astrocytic receptor scaling contributes to neuronal iGluR activation, we first evaluated to what extent homeostatic scaling occurred on neuronal AMPA and NMDA receptors in our system. Hippocampal slices were obtained from wild type mouse brains and were incubated in either 3.5 mM $[K^+]_o$ ACSF, 3.5 mM $[K^+]_o$ ACSF containing 1 μM TTX or 5.0 mM $[K^+]_o$ ACSF. Hippocampal CA1 pyramidal neurons were patch-clamped and gap-free recordings performed in 1 μM TTX for at least 10 minutes to monitor AMPA receptor-mediated mEPSCs. Magnesium was included in the ACSF to prevent NMDA mediated mEPSCs. As expected, CA1 neurons had similar resting membrane potentials in 3.5 mM $[K^+]_o$ ACSF and 3.5 mM $[K^+]_o$ ACSF containing 1 μM TTX, while neurons were significantly depolarized in 5.0 mM $[K^+]_o$ ACSF (figure 4.6 A). CA1 neurons had mEPSCs with average amplitude of 8.67 pA and frequency of 1.76 Hz (figure 4.6 B and C). Miniature EPSCs were identified as AMPA receptor mediated because they were completely blocked by the AMPA receptor-specific

antagonist NBQX (data not shown). Compared to CA1 neurons in control hippocampal slices, the amplitude of AMPA receptor mediated mEPSCs was significantly larger in TTX treated slices. There was no change in the amplitude of AMPA receptor mediated mEPSCs recorded in CA1 neurons after 4 to 6 hours of 5.0 mM $[K^+]_o$ treatment (figure 4.6 B). These data suggest that scaling of AMPA receptors occurs rapidly, as within 4-6 hr after block of neuronal action potentials. Neither TTX treatment nor 5.0 mM $[K^+]_o$ treatment led to change in the frequency of AMPA receptor mediated mEPSCs recorded in CA1 neurons, suggesting that there was no detectable change in spontaneous presynaptic release.

Ongoing experiments are testing: 1) whether NMDA receptor mediated mEPSCs also scale up following TTX treatment in CA1 neurons; and 2) whether there are changes in ambient glutamate or NMDA receptor mediated SICs in CA1 neurons following astrocyte mGluR scaling (see discussion below).

### 4.5 Discussion

Since metabotropic receptors are coupled to intracellular signaling cascades, the alterations in $Ca^{2+}$ signaling that we observe may include changes in expression levels of numerous Gq GPCR signaling molecules in addition to the surface receptors. Data gathered in experiments described in this chapter suggest that the changes observed in astrocytic group I mGluR $Ca^{2+}$ signaling are due to changes in expression of the group I mGluRs in astrocytes, while the intracellular signaling molecules activated by the Gq GPCRs remains unchanged. We were not able to directly measure the expression of

astrocytic group I mGluRs isolated from MrgA1R$^+$ brain slices, most likely due to failure of the mGluR5 antibody to bind the intracellular c-terminus of the receptor. However, the surface GPCRs seem to be the most likely targets based on the following: First, the changes observed in $Ca^{2+}$ signaling match well with previous studies that have explored the effects of manipulating Gq GPCR expression levels on evoked $Ca^{2+}$ activity. Wang and Thompson (1994) found that the loss of functional muscarinic M1 and histamine H1 receptors following desensitization resulted in a reduction in the total number of cells in the population responding to agonist as well as longer latencies between agonist application and the ensuing $Ca^{2+}$ responses (Wang and Thompson, 1994). This is exactly what we found for astrocytic DHPG responses after 4 to 6 hour incubation of hippocampal slices in 5 mM $[K^+]_o$. Second, Shao and McCarthy (1993, 1995) directly compared α1 adrenergic receptor expression levels on phenylephrine-evoked astrocyte $Ca^{2+}$ responses (Shao and McCarthy, 1993, 1995). In these experiments, higher GPCR expression levels correlated directly with an increased percentage of astrocytes in the population that responded to agonist and with shorter response latencies to agonist. This is also observed for astrocytic DHPG evoked responses after 4 to 6 hour incubation of hippocampal slices in TTX. Furthermore, studies in culture (Shao and McCarthy, 1995) and *in situ* (Fiacco et al., 2007) suggest that multiple astrocytic Gq GPCRs, including MrgA1 receptors, likely share the same signaling machinery and utilize common stores. Therefore in the present study we might also expect the agonist cocktail evoked responses in astrocytes to be significantly altered if components of the Gq GPCR signaling machinery were scaling. However, we have demonstrated that the scaling effect

is specific to astrocytic group I mGluRs by comparing $Ca^{2+}$ responses evoked by agonist to endogenous mGluRs to agonist evoked responses to multiple astrocytic Gq GPCRs in astrocytes. Furthermore, lack of changes in MrgA1R receptor evoked responses in the same astrocytes which exhibit changes in group I mGluR evoked responses provides compelling evidence that the receptor itself is what is affected rather than other components of the intracellular signaling machinery. Thus, the data suggest that the alterations observed in astrocyte $Ca^{2+}$ signaling mainly reflect changes in the surface group I mGluR expression levels.

We also attempted to directly measure the expression levels of mGluR5 in astrocytes from whole brain cell suspension by flow cytometry analysis. In this experiment, we asked: 1) whether we can take advantage of the GFP tag fused to the MrgA1 transcript in astrocytes to isolate astrocytes from the whole brain cell population; 2) whether total mGluR5 expression in astrocytes, and not only surface expression can be measured using flow cytometry; and, 3) whether mGluR5 expression in $MrgA1^{+}$ astrocytes changes after long-term manipulation of neuronal activity in whole brain slices. We have found that whole brain slices remained healthy after 4 to 6 hr incubation in 3.5 mM $[K^{+}]_o$ ACSF, and a large number of $GFP^{+}$ cells could be detected in slices from $MrgA1^{+}$ mice. Unfortunately, we could not detect mGluR5 staining in any cells from the whole brain population, which has prevented a direct measurement of mGluR5 expression levels in astrocytes for the time being. Future experiments are planned to further investigate this issue.

## 4.6 References

Angulo MC, Kozlov AS, Charpak S, Audinat E (2004) Glutamate released from glial cells synchronizes neuronal activity in the hippocampus. J Neurosci 24:6920-6927.

Cahoy JD, Emery B, Kaushal A, Foo LC, Zamanian JL, Christopherson KS, Xing Y, Lubischer JL, Krieg PA, Krupenko SA, Thompson WJ, Barres BA (2008) A transcriptome database for astrocytes, neurons, and oligodendrocytes: a new resource for understanding brain development and function. J Neurosci 28:264-278.

Dong X, Han S, Zylka MJ, Simon MI, Anderson DJ (2001) A diverse family of GPCRs expressed in specific subsets of nociceptive sensory neurons. Cell 106:619-632.

Fellin T, Pascual O, Gobbo S, Pozzan T, Haydon PG, Carmignoto G (2004) Neuronal synchrony mediated by astrocytic glutamate through activation of extrasynaptic NMDA receptors. Neuron 43:729-743.

Fiacco TA, McCarthy KD (2004) Intracellular astrocyte calcium waves in situ increase the frequency of spontaneous AMPA receptor currents in CA1 pyramidal neurons. J Neurosci 24:722-732.

Fiacco TA, Agulhon C, Taves SR, Petravicz J, Casper KB, Dong X, Chen J, McCarthy KD (2007) Selective stimulation of astrocyte calcium in situ does not affect neuronal excitatory synaptic activity. Neuron 54:611-626.

Garaschuk O, Milos RI, Konnerth A (2006) Targeted bulk-loading of fluorescent indicators for two-photon brain imaging in vivo. Nat Protoc 1:380-386.

Gossen M, Bujard H (2002) Studying gene function in eukaryotes by conditional gene inactivation. Annu Rev Genet 36:153-173.

Ibata K, Sun Q, Turrigiano GG (2008) Rapid Synaptic Scaling Induced by Changes in Postsynaptic Firing. Neuron 57:819-826.

Lembo PM, Grazzini E, Groblewski T, O'Donnell D, Roy MO, Zhang J, Hoffert C, Cao J, Schmidt R, Pelletier M, Labarre M, Gosselin M, Fortin Y, Banville D, Shen SH, Strom P, Payza K, Dray A, Walker P, Ahmad S (2002) Proenkephalin A gene products activate a new family of sensory neuron--specific GPCRs. Nat Neurosci 5:201-209.

Loane DJ, Stoica BA, Pajoohesh-Ganji A, Byrnes KR, Faden AI (2009) Activation of metabotropic glutamate receptor 5 modulates microglial reactivity and neurotoxicity by inhibiting NADPH oxidase. J Biol Chem 284:15629-15639.

Nimmerjahn A, Kirchhoff F, Kerr JN, Helmchen F (2004) Sulforhodamine 101 as a specific marker of astroglia in the neocortex in vivo. Nat Methods 1:31-37.

Ostasov P, Krusek J, Durchankova D, Svoboda P, Novotny J (2008) Ca2+ responses to thyrotropin-releasing hormone and angiotensin II: the role of plasma membrane integrity and effect of G11alpha protein overexpression on homologous and heterologous desensitization. Cell Biochem Funct 26:264-274.

Parri HR, Gould TM, Crunelli V (2001) Spontaneous astrocytic Ca2+ oscillations in situ drive NMDAR-mediated neuronal excitation. Nat Neurosci 4:803-812.

Shao Y, McCarthy KD (1993) Quantitative relationship between alpha 1-adrenergic receptor density and the receptor-mediated calcium response in individual astroglial cells. Mol Pharmacol 44:247-254.

Shao Y, McCarthy KD (1995) Receptor-mediated calcium signals in astroglia: multiple receptors, common stores and all-or-nothing responses. Cell Calcium 17:187-196.

Sullivan MR, Nimmerjahn A, Sarkisov DV, Helmchen F, Wang SS (2005) In vivo calcium imaging of circuit activity in cerebellar cortex. J Neurophysiol 94:1636-1644.

Wang SS, Thompson SH (1994) Measurement of changes in functional muscarinic acetylcholine receptor density in single neuroblastoma cells using calcium release kinetics. Cell Calcium 15:483-496.

Watt AJ, van Rossum MC, MacLeod KM, Nelson SB, Turrigiano GG (2000) Activity coregulates quantal AMPA and NMDA currents at neocortical synapses. Neuron 26:659-670.

Wierenga CJ, Ibata K, Turrigiano GG (2005) Postsynaptic Expression of Homeostatic Plasticity at Neocortical Synapses. The Journal of Neuroscience 25:2895-2905.

## Figure Legends

### Figure 4.1 Hippocampal astrocytes express functional MrgA1 receptors.

(A) Schematic diagram represents the design of $MrgA1^+$ transgenic mouse. Crossing hGFAP-tTA to tetO-MrgA1 mice results in the expression of MrgA1 exclusively in astrocytes in the absence of doxycycline. As GFP is fused to the MrgA1 receptor construct, GFP staining indicates MrgA1 receptor expression (B) [Adopted from figure 1 A (Fiacco et al., 2007)].

(B) A field from acute hippocampal slices of $MrgA1^+$ mice contains three hippocampal s.r. astrocytes. OGB-1 dye was delivered into cell 1 and 2, and green fluorescence can be seen in the soma and processes of both astrocytes. Cell 3 has no OGB-1 dye. The green fluorescence from the outline of cell 3 is resulted from the GFP expression along with MrgA1 receptor expression.

(C) A single hippocampal s.r. astrocyte filled with OGB-1 $Ca^{2+}$ indicator dye by patch clamp from a control incubated hippocampal slice. Top panels show the $Ca^{2+}$ elevation evoked by MrgA1 receptor agonist, FMRFa, in both the soma and the fine processes of the astrocyte. ROIs were placed over astrocyte processes to study microdomain Gq GPCR activity (lower right panel) and match corresponding $Ca^{2+}$ traces in the lower left panel. Scale bar: 10 μm; 100% $\Delta F/F_0$/100 seconds.

**Figure 4.2 Representative data of $Ca^{2+}$ imaging on s.r. astrocytes with multiple agonist applications in CA1 region from $MrgA1^{+}$ transgenic mouse by patch-clamp technique.**

(A) A single hippocampal s.r. astrocyte filled with OGB-1 $Ca^{2+}$ indicator dye by patch clamp from a control incubated hippocampal slice. Equal sized boxes of 3.6 μm per side (12.3 $\mu m^2$) were placed over astrocyte processes to study microdomain Gq GPCR activity (top middle panel) and match corresponding $Ca^{2+}$ traces in (B). Scale bar: 10 μm.

(B) Representative trace of $Ca^{2+}$ activities from all the ROIs in the same astrocytes shown in (A). The $Ca^{2+}$ trace at the bottom represents cell soma, which is ROI number 1. The $Ca^{2+}$ traces from each ROI arranged from bottoms to top. FMRFa induces similar patterns of $Ca^{2+}$ elevation as those produced by tACPD application and agonist cocktail application. The spontaneous microdomain activities from microdomain A and B are highlighted by solid and dashed rectangles, respectively. Scale bar: 100% $\Delta F/F_0$/100 seconds.

**Figure 4.3 Long-term incubation in TTX showed no effect on MrgA1 receptor mediated Gq GPCR signaling in s. r. astrocyte.**

(A) There was no change in rise times of 1 μM and 4 μM FMRFa induced $Ca^{2+}$ responses between TTX treated astrocytes and control cells (control: n = 9 microdomains/8 cells; TTX: n = 14 microdomains/10 cells). The rise times of tACPD induced $Ca^{2+}$ responses was significantly shorter in TTX treated astrocytes compared to those from control cells. Error bars represent S.E.M.

(B) There was no significant change in amplitude of agonist induced $Ca^{2+}$ responses by either FMRFa, tACPD or agonist cocktail between TTX treated astrocytes compared to controls (control: n = 9 microdomains/8 cells; TTX: n = 14 microdomains/10 cells). Error bars represent S.E.M.

(C) There was no significant change in latency of agonist induced $Ca^{2+}$ responses by FMRFa, tACPD or agonist cocktail between TTX treated astrocytes compared to controls (control: n = 9 microdomains/8 cells; TTX: n = 14 microdomains/10 cells). Error bars represent S.E.M.

**Figure 4.4 MrgA1$^+$ astrocytes can be identified based on their positive GFP expression by flow cytometry analysis.**

(A) Whole brain cell population (328965 cells) isolated from tetO-MrgA1 mice (littermate control, MrgA1 negative) was displayed in forward and side scatter channels Gated cells represent live, single cell population (135936 cells), which is about 41.3% of the whole brain cells (left panel). There were about 180 cells showed positive GFP expression, which was about 0.13% of all the living cells (right panel).

(B) Whole brain cell population (611870 cells) isolated from MrgA1$^+$ transgenic mice was displayed in forward and side scatter channels. Gated cells represent live, single cell population (261294 cells), which is about 42.7% of the whole brain cells (left panel). There were 2906 cells showed positive GFP expression, which was about 1.11% of all the living cells (right panel).

**Figure 4.5 Metabotropic $GluR_5$ antibodies did not reveal positive staining on astrocytes isolated from whole brain of MrgA-$1^+$ transgenic mouse.**

(A) The antibodies for mGluR5 showed no staining in any brain cells isolated from untreated MrgA$1^+$ transgenic mouse. Upper left panel: Single cell population stained with isotype control. 68530 cells isolated from two MrgA$1^+$ transgenic mice were displayed in forward and side scatter channels. Gated cells represent live, single cell population (30558 cells), which is about 44.6% of the whole brain cells. There were 3388 cells showed positive GFP expression, which was about 11.1% of all the living cells (upper right panel).

Lower panels: single cell population isolated from the same MrgA$1^+$ transgenic brains stained with mGluR5 antibodies. Within 316715 cells that were detected, 65.9% were living brain cells (208651 cells) (lower left panel). There were 23105 cells showed positive GFP expression, which was about 11.1% of all the living cells. Unfortunately, there was no detectable mGluR5 signaling from the entire population, which indicates problems with antibody staining (lower right panel).

(B) The antibodies for mGluR5 showed no staining in any brain cells isolated from untreated MrgA$1^+$ transgenic mouse. Upper left panel: Single cell population stained with isotype control. 68145 cells isolated from two MrgA$1^+$ transgenic mice were displayed in forward and side scatter channel. Gated cells represent live, single cell population (28875 cells), which is about 42.4% of the whole brain cells. There were 3717 cells showed

positive GFP expression, which was about 12.9% of all the living cells (upper right panel).

Lower panels: single cell population isolated from the same MrgA1$^+$ transgenic brains stained with mGluR5 antibodies. Within 186410 cells that were detected, 63.6% were living brain cells (118647 cells) (lower left panel). There were 15246 cells showed positive GFP expression, which was about 12.8% of all the living cells. Unfortunately, there was no detectable mGluR5 signaling from the entire population, which indicates problems with antibody staining (lower right panel).

**Figure 4.6 Homeostatic scaling on AMPA receptor mediated mEPSCs following 4 to 6 hr TTX treatment.**

(A) The resting membrane potential of CA1 neurons incubated in 5.0 mM $[K^+]_o$ (-51.67 mV ± 1.32 mV) is significantly more depolarized compared to the resting membrane potential of CA1 neurons incubated in 3.5 mM $[K^+]_o$ ACSF (without TTX: -54.94 mV ± 0.67 mV; with TTX: -53.57 mV ± 0.68 mV) (3.5 mM $[K^+]_o$ ACSF + TTX: n = 12 cells; 3.5 mM $[K^+]_o$ ACSF: n = 10 cells; 5.0 mM $[K^+]_o$ ACSF: n = 10 cells). Error bars represent S.E.M.

(B) The average amplitude of AMPAR-mediated mEPSCs recorded from CA1 neuron incubated with 1 μM TTX for 4 to 6 hrs (10.42 pA ± 0.52 pA) is significantly larger than those from recorded CA1 neurons incubated with control ACSF and 5.0 mM $[K^+]_o$ ACSF (control ACSF: 8.67 pA ± 0.60 pA; 5.0 mM $[K^+]_o$ ACSF: 8.76 pA ± 0.37 pA) (3.5 mM

$[K^+]_o$ ACSF + TTX: n = 12 cells; 3.5 mM $[K^+]_o$ ACSF: n = 10 cells; 5.0 mM $[K^+]_o$ ACSF: n = 10 cells). Error bars represent S.E.M.

(C) There is no significant difference in frequency of AMPAR-mediated mEPSCs among CA1 neurons incubated in different ACSF (3.5 mM $[K^+]_o$ ACSF + TTX: 2.06 ± 0.23 Hz, n = 12 cells; 3.5 mM $[K^+]_o$ ACSF: 1.76 ± 0.25 Hz, n = 10 cells; 5.0 mM $[K^+]_o$ ACSF: 1.64 ± 0.235 Hz, n = 10 cells). Error bars represent S.E.M.

Figure 4.1 Hippocampal s.r. astrocytes express functional MrgA1 receptors in both the soma and the fine processes

A Schematic diagram of the design of MrgA1 transgenic mouse line

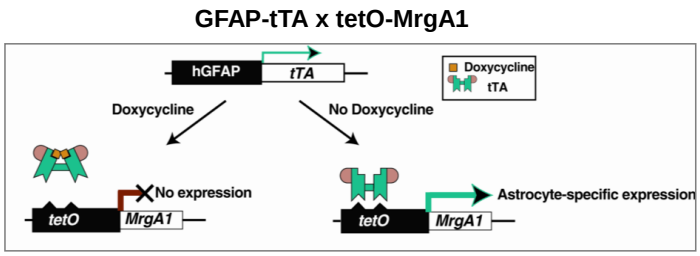


B A field of 3 astrocytes in CA1 s.r. region from P14 MrgA1 transgenic mouse. Cell 1 and 2 were filled with OGB-1 indicator dye and cell 3 has GFP expression. Note that the surface expression of GFP in MrgA1+ cells.

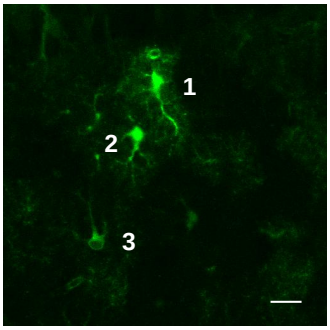


C

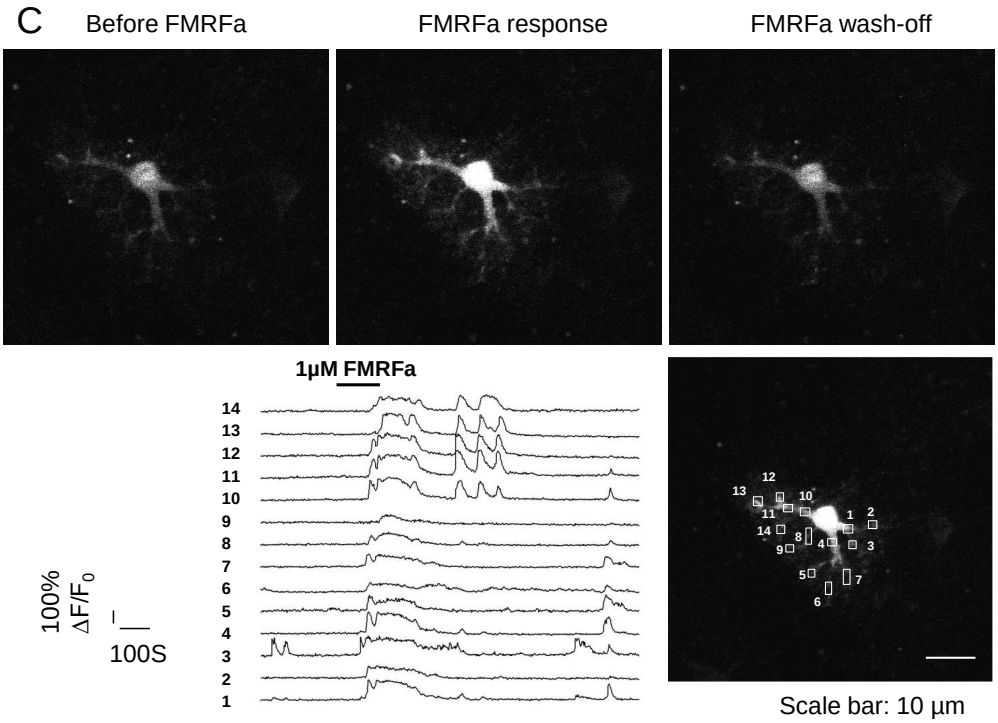

Figure 4.2 $Ca^{2+}$ imaging on s.r. astrocytes from MrgA-1 transgenic mouse with multiple agonist applications

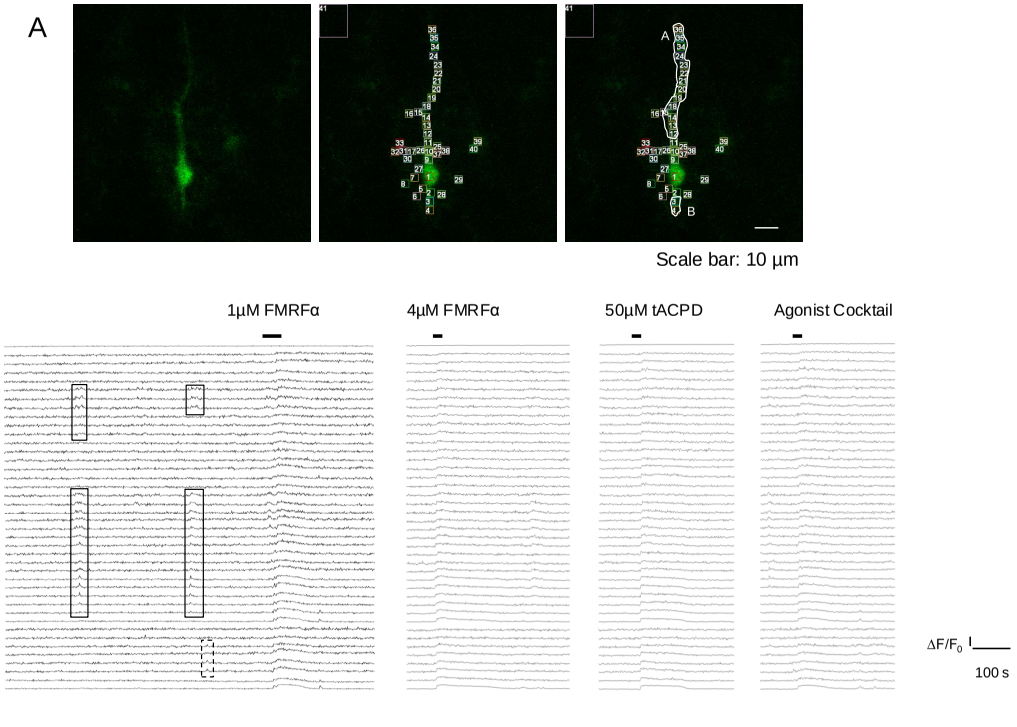

Figure 4.3 Long-term TTX incubation had no effect on MrgA1 receptor signaling

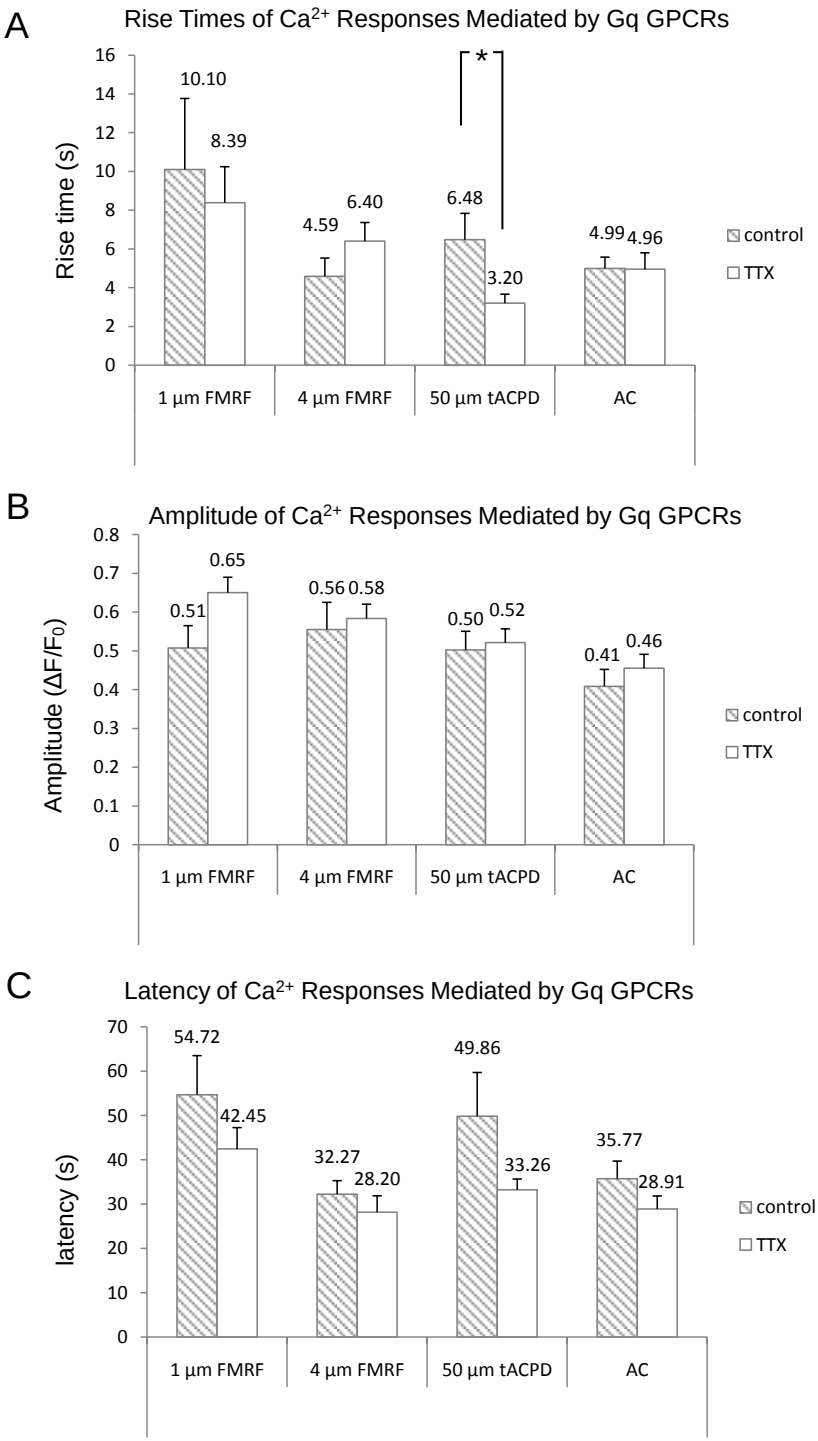

Figure 4.4 MrgA1 positive astrocytes can be identified by flow cytometry analysis

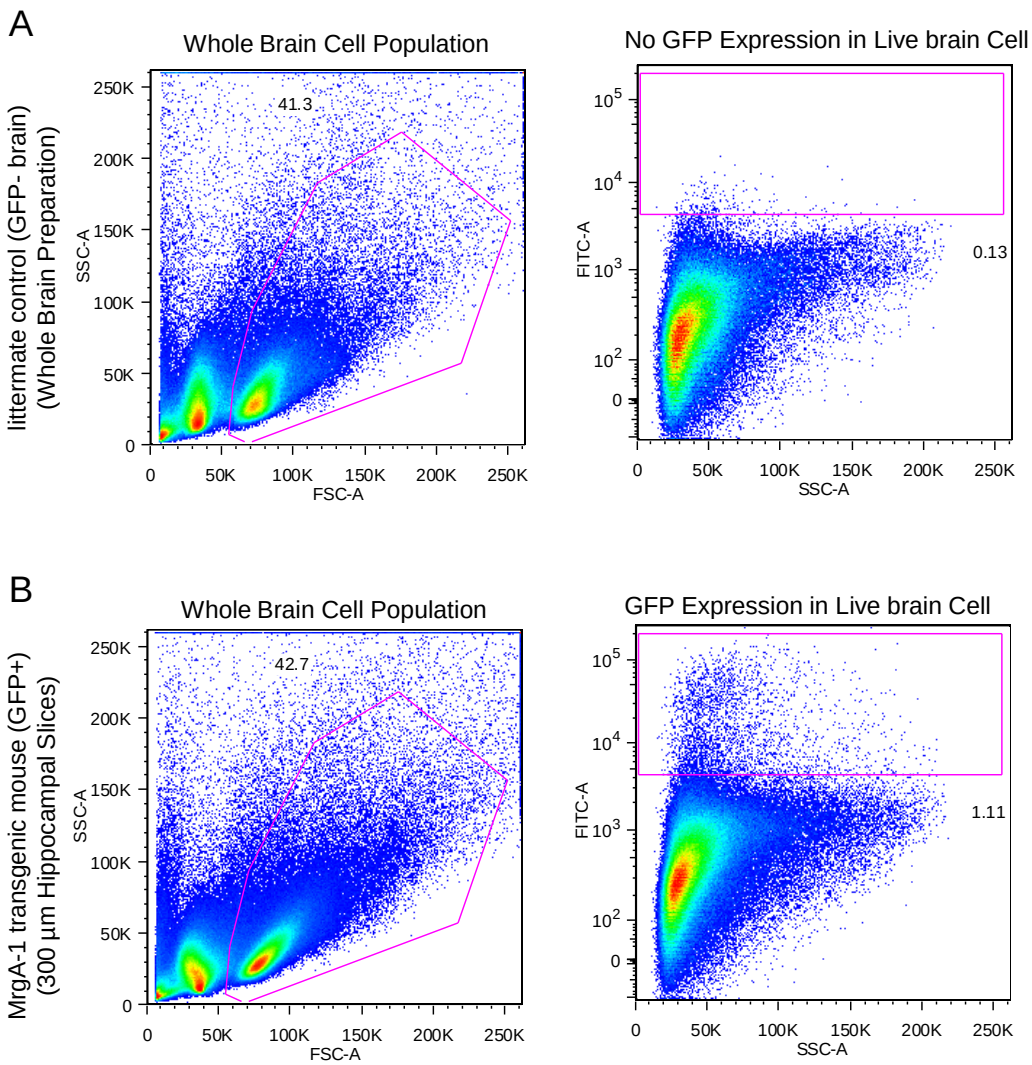

Figure 4.5 Metabotropic $GluR_5$ antibodies did not reveal positive staining on astrocytes isolated from whole brain of MrgA-1 transgenic mouse.

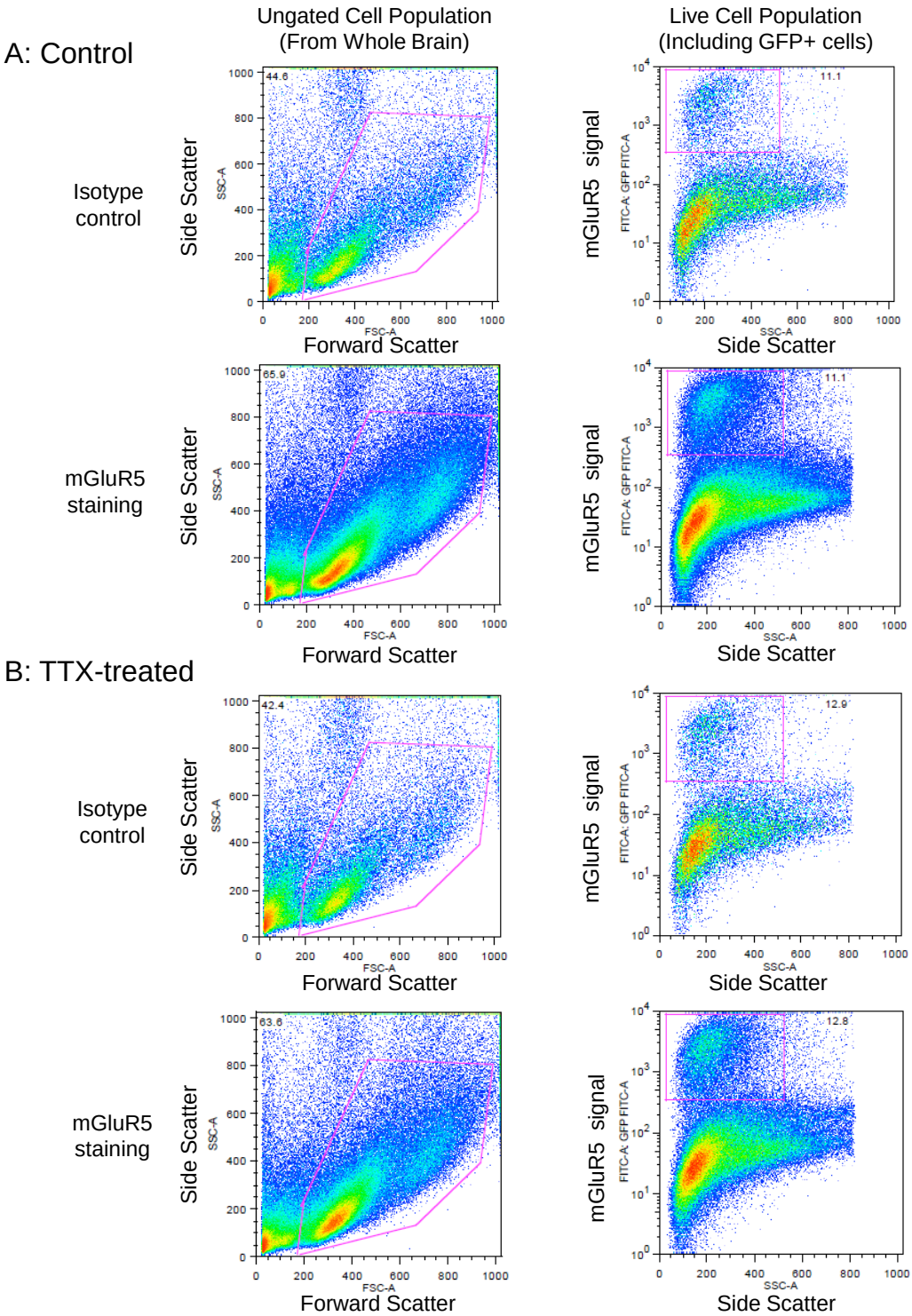

Figure 4.6 Scaling on AMPAR-mediated mEPSCs after 4 to 6 hrs TTX treatment.

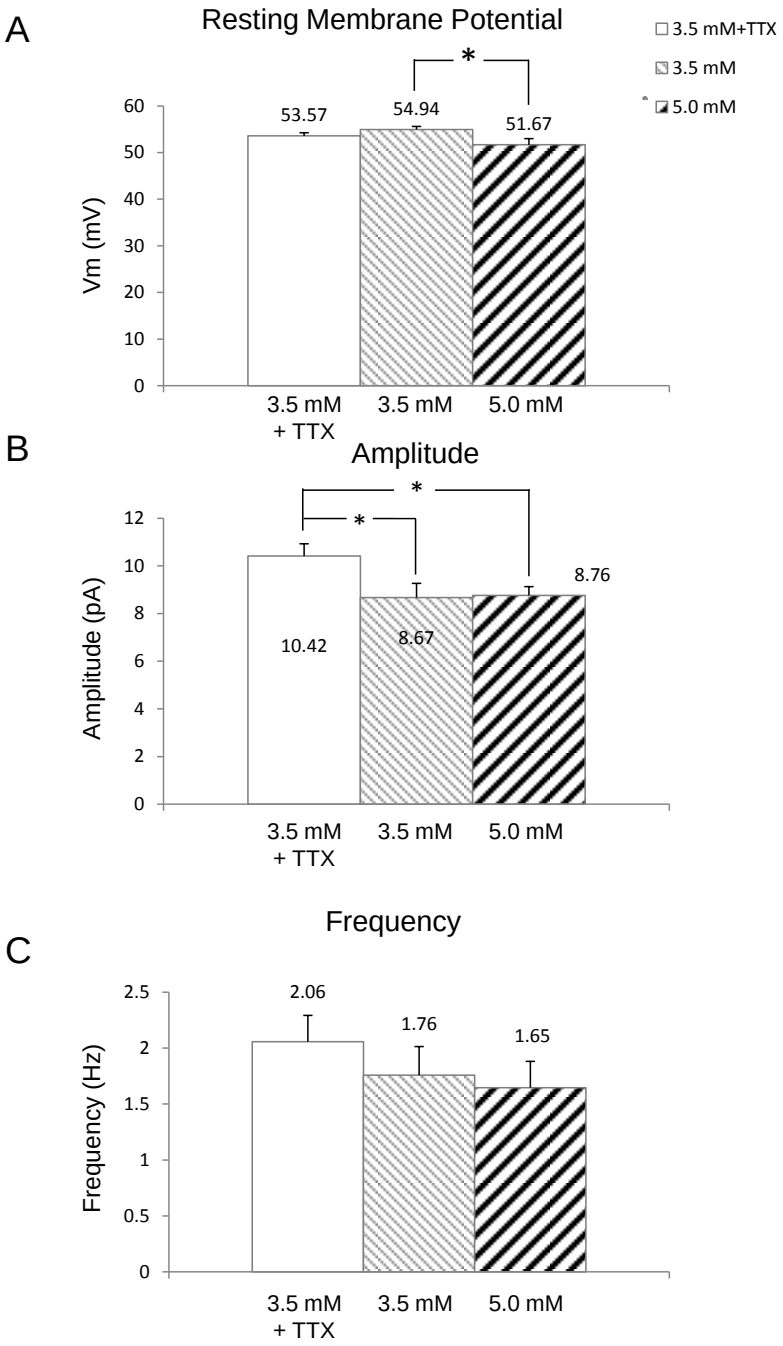

## Chapter 5: Discussion and Perspective

Astrocytes sense neuronal synaptic transmission through activation of their metabotropic receptors (Porter and McCarthy, 1995a, 1996; Pasti et al., 1997; Kang et al., 1998; Araque et al., 2002; Perea and Araque, 2005; Wang et al., 2006; Navarrete and Araque, 2008). Early studies indicated that cultured astroglia express metabotropic receptors that were coupled to second messenger cascades for almost all known neurotransmitters (Porter and McCarthy, 1997). The functional expression of these receptors on astrocytes *in situ* was confirmed using a variety of techniques, including immunocytochemistry, *in situ* hybridization, electrophysiology and $Ca^{2+}$ imaging (Van Der Zee et al., 1993; Duffy and MacVicar, 1995; Porter and McCarthy, 1995b, a; Azmitia et al., 1996; Porter and McCarthy, 1996, 1997; Shelton and McCarthy, 2000). In hippocampus, it is reported that astrocytes express metabotropic glutamate receptors (mGluRs) in the fine processes close to glutamatergic synapses (Porter and McCarthy, 1995b) which respond to neuronal glutamate release with elevations in intracellular $Ca^{2+}$ concentration (Porter and McCarthy, 1996). Hippocampal astrocytes are also reported to express $\alpha_1$-adrenergic receptors which respond to norepinephrine with $Ca^{2+}$ elevations (Duffy and MacVicar, 1995). The expression of purinergic receptors (Porter and McCarthy, 1995a), serotonergic receptors (Azmitia et al., 1996), muscarinic acetylcholine receptors (Van Der Zee et al., 1993) and histamine receptors (Shelton and McCarthy, 2000) was also shown in subpopulations of astrocytes in hippocampus. Their activity is coupled to activation of phospholipase C (PLC), conversion of phosphatidylinositol

bisphosphate ($PIP_2$) to inositol triphosphate ($IP_3$), and release of calcium from the endoplasmic reticulum (ER) (Porter and McCarthy, 1997).

In the 1990's, several pharmacological studies tested the nature of metabotropic receptor-mediated $Ca^{2+}$ release from the ER *in vitro* and *in situ*. $Ca^{2+}$ responses in astrocytes were carefully analyzed by applying neurotransmitters or agonists of the metabotropic receptors to astrocytes. There are some characteristics common to all Gq GPCR evoked $Ca^{2+}$ responses. First, astrocytes display all-or-none metabotropic receptor mediated $Ca^{2+}$ responses (Shao and McCarthy, 1993, 1995). Each ligand/agonist increases intracellular $Ca^{2+}$ levels to similar amplitudes, often occurring in the entire cell. Simultaneous application of multiple ligands does not produce an additive effect on $Ca^{2+}$ response amplitudes, even though clearly more receptors are being activated as compared to application of only one of the three agonists. These all-or-none type responses were also observed in the present study. The data presented in previous chapters show that astrocytes respond to the Gq GPCR agonists, including the group I mGluR agonist DHPG, group I and II mGluR agonist tACPD, a cocktail of agonists (including ATP for purinergic $P_2Y$ receptors, histamine for histamine H1 receptors, and carbachol for muscarinic AchRs), with $Ca^{2+}$ elevations of similar amplitudes. More interestingly, stimulation of a transgenic Gq GPCR (the MrgA1R) in astrocytes by its ligand FMRFa produces $Ca^{2+}$ responses with similar amplitudes as endogenous receptor evoked $Ca^{2+}$ responses in the same astrocytes. These data further confirm the all-or-none nature of Gq GPCR evoked $Ca^{2+}$ responses in astrocytes.

Is there a dose-dependent relationship between ligand/agonist and $Ca^{2+}$ responses? Previous studies using combined $Ca^{2+}$ imaging and receptor autoradiography showed that although the amplitude of $Ca^{2+}$ responses in astrocytes was independent of the receptor density and ligand concentration, the probability of a cell in the population giving a response was dependent on both parameters (Shao and McCarthy, 1993; Wang and Thompson, 1994). It has been reported that two subthreshold agonist applications applied simultaneously could evoke a full $Ca^{2+}$ response, which suggests that the key factors underlying the all-or-none responses are likely to be the level of $IP_3$ accumulation and the receptor desensitization (Shao and McCarthy, 1995). This leads to the second principle of Gq GPCR mediated $Ca^{2+}$ responses in astrocytes: The expression level of the Gq GPCRs correlates to the percentage of the cells in a population that respond to the agonist. Similarly, the percentage of the responding cells is dependent on the ligand/agonist concentration (Shao and McCarthy, 1993; Wang and Thompson, 1994). In both cases, the increased percentage of the responding cells in the population is due to increased number of receptors within each cell being activated (the probability of receptor-ligand interaction will increase with agonist concentration or by increasing receptor number). These studies were performed in astroglial cultures but the basic principles can be applied to astrocytes in intact systems, since cells in both cases express multiple Gq GPCR subtypes and the functional expression level of these Gq GPCRs varies among individuals (Shao et al., 1994; Porter and McCarthy, 1997). In the present study, the data also indicate that changes in the responsiveness of hippocampal s.r. astrocytes *in situ* are correlated with increased agonist concentration (Ref: data from

Chapters 2 and 3, where different DHPG concentrations were applied to the same treatment group). In addition, this phenomenon is also seen when different concentrations of FMRFa are applied to the transgenic MrgA1 Gq GPCR (Ref: data from Chapter 4, where 1 μM and 4 μM FMRFa are applied to MrgA1 expressing astrocytes). More importantly, significant differences in the percentage of cells in the population responding to the same agonist concentration have been detected between the control cells and the treated cells (Ref: data from Chapters 2 and 3, the difference between non-responders to within each DHPG concentration applied). These data in themselves suggest that long-term changes in neuronal action-potential driven neurotransmitter release directly affect the expression of astrocytic group I mGluRs.

In addition, it has been reported that the latency of Gq GPCR mediated $Ca^{2+}$ responses to agonist application is correlated to changes in Gq GPCR expression in cultured cells (Shao and McCarthy, 1993; Wang and Thompson, 1994). Rise times in these reports also appeared to be affected but they were not directly measured. In the present study, we found that the rise times of $Ca^{2+}$ elevations changes significantly in the group I mGluR mediated responses after treatment (Ref: data in Chapters 2 and 3 for DHPG evoked $Ca^{2+}$ responses). The latency of the response was significantly different only when measured in microdomains but not in the soma (Ref: data in Chapters 2 and 3 for DHPG evoked $Ca^{2+}$ responses). The lack of observed changes in latency in our hands might be due to the long time course it takes for agonist to diffuse into hippocampal slices vs. cultured cells. The astrocytes we imaged are mostly at a depth of at least 30 to

50 μm into the hippocampal slices, which makes rise time a more reasonable parameter with which to evaluate changes in the functional expression of the group I mGluRs.

Last, previous studies suggest that astrocytes *in vitro* and *in situ* respond to ligand/agonist application with different $Ca^{2+}$ elevation patterns (Murphy et al., 1993; Pasti et al., 1997; Shelton and McCarthy, 2000). Shelton and McCarthy showed that a single astrocytes that not respond to 2.5 μM tACPD but responded to 10 μM tACPD in oscillatory $Ca^{2+}$ elevation, and the same astrocytes responded to 40 μM tACPD with plateau-like $Ca^{2+}$ responses(Shelton and McCarthy, 2000). Activation of mGluRs by tACPD are known to induce $Ca^{2+}$ oscillations in astrocytes, and the frequency of the $Ca^{2+}$ oscillations increases with repetitive mGluR stimulation (Pasti et al., 1995; Pasti et al., 1997). The oscillatory $Ca^{2+}$ response is believed to result from the oscillatory pattern of PKC activation, in turn the production of $IP_3$, and the regenerative cycle of $Ca^{2+}$ release from the ER (Berridge and Galione, 1988; Berridge, 1993). Changes in the agonist response pattern can likely be involved in integration of signaling derived from multiple sites of Gq GPCR activation within the cell. In the present study, we observed a pattern shift in the both endogenous group I mGluR- and transgenic MrgA1 receptor-mediated $Ca^{2+}$ responses from single peak responses to plateau-like responses, with multi-peak oscillating responses in-between when agonist concentration is stepped up (Ref: data in Chapters 2, 3, 4). More importantly, the $Ca^{2+}$ responses in astrocytes evoked by the same concentration of group I mGluR agonist exhibit a significant pattern shift after long-term manipulation of neuronal activity. These data strongly indicate that there is a change in the functional expression level of astrocytic group I mGluRs after treatment.

While the present data suggest that astrocytes *in situ* change their metabotropic glutamate receptor expression in response to changes basal levels of neuronal activity, the findings do not conclusively and fully rule out the possibility that other endogenous Gq GPCRs expressed in hippocampal astrocytes are similarly sensitive to changes in neuronal activity. In the hippocampus, there are histaminergic inputs from the tuberomammillary nucleus (TMN) of the posterior hypothalamus (Panula et al., 1989) and rich cholinergic innervation arising mainly from the medial septum and the nucleus of the diagonal band of Broca (Woolf, 1991). In our experiment, a cocktail of agonists containing ATP, histamine and carbachol (10 μM each) was applied to astrocytes in order to stimulate purinergic $P_2Y$, histamine $H_1$, and muscarinic AchRs, respectively, as a positive control for astrocytic viability and to determine if changes in astrocytic Gq GPCR signaling activity are a ubiquitous process. There were no significant changes in either the rise times or the patterns of the agonist cocktail evoked $Ca^{2+}$ responses between control and treated astrocytes. However, the combined concentration of the multiple agonists we used are relatively high, and cannot fully distinguish potential changes to response patterns. Furthermore, the combination of 3 different kinds of agonist does not yield data about potential changes in the percentage of cells responding to each agonist. Thus, the data do not rule out the possible scaling effect on other astrocytic Gq GPCRs. Although, the histaminergic and cholinergic fibers in the hippocampal slice preparation have been deafferented from the neuron cell bodies in the basal forebrain area and hypothalamus. Therefore, it is unlikely that TTX or 5.0 mM $[K^+]_o$ application to hippocampal slices could cause significant change in the release of these

neurotransmitters. However, ATP has been shown to be co-released at glutamatergic synapses in the hippocampus under certain conditions (Rodrigues et al., 2006), raising the possibility that manipulation of neuronal firing also influenced the release of ATP and therefore led to a scaling effect on purinergic $P_2Y$ receptors.

It is a very interesting to consider the possibility that the scaling effect on group I mGluRs we observed in the present study can be applied to other Gq GPCRs when there is long-term change in release of the corresponding neurotransmitters. Future experiments are needed to test this hypothesis.

What is the possible mechanism underlying the changes in functional expression of group I mGluRs? Does manipulation of neuronal activity cause an increased group I mGluR protein expression in all s.r. astrocytes? Homeostatic scaling in neurons could be induced by blocking postsynaptic firing in individual neurons, which was mediated through a drop in somatic calcium influx, reduced activation of CaMKIV, and an increase in transcription (Ibata et al., 2008). However, astrocytes *in vivo* lack CaMKIV expression and CREB dependent gene transcription through CaMKIV (Impey et al., 2004; Murray et al., 2009). Recent reports suggest that ligand induced $Ca^{2+}$ oscillations in non-excitable cells regulate nuclear transcription factor NF-κB-driven gene transcription, which can function as one of the pathways that link Gq GPCR activity to changes in receptor expression (Dolmetsch et al., 1998; Hu et al., 1999).

Beta-arrestins are known to be involved in the desensitization and internalization of Gq GPCRs (Luttrell and Lefkowitz, 2002; DeWire et al., 2007; Defea, 2008). In

receptor desensitization, after G protein coupled kinases (GRKs) phosphorylate the ligand/agonist activated Gq GRCRs (Bunemann and Hosey, 1999), β-arrestins can inhibit the receptor from interacting with G proteins (Lohse et al., 1990). Following desensitization, β–arrestins also participate in the internalization of Gq GPCRs by binding to elements of clathrin-coated vesicles and targeting Gq GPCRs for endocytosis (Zhang et al., 1996; Laporte et al., 2002). Group I mGluRs have been shown to interact with arrestins and to undergo agonist-dependent endocytosis (Mundell et al., 2001). It has been shown that astrocytes express β-arrestins and that the binding of β -arrestins to Gq GPCRs does not simply uncouple GPCRs from further G-protein activation, but also initiates an alternative signaling pathway leading to activation of mitogen-activated protein kinase (MAPK) (Lefkowitz, 1998; McLennan et al., 2008; Miyatake et al., 2009). The activity of β-arrestins in relation to Gq GPCRs might a play role in both receptor internalization and gene transcription.

Another important remaining question pertains to the possible physiological significance of this form of plasticity in astrocytes. This is a somewhat difficult question to answer, as the function of neuron-to-astrocyte Gq GPCR signaling remains an open and heavily investigated area. One of the most significant overarching functions of astrocytes *is* homeostasis, not just of their own activity but in support of normal brain physiology. For example, neuron-to-astrocyte receptor communication may be important in regulating cerebral blood flow to active neurons (Simard et al., 2003; Zonta et al., 2003; Gordon et al., 2008) and in modulating uptake of $K^+$ and glutamate released by neurons to control neuronal excitability (Porter and McCarthy, 1997; Ye and Sontheimer,

1999). Secretion of molecules from astrocytes has been reported to play an important role in neuronal homeostatic plasticity (Kaneko et al., 2008). In addition to these supportive functions, many research groups have reported reciprocal astrocyte-to-neuron communication via release of gliotransmitters under certain conditions (Fiacco and McCarthy, 2006; Halassa et al., 2007; Agulhon et al., 2008). Transcriptome analysis of astrocytes suggests that they are highly secretory cells (Cahoy et al., 2008), and that the changes in astrocytic Gq GPCRs and $Ca^{2+}$ signaling may code for changes in gene transcription (Dolmetsch et al., 1998; Li et al., 1998; Hu et al., 1999) to affect the production and secretion of neuroactive molecules. In light of these important supportive astrocytic functions, it is possible that astrocytes adjust their secretion of neurotransmitters, including glutamate, in a homeostatic manner to adjust to long-term changes in neuronal activity. Ongoing experiments are testing the potential influence of astrocytic receptor plasticity on ambient glutamate and swelling-induced release of glutamate by astrocytes contributing to NMDA receptor-mediated slow inward currents in hippocampal CA1 pyramidal neurons.

**References**

Agulhon C, Petravicz J, McMullen AB, Sweger EJ, Minton SK, Taves SR, Casper KB, Fiacco TA, McCarthy KD (2008) What is the role of astrocyte calcium in neurophysiology? Neuron 59:932-946.

Araque A, Martin ED, Perea G, Arellano JI, Buno W (2002) Synaptically released acetylcholine evokes Ca2+ elevations in astrocytes in hippocampal slices. J Neurosci 22:2443-2450.

Azmitia EC, Gannon PJ, Kheck NM, Whitaker-Azmitia PM (1996) Cellular localization of the 5-HT1A receptor in primate brain neurons and glial cells. Neuropsychopharmacology : official publication of the American College of Neuropsychopharmacology 14:35-46.

Berridge MJ (1993) Cell signalling. A tale of two messengers. Nature 365:388-389.

Berridge MJ, Galione A (1988) Cytosolic calcium oscillators. The FASEB journal : official publication of the Federation of American Societies for Experimental Biology 2:3074-3082.

Bunemann M, Hosey MM (1999) G-protein coupled receptor kinases as modulators of G-protein signalling. The Journal of physiology 517 ( Pt 1):5-23.

Cahoy JD, Emery B, Kaushal A, Foo LC, Zamanian JL, Christopherson KS, Xing Y, Lubischer JL, Krieg PA, Krupenko SA, Thompson WJ, Barres BA (2008) A transcriptome database for astrocytes, neurons, and oligodendrocytes: a new

resource for understanding brain development and function. J Neurosci 28:264-278.

Defea K (2008) Beta-arrestins and heterotrimeric G-proteins: collaborators and competitors in signal transduction. British journal of pharmacology 153 Suppl 1:S298-309.

DeWire SM, Ahn S, Lefkowitz RJ, Shenoy SK (2007) Beta-arrestins and cell signaling. Annual review of physiology 69:483-510.

Dolmetsch RE, Xu K, Lewis RS (1998) Calcium oscillations increase the efficiency and specificity of gene expression. Nature 392:933-936.

Duffy S, MacVicar BA (1995) Adrenergic calcium signaling in astrocyte networks within the hippocampal slice. J Neurosci 15:5535-5550.

Fiacco TA, McCarthy KD (2006) Astrocyte calcium elevations: properties, propagation, and effects on brain signaling. Glia 54:676-690.

Gordon GR, Choi HB, Rungta RL, Ellis-Davies GC, MacVicar BA (2008) Brain metabolism dictates the polarity of astrocyte control over arterioles. Nature 456:745-749.

Halassa MM, Fellin T, Haydon PG (2007) The tripartite synapse: roles for gliotransmission in health and disease. Trends Mol Med 13:54-63.

Hu Q, Deshpande S, Irani K, Ziegelstein RC (1999) [Ca(2+)](i) oscillation frequency regulates agonist-stimulated NF-kappaB transcriptional activity. J Biol Chem 274:33995-33998.

Ibata K, Sun Q, Turrigiano GG (2008) Rapid Synaptic Scaling Induced by Changes in Postsynaptic Firing. Neuron 57:819-826.

Impey S, McCorkle SR, Cha-Molstad H, Dwyer JM, Yochum GS, Boss JM, McWeeney S, Dunn JJ, Mandel G, Goodman RH (2004) Defining the CREB regulon: a genome-wide analysis of transcription factor regulatory regions. Cell 119:1041-1054.

Kaneko M, Stellwagen D, Malenka RC, Stryker MP (2008) Tumor necrosis factor-alpha mediates one component of competitive, experience-dependent plasticity in developing visual cortex. Neuron 58:673-680.

Kang J, Jiang L, Goldman SA, Nedergaard M (1998) Astrocyte-mediated potentiation of inhibitory synaptic transmission. Nat Neurosci 1:683-692.

Laporte SA, Miller WE, Kim KM, Caron MG (2002) beta-Arrestin/AP-2 interaction in G protein-coupled receptor internalization: identification of a beta-arrestin binging site in beta 2-adaptin. J Biol Chem 277:9247-9254.

Lefkowitz RJ (1998) G protein-coupled receptors. III. New roles for receptor kinases and beta-arrestins in receptor signaling and desensitization. J Biol Chem 273:18677-18680.

Li W, Llopis J, Whitney M, Zlokarnik G, Tsien RY (1998) Cell-permeant caged InsP3 ester shows that Ca2+ spike frequency can optimize gene expression. Nature 392:936-941.

Lohse MJ, Benovic JL, Codina J, Caron MG, Lefkowitz RJ (1990) beta-Arrestin: a protein that regulates beta-adrenergic receptor function. Science 248:1547-1550.

Luttrell LM, Lefkowitz RJ (2002) The role of beta-arrestins in the termination and transduction of G-protein-coupled receptor signals. Journal of cell science 115:455-465.

McLennan GP, Kiss A, Miyatake M, Belcheva MM, Chambers KT, Pozek JJ, Mohabbat Y, Moyer RA, Bohn LM, Coscia CJ (2008) Kappa opioids promote the proliferation of astrocytes via Gbetagamma and beta-arrestin 2-dependent MAPK-mediated pathways. Journal of neurochemistry 107:1753-1765.

Miyatake M, Rubinstein TJ, McLennan GP, Belcheva MM, Coscia CJ (2009) Inhibition of EGF-induced ERK/MAP kinase-mediated astrocyte proliferation by mu opioids: integration of G protein and beta-arrestin 2-dependent pathways. Journal of neurochemistry 110:662-674.

Mundell SJ, Matharu AL, Pula G, Roberts PJ, Kelly E (2001) Agonist-induced internalization of the metabotropic glutamate receptor 1a is arrestin- and dynamin-dependent. Journal of neurochemistry 78:546-551.

Murphy TH, Blatter LA, Wier WG, Baraban JM (1993) Rapid communication between neurons and astrocytes in primary cortical cultures. J Neurosci 13:2672-2679.

Murray PD, Kingsbury TJ, Krueger BK (2009) Failure of Ca2+-activated, CREB-dependent transcription in astrocytes. Glia 57:828-834.

Navarrete M, Araque A (2008) Endocannabinoids mediate neuron-astrocyte communication. Neuron 57:883-893.

Panula P, Pirvola U, Auvinen S, Airaksinen MS (1989) Histamine-immunoreactive nerve fibers in the rat brain. Neuroscience 28:585-610.

Pasti L, Pozzan T, Carmignoto G (1995) Long-lasting changes of calcium oscillations in astrocytes. A new form of glutamate-mediated plasticity. J Biol Chem 270:15203-15210.

Pasti L, Volterra A, Pozzan T, Carmignoto G (1997) Intracellular calcium oscillations in astrocytes: a highly plastic, bidirectional form of communication between neurons and astrocytes in situ. J Neurosci 17:7817-7830.

Perea G, Araque A (2005) Glial calcium signaling and neuron-glia communication. Cell Calcium 38:375-382.

Porter JT, McCarthy KD (1995a) Adenosine receptors modulate [Ca2+]i in hippocampal astrocytes in situ. Journal of neurochemistry 65:1515-1523.

Porter JT, McCarthy KD (1995b) GFAP-positive hippocampal astrocytes in situ respond to glutamatergic neuroligands with increases in [Ca2+]i. Glia 13:101-112.

Porter JT, McCarthy KD (1996) Hippocampal astrocytes in situ respond to glutamate released from synaptic terminals. J Neurosci 16:5073-5081.

Porter JT, McCarthy KD (1997) Astrocytic neurotransmitter receptors in situ and in vivo. Prog Neurobiol 51:439-455.

Rodrigues RJ, Almeida T, de Mendonca A, Cunha RA (2006) Interaction between P2X and nicotinic acetylcholine receptors in glutamate nerve terminals of the rat hippocampus. Journal of molecular neuroscience : MN 30:173-176.

Shao Y, McCarthy KD (1993) Quantitative relationship between alpha 1-adrenergic receptor density and the receptor-mediated calcium response in individual astroglial cells. Mol Pharmacol 44:247-254.

Shao Y, McCarthy KD (1995) Receptor-mediated calcium signals in astroglia: multiple receptors, common stores and all-or-nothing responses. Cell Calcium 17:187-196.

Shao Y, Porter JT, McCarthy KD (1994) Neuroligand receptor heterogeneity among astroglia. Perspect Dev Neurobiol 2:205-215.

Shelton MK, McCarthy KD (2000) Hippocampal astrocytes exhibit Ca2+-elevating muscarinic cholinergic and histaminergic receptors in situ. Journal of neurochemistry 74:555-563.

Simard M, Arcuino G, Takano T, Liu QS, Nedergaard M (2003) Signaling at the gliovascular interface. J Neurosci 23:9254-9262.

Van Der Zee EA, De Jong GI, Strosberg AD, Luiten PG (1993) Muscarinic acetylcholine receptor-expression in astrocytes in the cortex of young and aged rats. Glia 8:42-50.

Wang SS, Thompson SH (1994) Measurement of changes in functional muscarinic acetylcholine receptor density in single neuroblastoma cells using calcium release kinetics. Cell Calcium 15:483-496.

Wang X, Lou N, Xu Q, Tian GF, Peng WG, Han X, Kang J, Takano T, Nedergaard M (2006) Astrocytic Ca2+ signaling evoked by sensory stimulation in vivo. Nat Neurosci 9:816-823.

Woolf NJ (1991) Cholinergic systems in mammalian brain and spinal cord. Prog Neurobiol 37:475-524.

Ye ZC, Sontheimer H (1999) Metabotropic glutamate receptor agonists reduce glutamate release from cultured astrocytes. Glia 25:270-281.

Zhang J, Ferguson SS, Barak LS, Menard L, Caron MG (1996) Dynamin and beta-arrestin reveal distinct mechanisms for G protein-coupled receptor internalization. J Biol Chem 271:18302-18305.

Zonta M, Angulo MC, Gobbo S, Rosengarten B, Hossmann KA, Pozzan T, Carmignoto G (2003) Neuron-to-astrocyte signaling is central to the dynamic control of brain microcirculation. Nat Neurosci 6:43-50.